SUSPENDED PARTICULATE MATTER DISTRIBUTION. TRANSPORT, AND PHYSICAL CHARACTERISTICS IN THE NORTH ALEUTIAN SHELF AND ST. GEORGE BASIN LEASE AREAS

by

Edward T. Baker

Pacific Marine Environmental Laboratory
National Oceanic and Atmospheric Administration

Final Report
Outer Continental Shelf Environmental Assessment Program
Research Unit 594

January 1983

TABLE OF CONTENTS

LIST OF FIGURES

Figure 44. Incremental cumulative curves from the NASTE 2 surface (top) and bottom (middle) waters. Curve envelopes (bottom) demonstrate the similarity of the two populations.

Figure 45. Incremental cumulative curves from NASTE 3 PL_1 surface (A), minimum turbidity (B), and bottom (C) zones. Panels D, E, and F show analogous curves for the PL_2 transect.

Figure 46. Net particle attenuation profiles, stability profiles, and density profiles from the coastal (top), middle (middle), and oceanic (bottom) domains. Note the stability maximum at the top of each bottom nepheloid layer.

Figure 47. Attenuation (open circles) and salinity (closed circles) gradients normal to the Alaska Peninsula for each cruise. Mean attenuation and salinity values from each NA station were grouped and averaged over 10-m station depth increments.

Figure 48. Salinity and $\Delta\sigma_t$ gradients along the PL line during NASTE 1 and NASTE 3.

Figure 49. Changes in the attenuation value in the turbidity minimum and in the concentration of surface-and bottom chlorophyll a along the PL line. Compare the position of these changes with the hydrographic changes in Figure 48.

LIST OF TABLES

I. SUMMARY OF OBJECTIVES, CONCLUSIONS, AND IMPLICATIONS WITH RESPECT TO OCS OIL AND GAS DEVELOPMENT

A. Objectives

The principal objective of this research unit was to describe the distribution, transport, and physical characteristics of suspended particulate matter (SPM) in the area of the North Aleutian Shelf (NAS) and St. George Basin (SGB). These data are required to assess the effect that the natural particle population in these waters might have on the transport and dispersal of spilled oil.

B. Conclusions and Implications

1. The oceanographic conditions which result in the creation of hydrographic structural domains and frontal regions (Kinder and Schumacher, 1981a) also create characteristic SPM distributions in each of these domains. Particle gradients in the coastal domain were very low or non-existant in the vertical and very steep in the horizontal, with particle concentrations decreasing rapidly offshore. The middle and outer domains were typified by a three-layer structure: a high-turbidity surface layer resulting from in-situ phytoplankton growth and offshore advection and diffusion of shore and river derived particles, a broad middle zone of horizontally and vertically uniform particle concentrations, and a bottom layer of increased turbidity largely resulting from local resuspension of bottom sediments. This structure was always found in the outer domain. In the middle domain it can be weakened or destroyed when the normal two-layer density structure is weakened or obliterated, as in winter or during severe storms. Frontal zones were

sites of increased horizontal particle concentration gradients, especially in the mid-depth low turbidity layer.

2. Seasonal particle concentrations in the NAS region varied by <25% and were not significantly different during any of the three cruises. Seasonal salinity changes were likewise small but did vary inversely with the particle concentration.

3. The offshore gradient of mean particle concentration fell rapidly from shore to about the 50-m isobath and then varied little with increasing water depth. This pattern was evident irrespective of season (i.e., the presence or absence of the coastal front) or of location along the NAS.

4. The particle size distribution data followed the power law curve characteristic of many aqueous and terrestrial fine-particle suites. The slope of the power curve normally fell between 3.0 and 4.5 in agreement with numerous other marine studies and corresponding to median diameters of ~8-25 pm. Lower slopes, characteristic of a larger proportion of coarse-grained particles in the distribution, were normally found in near-shore waters. Organic matter loading in the SPM ranged from a low of ~25% for inshore stations during the winter to >50% for surface water samples from the offshore stations during the spring.

5. Areal distribution maps depict an SPM distribution in which particles from point sources along the coast are largely retained in the nearshore zone and dispersed parallel to the coast. Particle flux measurements from long term current meter/transmissometer deployments support this view.

Three moorings in the nearshore (z < 32 m) waters to the west of Port Moller recorded a net SPM alongshore transport to the southwest, away from Port Moller. A mooring in the coastal front zone (z = 59 m) recorded near-bottom SPM flux predominantly onshore. Two moorings seaward of the coastal front (z > 68 m) recorded near-bottom SPM flux offshore and to the northeast. This pattern is consistent with a transport divergence creating a particle minimum in the near-bottom waters under the coastal front, an interpretation which agrees with the minimums in SPM concentration around the 50-m isobath observed in fall and spring.

6. Maximum concentrations of particulate-associated oil resulting from an oil spill in NAS waters can be roughly estimated by combining the SPM data from this report with oil-loading studies performed by Payne et al., (1981) at Science Applications, Inc. (SAI). Based on the range of oil loading for different marine sediment types found by MI, particulate-associated oil concentrations might reach 0.7-7 ppb in the water column of the nearshore zone (10-19 m deep) and 0.06-1.1 ppb in the offshore zone (40-90 m deep]. Sedimentation of this oil to the benthos, calculated on the basis of sediment trap data from this report, could be expected to be in the range of 1-10 mg oil $m^{-2} day^{-1}$.

II. INTRODUCTION

A. Purpose of the Study

If petroleum hydrocarbons are introduced into the water column either through natural seepage or unintentional spills, a significant fraction will become associated with the ambient particles (Meyers and Quinn, 1973; Baker et al., 1978; Payne et al., 1981). Oil trajectories and sedimentation will then be governed not only by the water trajectories but also by the trajectories and sedimentation of natural particles accommodating the oil. The purpose of this study, then, was to quantify the distribution and transport of particles which could affect oil movement. In addition, the study sought to define the relationships between the hydrographic structure of the southeastern Bering Sea (Kinder and Schumacher, 1981a) and the variability in particle distributions.

B. Specific Objectives

Specific objectives under this research unit included:

(1) Seasonal distributions of SPM concentrations in the vicinity of the NAS and SGB lease areas.

(2) Direct information concerning the horizontal and vertical SPM flux at several locations on the NAS by means of moored current ❑ eter/transmissometer and sediment trap measurements.

(3) Characterizations of the SPM at several locations along and across the inner front on the NAS in terms of particle size distribution, organic matter content, and x-ray clay mineralogy.

(4) Using pertinent data from other research units, estimate the water column loading and sedimentation rates of sediment' accommodated oil for various areas on the NAS and SGB.

C. Relevance to OCSEAP

One factor in determining which potential lease areas may be inappropriate for development is the predicted fate of spilled oil from a particular location. Furthermore, OCSEAP is charged with providing information from which spilled oil trajectories and landfalls ❑ ay be projected. Because natural particles will provide vehicles for the transport and sedimentation of spilled oil, knowledge of particle distributions and transport is necessary to improve OCSEAP's predictions concerning the fate of spilled oil.

III. STUDY AREA AND OCEANOGRAPHIC SETTING

The study area for the North Aleutian Shelf Transport Experiment (NASTE) was the southeastern Bering Sea. Sampling was concentrated in two specific areas: (1) along the North Aleutian Shelf (NA stations, Fig. 1), and (2) in St. George Basin between the Pribilof Islands and Unimak Island (SG, PL, UP, and Y stations, Fig. 2). Each area was visited during three cruises: RP4SU80A between 13 August and 8 September, 1980 (NASTE 1); RP4SU81A between 30 January and 17 February, 1981 (NASTE 2); and RP4DI81A between 13 May and 2 June, 1981 (NASTE 3); moored instruments were deployed between NASTE 1 and NASTE 2 and between NASTE 2 and NASTE 3 at the locations shown in Fig. 3.

A. Hydrographic Domains

The hydrographic structure of the southeastern Bering Sea has been summarized by Kinder and Schumacher (1981a). The structure is developed not in reponse to mean flow patterns but rather as a result of boundary processes: tidal and wind mixing; buoyancy input from surface heating, cooling, and freshwater melt; and lateral exchange with the offshore oceanic water ❑ass. Three distinct hydrographic domains can be identified from the vertical structure of the water column, as illustrated by three stations sampled during NASTE 1 along the PL line in St. George Basin (Fig. 4). The coastal domain (PL 24) is vertically homogeneous in water properties and is separated

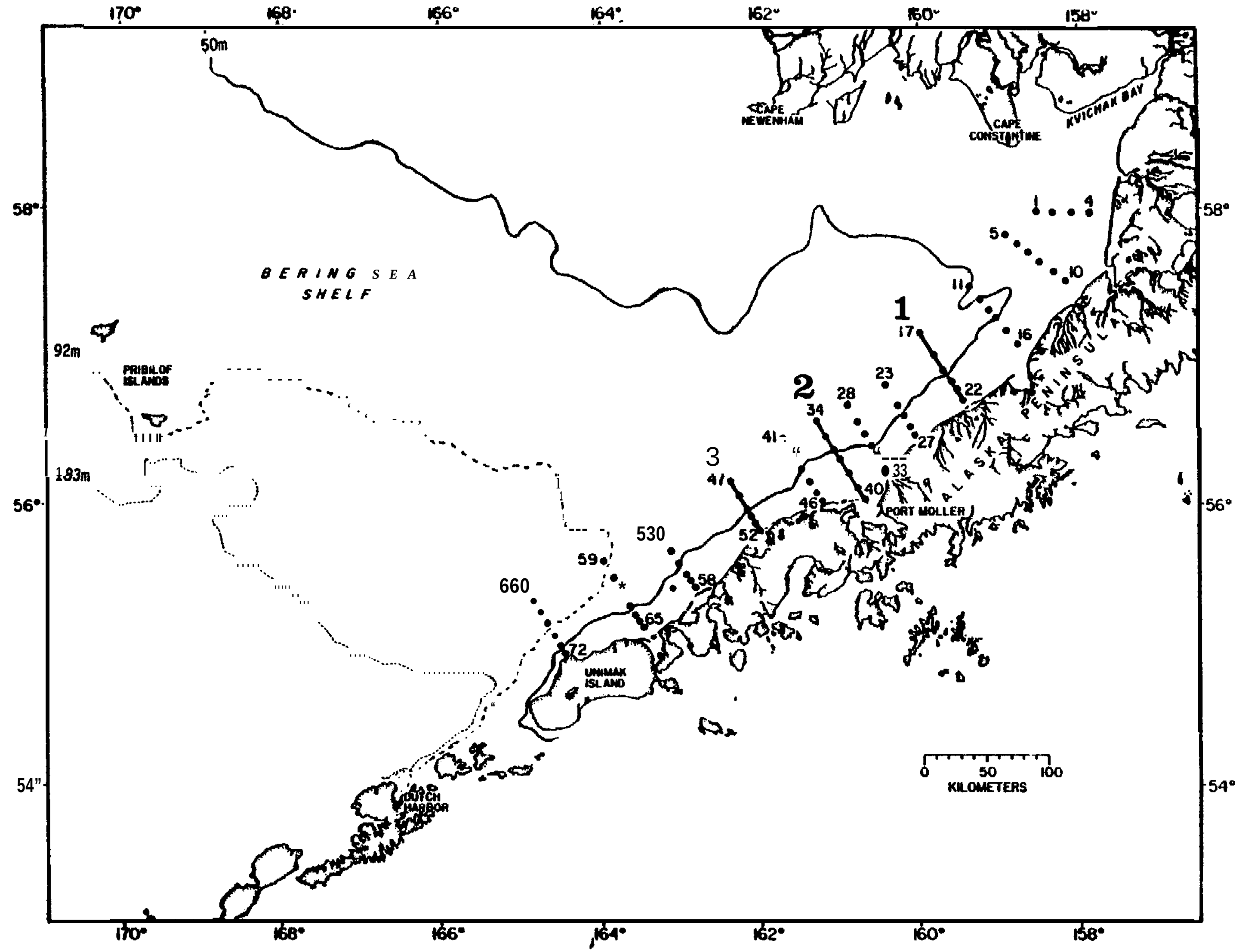

Figure 1. Map of north Aleutian Shelf (NAS) region showing bathymetry and all NA station locations. Lines 1, 2 and 3 are the locations chosen for the vertical cross-sections of attenuation and density shown in subsequent figures.

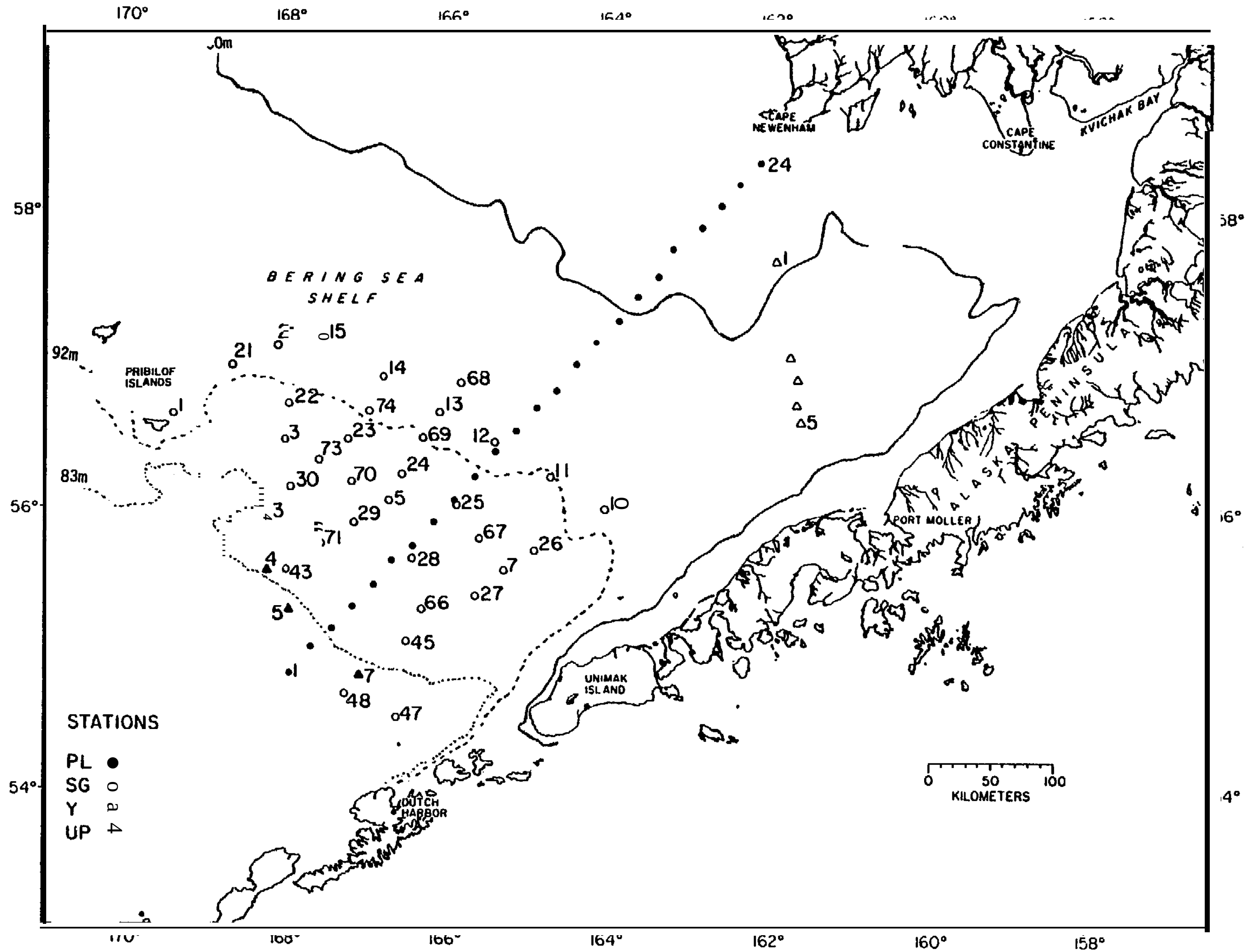

Figure 2. Map of the St. George Basin area showing all SG, PL, Y, and UP station locations occupied during one or more NASTE cruises. PL stations are numbered from 1 to 24 starting at the southwest end of the line.

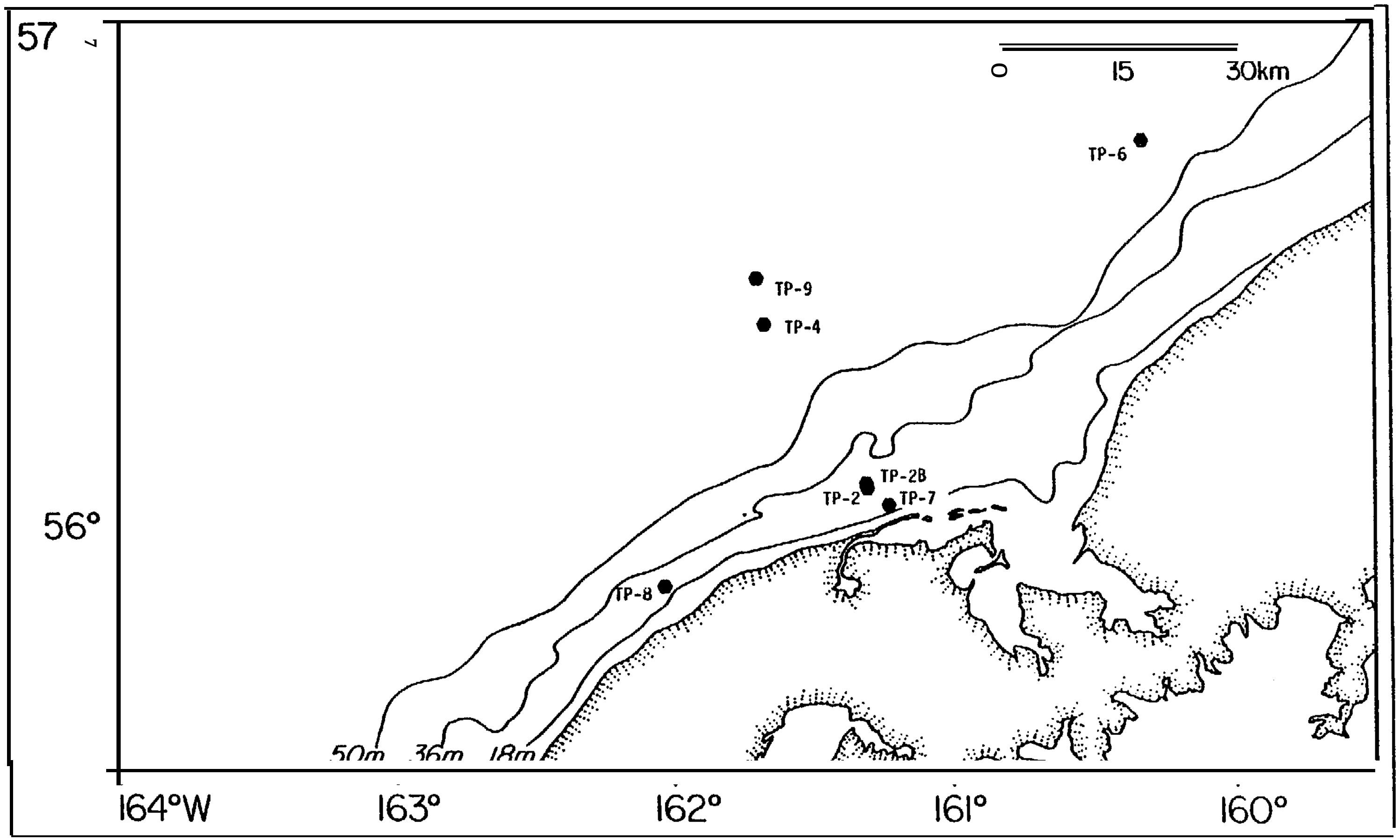

Figure 3. Map of the North Aleutian Shelf region near Port Moller showing bathymetry and mooring locations.

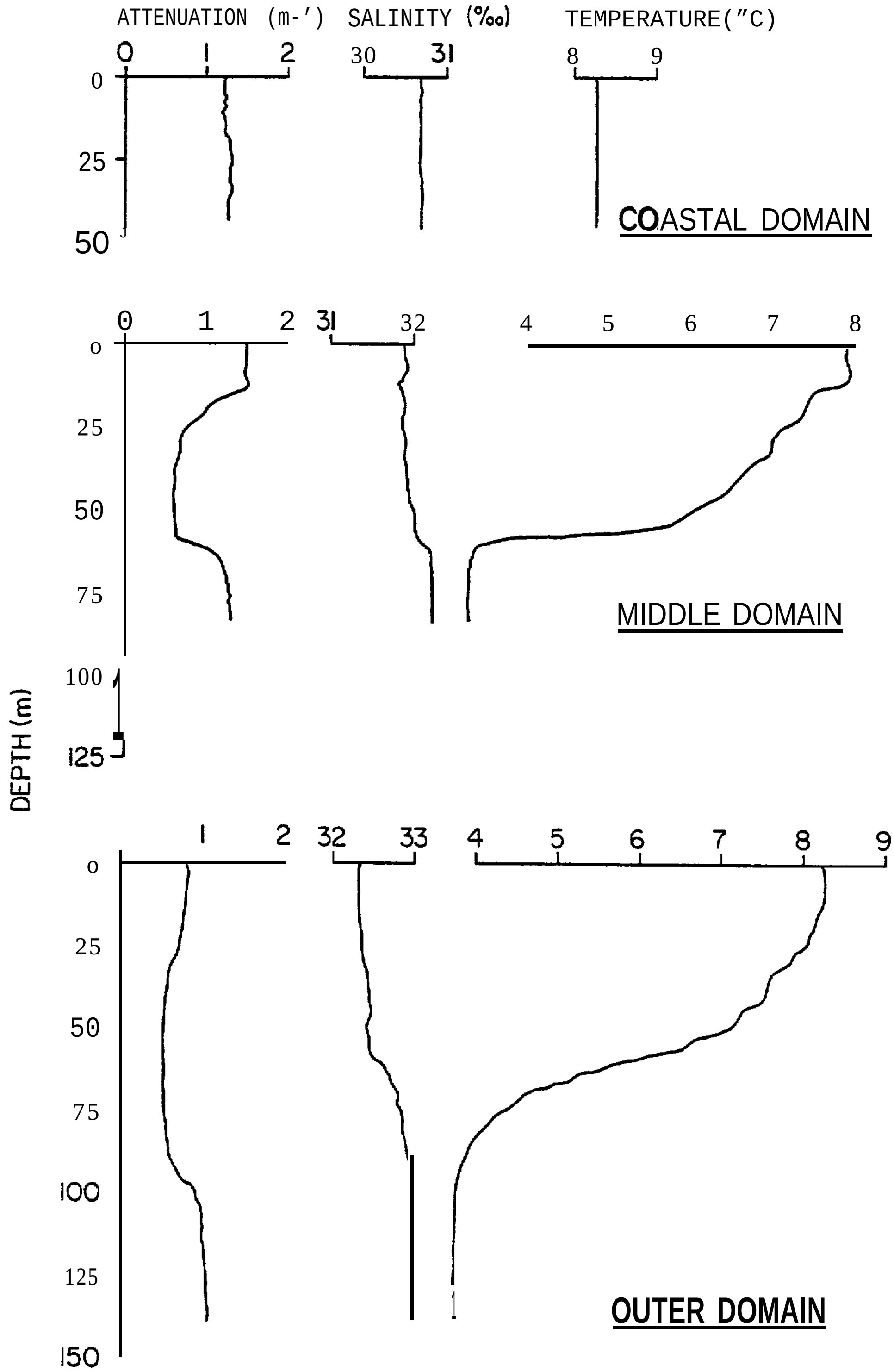

Figure 4. Typical water property and particle concentration profiles for hydrographic domains in the southeastern Bering Sea.

from the middle domain by a narrow (-10 km) front normally centered along the 50-m isobath. Seaward of this front, the middle domain is basically two-layered: a wind-mixed surface layer separated from a tidally-mixed bottom layer by a sharp pycnocline (PL 11). This domain extends to about the 100-m isobath where the broad (-50 km) middle front is located. Seaward of this front is the outer domain. This domain also has surface and bottom mixed layers, but the increased water depths prevent these layers from meeting and results in a broad *zone* of weak stratification and pronounced temperature and salinity fine structure (PL 4}. As will be discussed in this report, these domains, as well as the fronts separating them, also are a ❑ ajor influence on the vertical distribution of suspended particulate matter and its transport through the southeastern Bering Sea.

B. Bottom Sediments

Sharma (1979) has summarized much of the available information on bottom sediments of the southeastern Bering Sea. Most of the NASTE study" area is covered by sand and silt, with locally important amounts of gravel and clay. Mean sediment size contours closely follow isobaths, grading from very coarse sand (l-2 mm diameter) in Kvichak Bay to fine silt (8-18 pm) in St. George Basin between Unimak Island and the Pribilofs. Mean size is closely controlled by water depth (Fig. 5): at depths <~60 m the mean size is nearly always found to be >125 µm; at depths >~75 m the mean size is <125 pm. The interval between 60 and 75 m is a broad transition zone where mean size is highly variable. This transition zone roughly corresponds to the position of the coastal front.

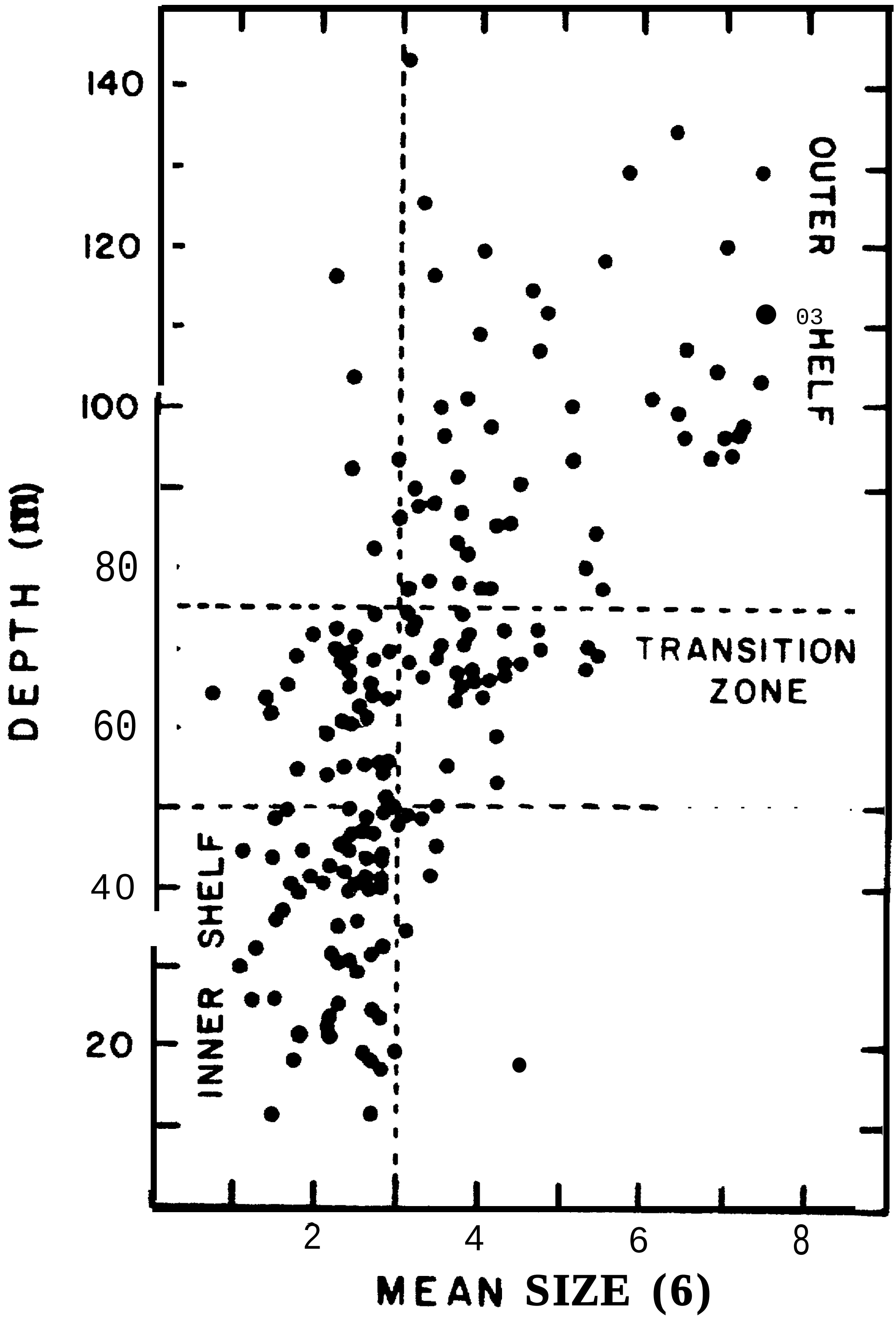

Figure 5. Bottom sediment data from the Bering Sea (Sharma,1979) showing the depth control of mean size.

C. Suspended Particulate Matter

Detailed information on SPM concentrations in the southeastern Bering Sea is scarce. Sharma (1979) found surface concentrations of 0.2 to 2.2 mg l^{-1} during June and July of 1973, but station spacing was too coarse to define any pattern in the NASTE study area. Feely et al. (1981) occupied ~50 stations at 50 to 100 km spacing in the southeastern Bering Sea during the fall of 1975 and the summer of 1976. Surface concentrations ranged from 1 to >6 mg l^{-1} in the near-shore zone and were generally <1 mg l^{-1} seaward of ~75 km from the Alaska Peninsula. Near-bottom concentrations also showed a bathymetric influence and were higher than their surface counterparts, indicating that resuspension activity was common. Of particular interest to the present study was the indication in Feely's data of a narrow band of relatively low (<1.0 mg l^{-1}) near bottom SPM values running parallel to the Alaska Peninsula at or just seaward of the 50 m isobath; that is, at about the position of the coastal front.

IV. METHODOLOGY

A. Data Collection

1. Water samples

Water samples for SPM filtration, mineralogy samples, pigment analyses, and particle size distribution measurements were collected from 5-ℓ Niskin or Go-Flo sampling bottles lowered by a CTD-mounted rosette system. Upon recovery, separate samples were drawn for particle size distribution and pigment analyses. During NASTE 1 and 2, SPM samples were filtered by transferring a portion of the bottle sample to a separate filtering apparatus. During NASTE 3, SPM samples were filtered directly from the sample bottles. In each case, seawater was drawn through preweighed 0.4 µm pore size, 47 mm diameter polycarbonate filters under a 15 psi vacuum. Filters were rinsed three times with particle-free distilled water to remove sea salts, dessicated at room temperature, sealed, and returned to the laboratory for reweighing and analysis.

2. Light attenuation profiles

Light attenuation data were recorded at every CTD station and on seven of the Aanderaa current meter deployments. The beam transmissometers used are fully described by Bartz et al. (1978). The light source is a light-emitting diode with a wavelength of 660 nm to eliminate attenuation resulting from dissolved humic acids ("yellow matter"). Accuracy and stability are sufficient to provide data with an error of <0.5% of the true light transmission. The path length is 0.25 m to provide excellent resolution in coastal waters where SPM concentrations typically range from 1 mg l^{-1} to 20 mg l^{-1}.

For profiling work, the transmissometer readout was converted from the normal DC output to a frequency modulated signal compatible with the CTD data flow. The transmission signal was then recorded on the CTD data tape along with temperature, salinity, and depth. A realtime strip chart record was also available to provide a guide to choosing appropriate depths for discrete water samples.

By correlating the absolute SPM concentrations from filter samples with the transmissometer reading from the same depth and location, transmissometer calibration curves were developed for each cruise. Light transmission values were first converted to the optical parameter of attenuation (α) using:

$$\alpha = \frac{-\ln (T/100)}{R}$$

where T = percent transmission and R = path length of the instrument (0.25 m). Plots of particle mass concentration (C) versus light attenuation (α) are shown in Fig. 6; statistical parameters of the least-squares regression are given in Table 1. Figure 6 and Table 1 indicate that correlations between light attenuation and SPM concentration were significant at the 0.05 probability level for each cruise. Furthermore, the 95% confidence intervals for the slope of the lines all overlap, implying that the two variables possessed a similar functional relationship during all three cruises. Inspection of Fig. 6 reveals that for NASTE 2 and 3 the most dilute samples fall below the regression line. To accurately predict SPM values of <~1.5 mg l^{-1} from attenuation readings, a separate regression line is necessary (Table 1). The most notable change is that the intercept of the lines for the dilute NASTE 2 and 3 samples average ~0.41 m^{-1}. One measure of the effectiveness of transmissometer readings in predicting the true SPM concentration is a comparison of the value of α at the zero SPM intercept to that for particle-free water. Tyler et al. (1974) present laboratory data which show that at 660 nm α lies between 0.34 and 0.43 m^{-1}. Both the NASTE 2 and NASTE 3 intercepts are within or close to that range, indicating that the variation in particle concentration was indeed the primary influence affecting the transmissometer readings. Although mass concentration of particles is commonly the primary influence on attenuation, factors such as size, shape, number, and index of refraction of the particles are also

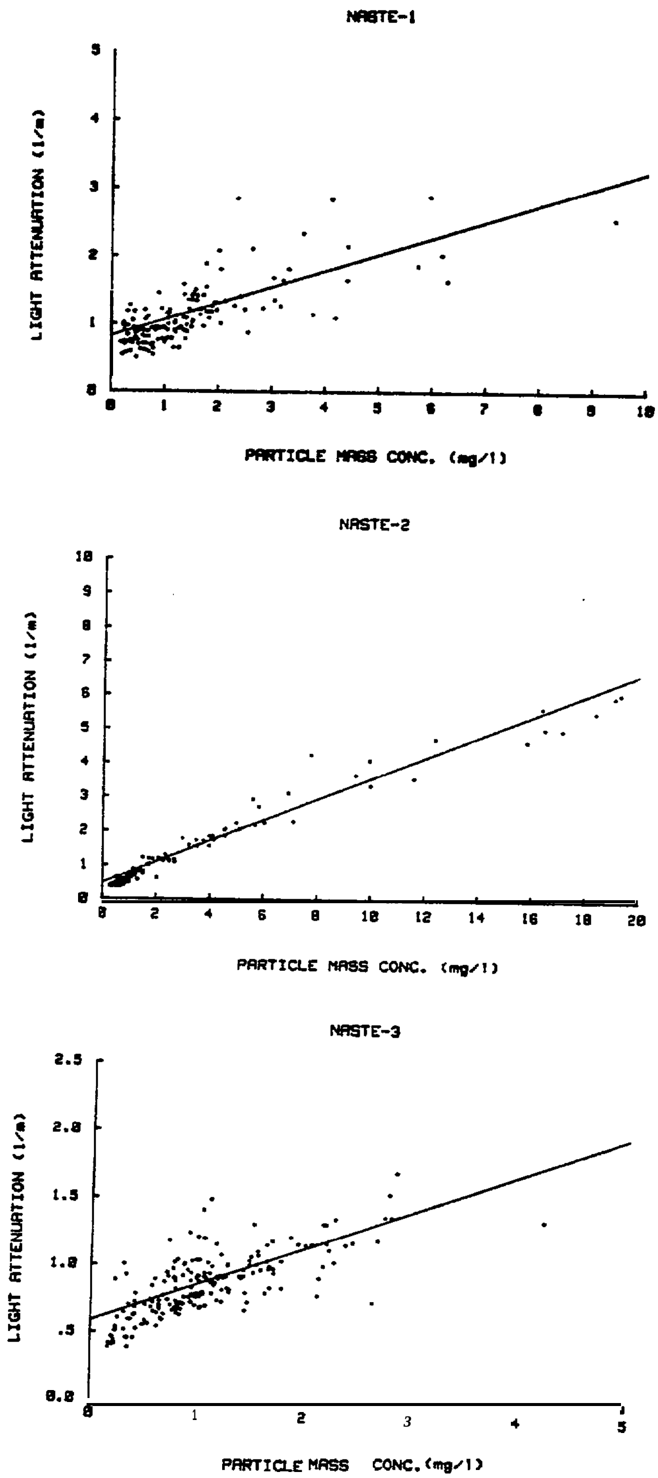

Figure 6. Transmissometer calibration curves for (top) August 1980, (middle) January 1981, and (bottom) May 1981.

important. The consistent difference in regression parameters between NASTE 1 and the following cruises suggests that the particles may have had somewhat different average characteristics during the late summer than during winter and spring.

TABLE 1

Linear least squares parameters for regressions of particle mass concentration (C) and light attenuation (a)

	NASTE 1	NASTE 2	NASTE 3
All Samples			
No. of samples pairs	144	126	187
Regression equation	α=.80+.26C	α=.50+.31C	α=.59+.28C
Correlation (r)	.72	.98	.74
Standard error of estimate	.30	.26	.16
95% confidence interval			
Slope	.22-.30	.30-.32	.24-.31
Intercept	.72-.88	.45-.55	.54-.64
Dilute Samples			
SPM range (mg 1^{-1})	0-1.5	0-1.5	0-1.0
No. of sample pairs	98	79	104
Regression equation	α=.80+.22C	α=.36+.41C	α=.46+.47C
Correlation (r)	.40	.86	.65
Standard error of estimate	.20	.077	.14
95% confidence interval			
Slope	.18-.32	.32-.40	.36-.57
Intercept	.72-.89	.35-.47	.39-.54

3. Flux measurements

Measurements of horizontal SPM flux and vertical mass flux were made at the times and locations given in Table 2. Horizontal SPM flux data were acquired by means of a transmissometer (identical to the profiling model) coupled to the directional vane of Aanderaa current meters deployed by J. Schumacher, PMEL. The attenuation data were recorded internally on the current meter's pressure charnel. The record length for the transmissometer data varies from 16 to 93 days depending on equipment failures and degradation of the signal as a result of organic growth on the lens surfaces. Transport flux was obtained by vector addition of the mean and variable portions of the flow along two component axes:

TABLE 2

Flux measurements during the NASTE project

Mooring	Location	Water Depth (m)	Transmissometer Sampling Interval	Transmissometer Meter Depth (m)	Sediment Trap Sampling Interval	Sediment Trap Trap Depth (m)
TP2	56.07°N 161.30°W	32	19 Aug-25 Sep	20	--	--
TP6	56.78°N 160.30°W	59	20 Aug-17 Sep	55	--	--
TP4	56.41°N 161.68°W	68.5	19 Aug-20 Sep	63	--	--
TP7	56.03°N 161.22°W	24.5	30 Jan-5 May	15	3 Feb-15 May	13.5
TP8	55.86°N 162.04°W	31	2 Feb-19 Feb	21	5 Feb-17 May	17
TP2B	56.08°N 161.30°W	35	No record	25	3 Feb-15 May	21
TP9	56.50°N 161.71°W	89	31 Jan-27 Mar	79	4 Feb-16 May	77

$$\text{Flux} = [(\bar{u}\,\bar{c} + \frac{1}{n}\,\Sigma u'c')^2 + (\bar{v}\,\bar{c} + \frac{1}{n}\,\Sigma v'c')^2]^{\frac{1}{2}},$$

where $\bar{u}$, u' and $\bar{v}$, v' = the mean and fluctuating components of the flow along the east-west and north-south axes, respectively, and $\bar{c}$ and c' = the mean and fluctuating components of the SPM concentration. Transport direction relative to the component axes is given by

$$\theta = \tan^{-1}\left(\frac{\bar{u}\,\bar{c} + 1/n\ \Sigma u'c'}{\bar{v}\,\bar{c} + 1/n\ \Sigma v'c'}\right).$$

Vertical mass flux was measured by newly designed Sequentially Sampling Sediment Traps (S^3T) which collect up to 10 separate flux samples per deployment (Baker and Milburn, in press). The traps are cylindrical with a diameter of 25 cm and a height/width ratio of 3.25. These dimensions follow those recommended by several field and laboratory tests (Gardner, 1980a,b). A steep asymmetric funnel at the bottom of the trap focuses the settling particles into one of 10 acrylic sample collectors which rotate into position beneath the funnel at preset intervals. In this study, a new sample was collected every 11.25 days. Interpretation of the sediment trap data should be made with caution, however. Instantaneous current speeds at the trap locations often exceed 50 cm see-l, and in high flow conditions sediment traps may be biased samplers in a way that is not yet fully understood (Hannan and Grant, 1982).

B. Sample Analyses

1. Gravimetry

Total suspended ❑ atter concentrations were determined gravimetrically. Volumetric samples were collected on 0.4 µm pore size, 47 mm diameter

polycarbonate filters weighed on a Cahn **4700®** **electrobalance** before and after filtration. Suspended matter loadings were determined by difference after correction for weight changes due to the freshwater rinse. This correction averaged 0.030 mg, 0.021 mg and 0.099 mg for NASTE 1, 2, and 3 applied to an average sample mass of ~2 ❑ g (1.1 - 2.5%). The weighing precision ($2\sigma = \pm 0.011$ mg) and volume reading error (±10 ml) yield a combined coefficient of variation in SPM concentration of - 1% at mean sample loading and volume.

2. Particle size

Particle size distributions were determined using a **Coulter** Electronics **ZBI®** particle size analyzer and **C1000®** **channelizer.** Water samples were analyzed shortly after collection. No preservatives were added. Fifty µm and 200 µm aperture tubes were used for the analyses during NASTE 1 and NASTE 2. Particles with equivalent spherical diameters of 1-80 µm were counted with this combination of aperture tubes. In order to avoid problems in matching the overlap region of the 50 and 200 µm aperture tubes, size analyses during NASTE 3 were run on an intermediate (100 pm) aperture tube only, This tube covered the size range 2-40 pm, which included all particles of interest to this study.

Coulter Counter analyses of particle suspensions yield a very detailed data distribution. The size range covered by each aperture is broken down into 100 logarithmically spaced charnels of population information. In order to compare samples, it was necessary to fit the data to a specific distribution. **Bader** (1970) has shown that many natural collections of **small** particles, such as cosmic and terrestrial dust, oceanic suspended particles, and fine sediments, have a size distribution well fitted by a hyperbolic (or power) curve: $N = -K D^{-c}$, where N = the number of particles > a given size, D = particle diameter (or some other parameter), and K and c are constants. The derivative with respect to size of this cumulative distribution is an incremental distribution: $dN/dD = aD^{-b}$, where a = CK and b = c + 1. This distribution has been used by several authors to describe the observed particle populations in seawater (Carder and Schlemmer, 1973; Lal and Lerman, 1975; McCave, 1975; Brun-Cottan, 1976; Lerman et al., 1977, Baker et al., 1979): a represents the dN/dD value at D = 1 μm, and b represents the slope of the distribution (linear on full logarithmic paper). The slope is thus a measure of the number of large particles relative to the number of small particles; the larger the slope, the greater the relative proportion of small particles. Material having a slope b = 3 contains equal volumes of particles in logarithmically increasing size grades (McCave, 1975). Values of $b < 3$ indicate that the volume concentration is skewed towards the larger size grades and values of $b > 3$ indicates a skewness towards the finer size grades. Values of b for deep-sea sediments and suspended particulate matter commonly lie between 3.5 and 4.5 (Lal and Lerman, 1975; Brun-Cottan, 1976; Baker et al., 1979). Inshore and surface waters commonly have values of $b < 3$ due to the influence of large amounts of coarse grained organic (i.e., phytoplankton) and inorganic particles (Carder and Schlemmer, 1973; Kitchen et al., 1978). In the present study, variations in slope and intercept of the power distribution served to distinguish different particle populations.

Sampling variations in the Coulter Counter technique were periodically assessed by comparing measured particle volumes from replicate samples. In the example illustrated in Table 3, two Niskin bottles were tripped at the same depth, two subsamples were drawn from each bottle, and three replicate

TABLE 3

Coulter counter sampling variations

NASTE 1 Sta. SG 2 Depth 72 m

Niskin Bottle	Subsample	Replicate Analysis	Total Particle Volume ($\mu m^3 ml^{-1}$) 1.18-6.32 μm[1]	6.36-41.1 μm[1]
1	1	1	28.5×10^4	36.2×10^4
		2	29.6×10^4	63.4×10^4
		3	30.4×10^4	94.9×10^4
1	2	1	28.5×10^4	68.2×10^4
		2	29.2×10^4	80.4×10^4
		3	29.3×10^4	68.6×10^4
2	1	1	27.5×10^4	74.4×10^4
		2	26.4×10^4	45.4×10^4
		3	$27,4 \times 10^4$	69.4×10^4
2	2	I	27.3×10^4	33.3×10^4
		2	26.4×10^4	46.5×10^4
		3	27.7×10^4	55.4×10^4

[1] Diameter (D) range of the volume calculation, assuming all particles are spheres

analyses were performed on each subsample. Comparison of the means of the particle volume for each subsample (Natrella, 1963), at the 0.01 level of significance, indicates that there is no basis for concluding that the average volume for either diameter range (i.e., the 50µm and 200µm apertures) differs between subsamples or sampling bottles.

Examination of the volume measured in the 6.36 - 41.1 µm range reveals much larger variations than in the finer size range. This condition arises from the fact that at the coarse end of the particle range (D>~20µm) particle counting statistics are poor because of a small concentration of particles (<~5 per ml for each one µm interval; Fig. 7). And since volume is proportional to the cube of the radius, a small change in the number of large particles results in a large change in total volume.

3. Organic matter concentrations

The efficiency of hydrogen peroxide in oxidizing particulate organic matter from seawater samples has been demonstrated by Crecelius et al. (1974) and Landing (1978). The filters were placed in 20 ❑ l of 10% H_2O_2 for 30-45 ❑ inutes at room temperature, sonicated for one minute to remove the particles, then taken from the H_2O_2 and rinsed. The particles remained in the hydrogen peroxide for 24 hours in a 60°C oven. Each H_2O_2-particle suspension was then poured back through the original sample filter, dried in a dessicator, and weighed. The concentration of organic matter was determined by the weight difference after treatment with hydrogen peroxide.

4. X-ray diffraction mineralogy

Selected samples for clay mineral determination were collected on cellulose membrane filters (Baker, 1973). Organic matter was removed from

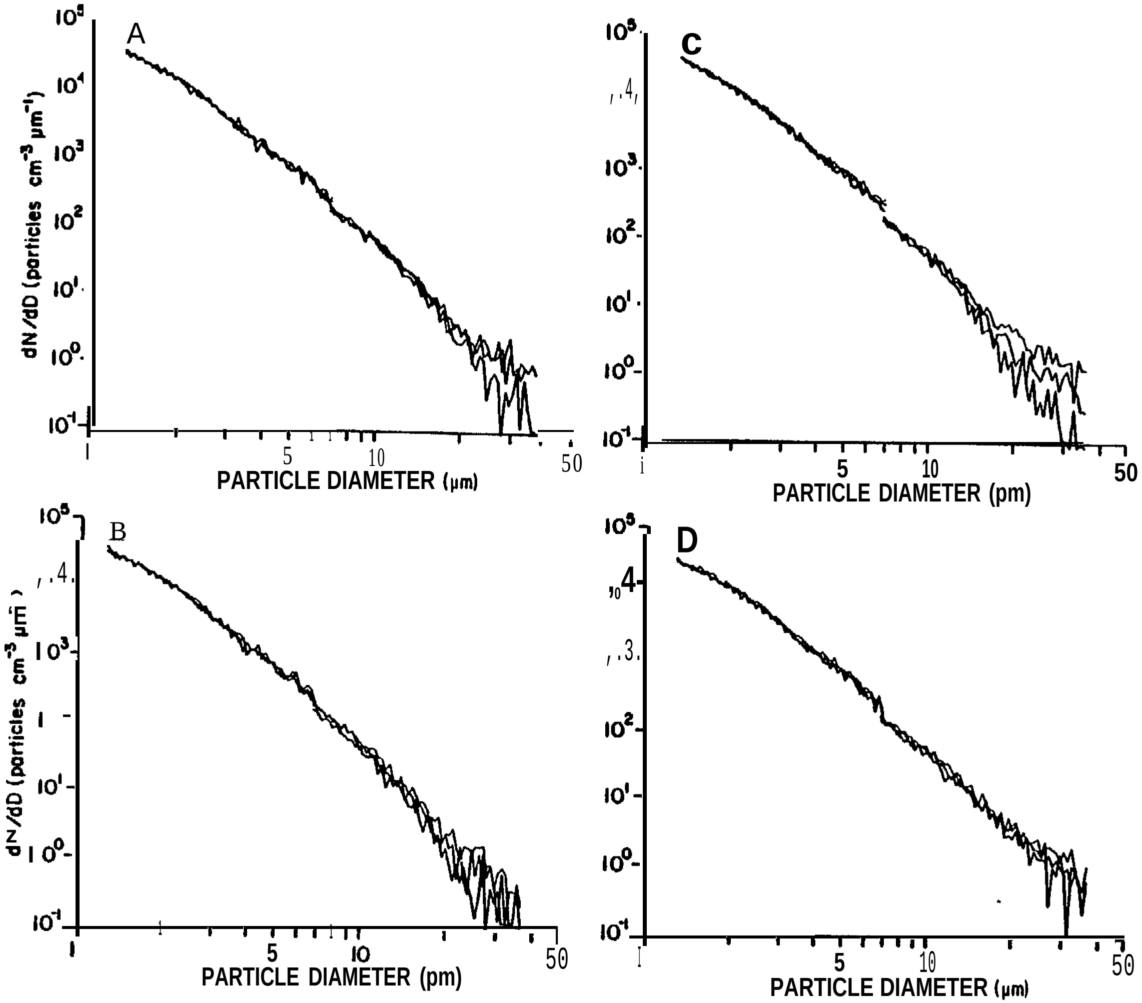

Figure 7. **Incremental** particle distribution, **dN/dD,** for replicate **Coulter** Counter samples.

the samples by hydrogen peroxide treatment in order to improve the quality of the diffractograms. Afterwards, the filters were dissolved in acetone until all traces of the filter material had disappeared. The resulting suspension was then refiltered through a Selas Flotronics® pure silver membrane filter (47mm diameter, mean pore size 0.45µm) in order to prepare an oriented mount for x-ray analysis. All samples were analyzed on a Phillips diffractometer with CuK_α radiation and graphite focusing monochromator, scan speed $1°2\theta$/min.

5. Phytoplankton pigments

The concentration of phytoplankton pigments was measured in selected samples. Subsamples (100 ml) were drawn from the sample bottles and filtered onto a glass fiber filter. The filter was then immersed in 90% acetone and sonicated for five minutes. Solids were separated by centrifugation. Chlorophyll a and pheophorbide a were measured by the fluorometric method of Helm-Hansen et al. (1965) using a Turner model 111 fluorometer.

V. RESULTS

A. North Aleutian Shelf Region

1. Areal suspended matter and salinity distributions

Comparison of surface attenuation and salinity (Fig. 8) during NASTE 1 shows considerable agreement in terms of source areas and gradients. In

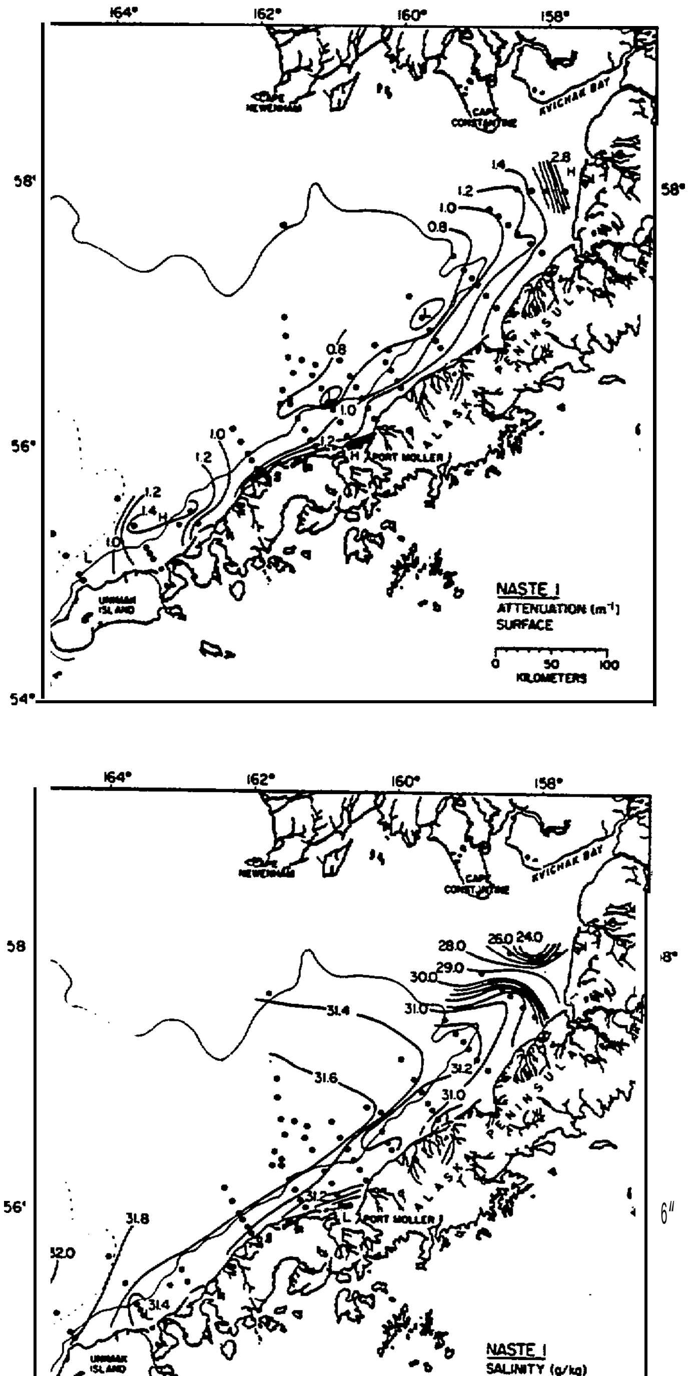

Figure 8. **Areal** maps of **light** attenuation (top) and salinity (bottom) at the surface during August 1980. Contour interval is **$0.2\ m^{-1}$** for attenuation and 0.2 ‰ for salinity.

general, attenuation and salinity contours ran predominantly alongshore, closely following the trend of the bathymetry. Prominent freshwater sources such as the Izembek Lagoon area (just east of Unimak Island), the Port Moller area, and Kvichak Bay, also showed high attenuation values. Isolated high values of attenuation at nearshore stations (e.g. station NA52, Fig. 1), were caused by tidal resuspension in shallow water.

Attenuation and salinity (Fig. 9) 5m above bottom (mab) showed patterns similar to the surface values, especially for salinity. A source of deep, high salinity water intruded from the northwest. Organization of the salinity contours along isobaths was more pronounced than in the surface waters. The influence of coastal freshwater sources was diminished, except for large sources such as Port Moller and Kvichak Bay. Because near-bottom attenuation is strongly influenced by local changes caused by bottom resuspension (e.g., station NA52), the contour pattern was more complicated than that of salinity. The trend of the contours was still alongshore, however. Superimposed upon this trend was a tendency for low attenuation values to occur near the center of each transect, roughly at the 50-m isobath. This pattern was particularly evident in the transects east of Port Moller. West of Port Moller the pattern was intermittent and not well described by the contour interval of Fig. 9. Note that the 50-m isobath is the approximate dividing line between the middle and coastal domains (Kinder and Schumacher, 1981a).

Oceanographic conditions during the winter (NASTE 2) resulted in a very close association between attenuation and salinity in both surface and bottom waters. Attenuation and salinity (Fig. 10) contours in the surface waters followed the isobath trends closely. Asymmetric trends of attenuation and salinity contours inshore of ~50 m suggest net transport to the northeast.

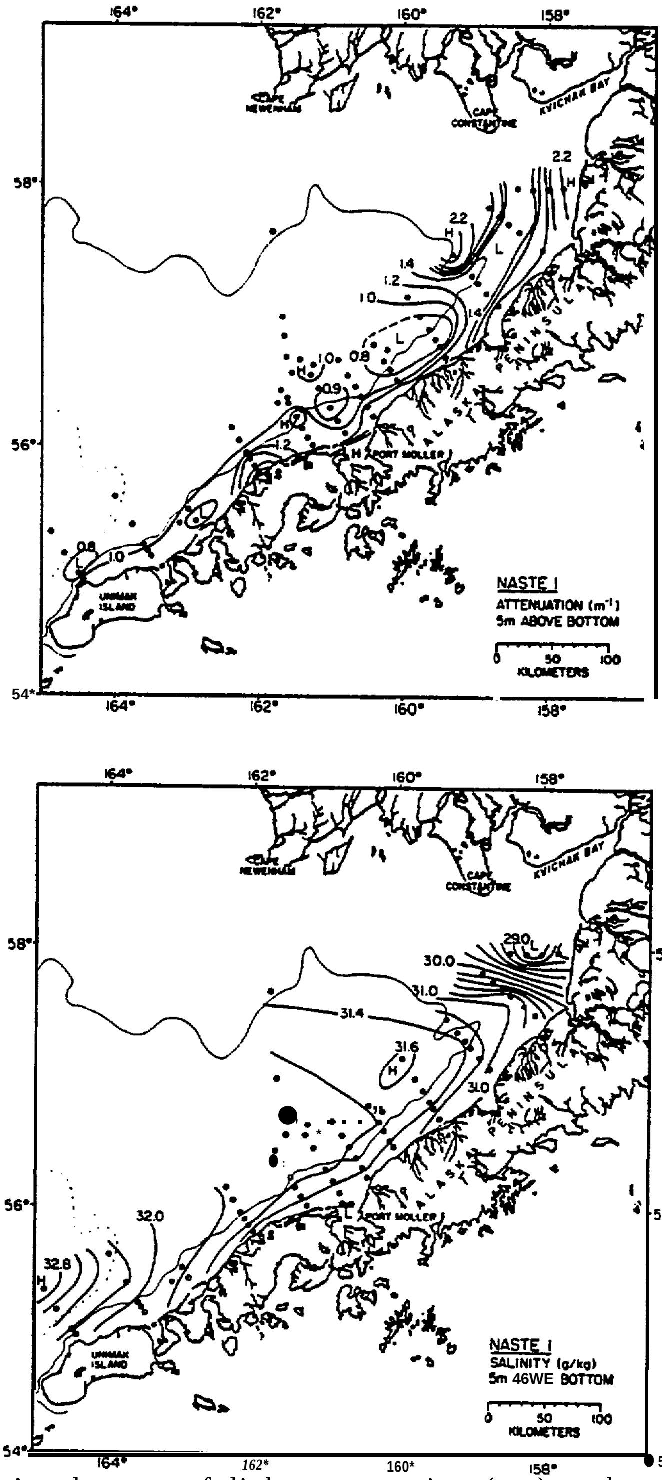

Figure 9. Areal maps of light attenuation (top) and salinity (bottom) at the bottom during August 1980. Contour interval is 0.2 m^{-1} for attenuation and 0.2 ‰ for salinity.

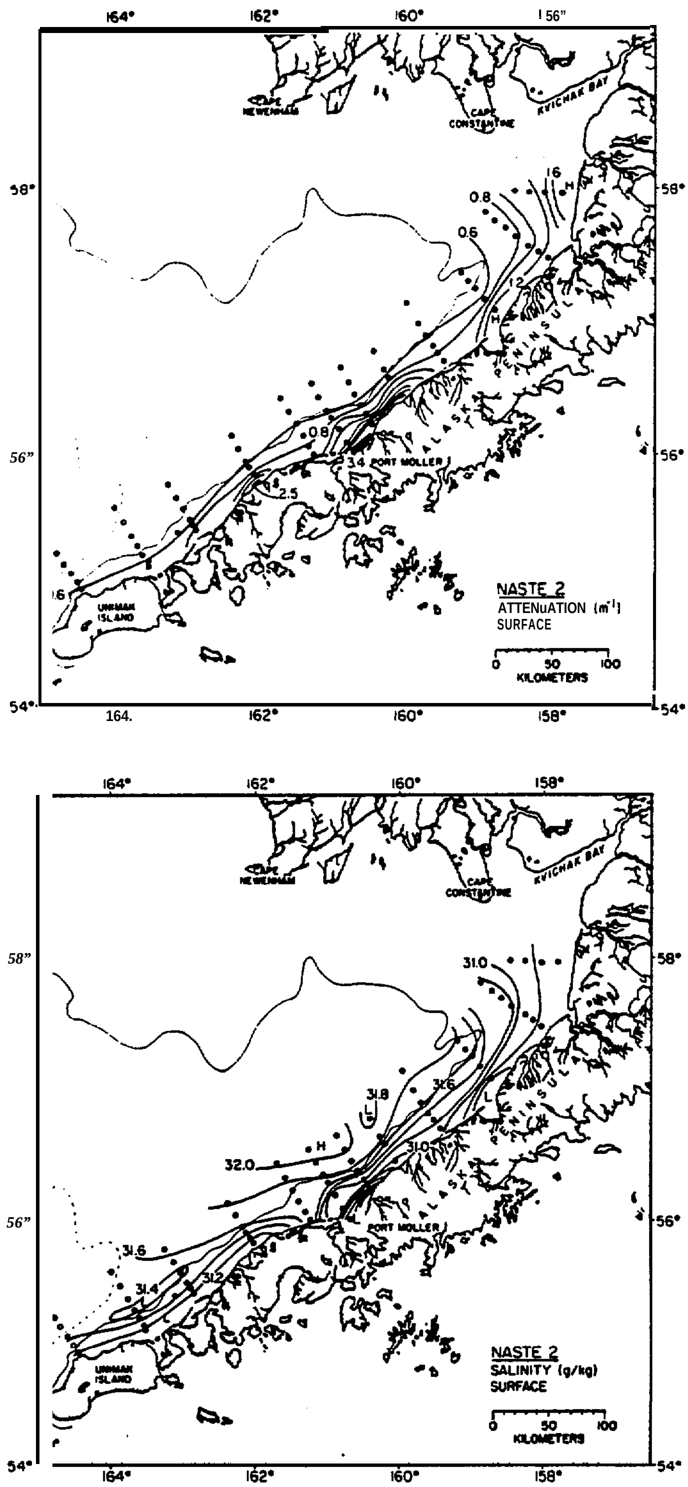

Figure 10. Areal maps of light attenuation (top) and salinity (bottom) at the surface during January 1981. Contour interval is 0.2 m^{-1} for attenuation and 0.2 ‰ for salinity.

A strong particle and freshwater source at Port Moller, for example, appeared to be elongated eastward along the coast. Another fresh water source was the Izembeck Lagoon area, but this area was not a significant particle source. These pockets of high turbidity and/or low salinity were separated by small areas of low attenuation and high salinity (e.g., stations NA46 and NA22). Seaward of ~50 m both alongshore and offshore gradients of salinity and attenuation became very low. Particle concentrations in this zone were nearly identical throughout the study area.

Descriptions of attenuation and salinity (Fig. 11) distributions in the bottom water during NASTE 2 are essentially the same as those presented for the surface water: Stations NA46 and NA22 separated regions of higher attenuation and freshwater content. Alongshore and offshore gradients were very low seaward of the 50-m isobath. Unlike NASTE 1, the near-bottom attenuation distribution showed little indication of isolated highs or lows attributable to resuspension activities. The weak vertical stratification throughout the region in winter (see section V. A2. below) evidently encouraged vertical mixing and thus prevented the creation of a bottom nepheloid layer other than that associated with isolated coastal sites where freshwater input was significant.

The NASTE 3 cruise encountered a return to conditions similar to those observed during NASTE 1. Surface salinity (Fig. 12) contours were parallel to the isobaths as usual and freshwater sources were evident in Port Moller and Port Heiden (no data was collected from the two easternmost transects). Prominent particle sources (Fig. 12) were Izembek Lagoon, Port Moller, and, Port Heiden. In addition, isolated highs throughout the region, always associated with a high chlorophyll a concentration, were indicative of phytoplankton patchiness.

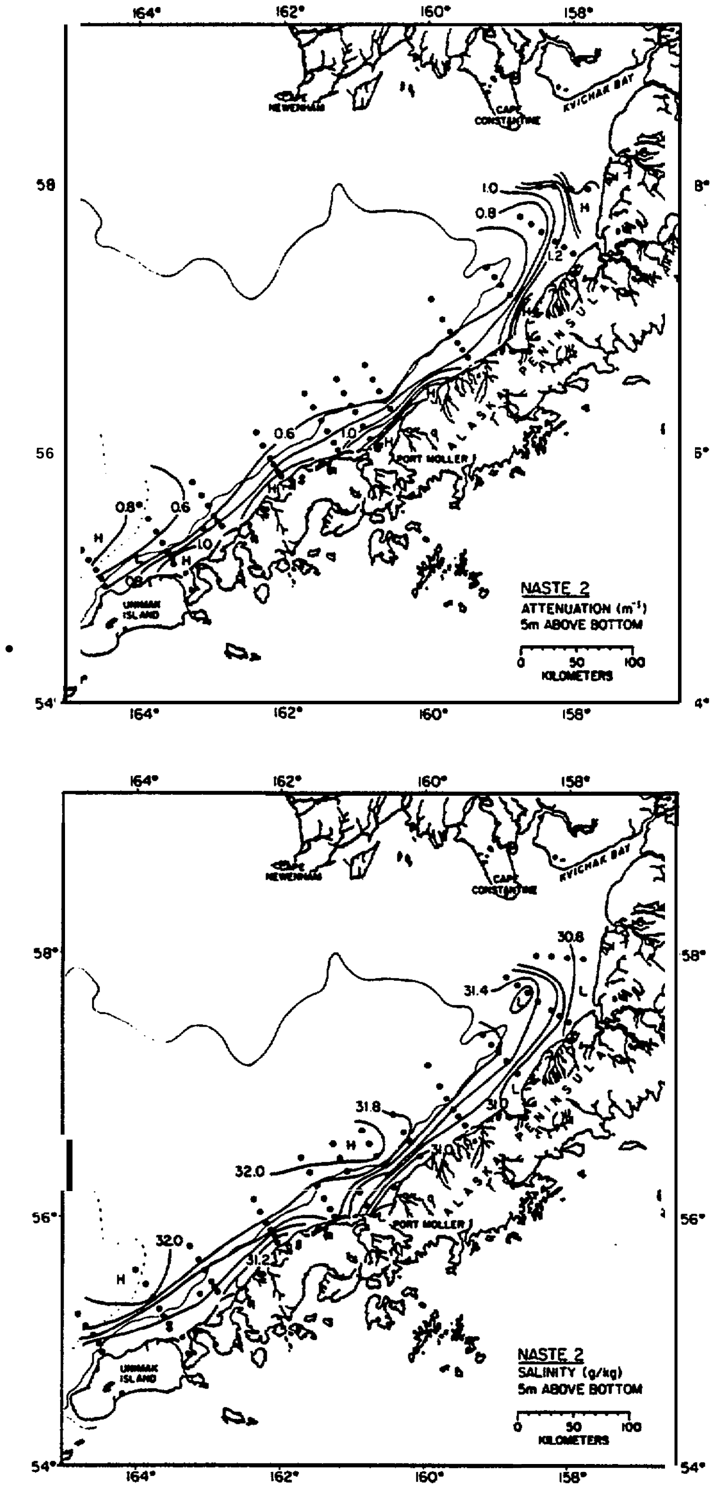

Figure 11. **Areal** ❑ aps of light attenuation (top) and salinity (bottom) at the bottom during January 1981. Contour interval is **$0.2\ m^{-1}$** for attenuation and 0.2 ‰ for salinity.

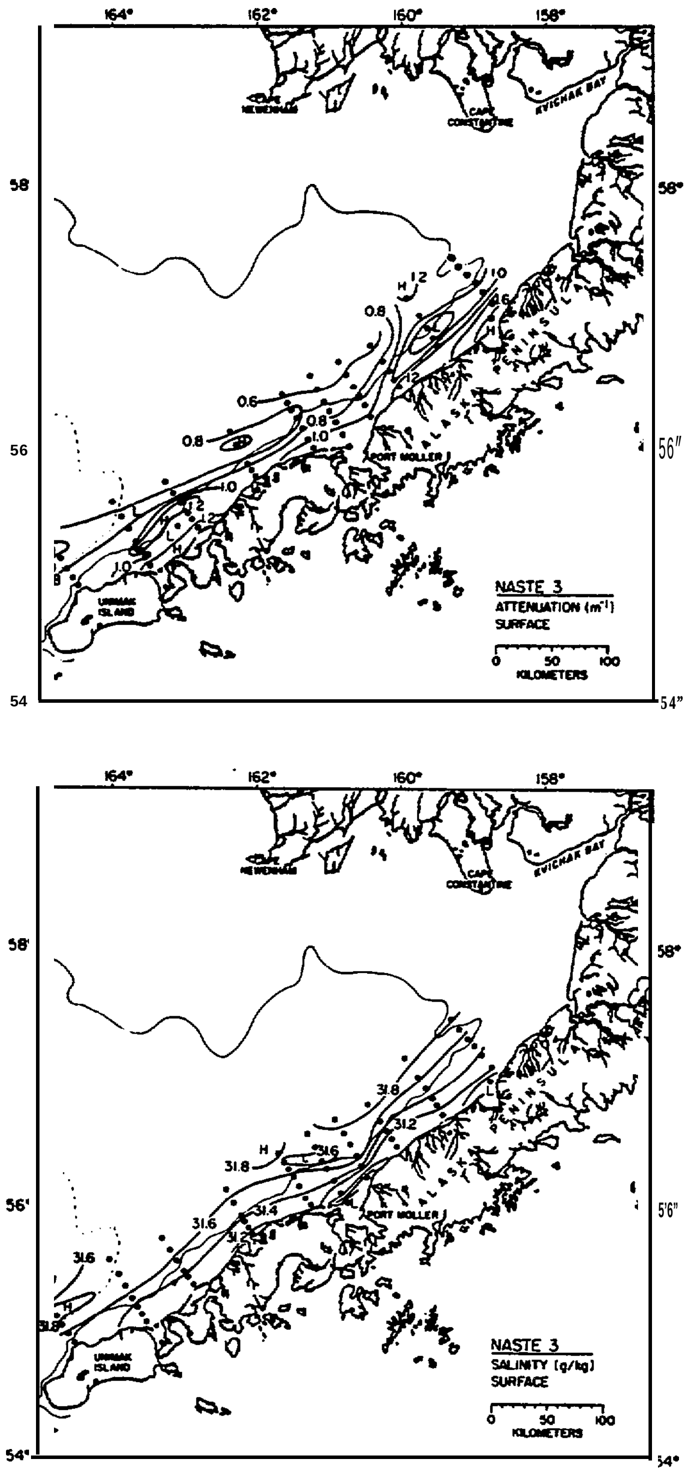

Figure 12. Areal maps of light attenuation [top)-and salinity (bottom), at the surface during May 1981. Contour interval is 0.2 m for attenuation and 0.2 $^{\circ}/_{\circ\circ}$ for salinity.

The salinity distribution in the deep water (Fig. 13) again showed an intrusion of high salinity water from the west and a strict correlation between bathymetric and salinity isolines. Offshore gradients became very low seaward of -50 m. Attenuation contours (Fig. 13) clearly described an SPM minimum zone along the 50-m isobath on every transect but the shallowest (the easternmost transect). This pattern was ❑ uch ❑ ore pronounced than during NASTE 1 and generally was not interrupted by isolated highs caused by resuspension.

The relationship between salinity and SPM concentrations in the surface waters of the North Aleutian Shelf region can be described by the use of a salinity vs. attenuation scatter plot analogous to the mixing diagrams used to trace the loss or addition of dissolved (Liss, 1976) or particulate (Baker, 1982) constituents in estuarine regions. During NASTE 1 and 3, correlations between attenuation and salinity were similar: $r \cong -0.56$ with a slope of -0.16 during NASTE 1 and -0.47 during NASTE 3 (Fig. 14). Salinity was a poor predictor of SPM concentration during these times, because particle sources other than freshwater runoff were important. These sources included resuspension and subsequent vertical mixing of particles into the surface waters (in the nearshore zone) and *in-situ* phytoplankton production.

The shape of the salinity-attenuation scatter plot was noticeably different during NASTE 2 (Fig. 14). Attenuation values fell rapidly with increasing salinity up to -31.5°/00; above that value very little change was observed in attenuation. The areal plots (Fig. 10) indicate that this point marks the transition between steep offshore gradients of attenuation landward of -50 m and essentially uniform attenuation values to seaward.

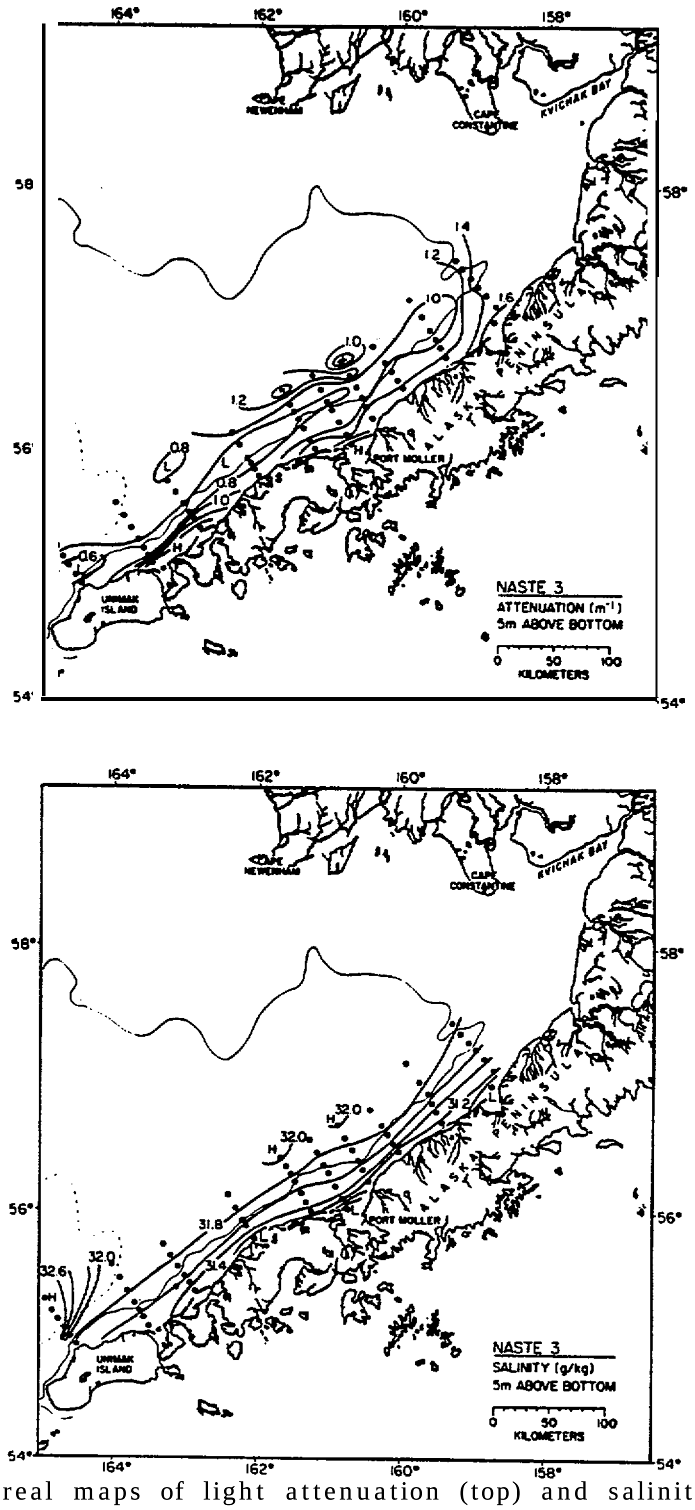

Figure 13. Areal maps of light attenuation (top) and salinity (bottom) at the bottom during May 1981. Contour interval is 0.2 m^{-1} for attenuation and 0.2 ‰ for salinity.

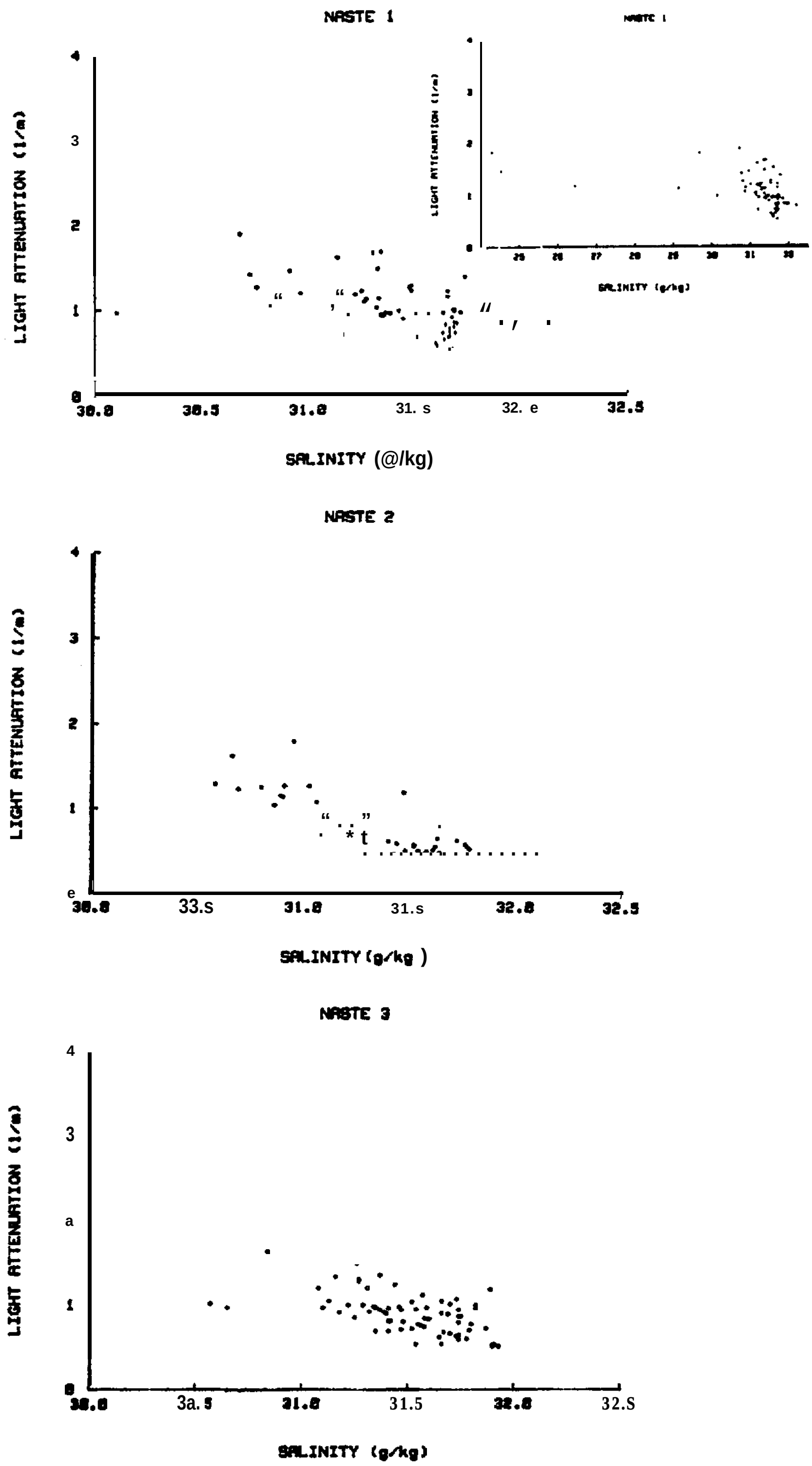

Figure 14. Light attenuation vs. salinity in the surface water at NA stations for (top) August 1980, (middle) January 1981, and (bottom) May 1981. Inset for NASTE 1 data shows the complete data set.

Seasonal changes in the average water column attenuation and salinity (based on l-m averaged data from CTD casts at each NA station) in the NAS region were small. Attenuation decreased from 1.17 ± 0.86 m^{-1} during NASTE 1 to 0.97 ± 0.90 m^{-1} and 0.92 ± 0.25 during succeeding cruises. These means are identical at a significance level of 0.05 (Natrella, 1963). Salinity changes are also small and statistically non-significant, but it is instructive to. note that the steady increase in salinity from NASTE 1 to 3 mirrored the decrease in attenuation, just as salinity was inversely proportional to attenuation during each cruise.

2. Density and SPM cross-sections

Vertical cross-sections for lines 1 (NA17-NA22), 2 (NA34-NA40), and 3 (NA47-NA52) normal to the Alaskan Peninsula (Fig. 1) were constructed from CTD casts on each cruise. These lines were chosen to reflect SPM conditions in different sections of the NAS study area.

Density cross-sections during NASTE 1 (Figs. 15, 16, and 17) typically showed isopycnals sloping landward, indicative of a weakly stratified two-layer system. Horizontal σ_t contours were found only at the westernmost line, where a reverse slope to the isopycnals clearly indicated an intrusion of relatively dense, deep water as close to shore as the 30-m isobath. Inshore stations on lines 2 and 3 showed nearly complete vertical ❑ ixing, whereas the density profile at Station NA22 on line 1 showed a prominent gradient due to freshwater influence from rivers in the Kvichak Bay area.

SPM distributions (Figs. 15, 16, and 17) closely followed the observed density pattern. Sites of strong horizontal density gradients on lines 1 (Station NA20), 2 (Station NA37), and 3 (Station NA51), were also sites of strong horizontal SPM gradients. Landward of these points, SPM contours

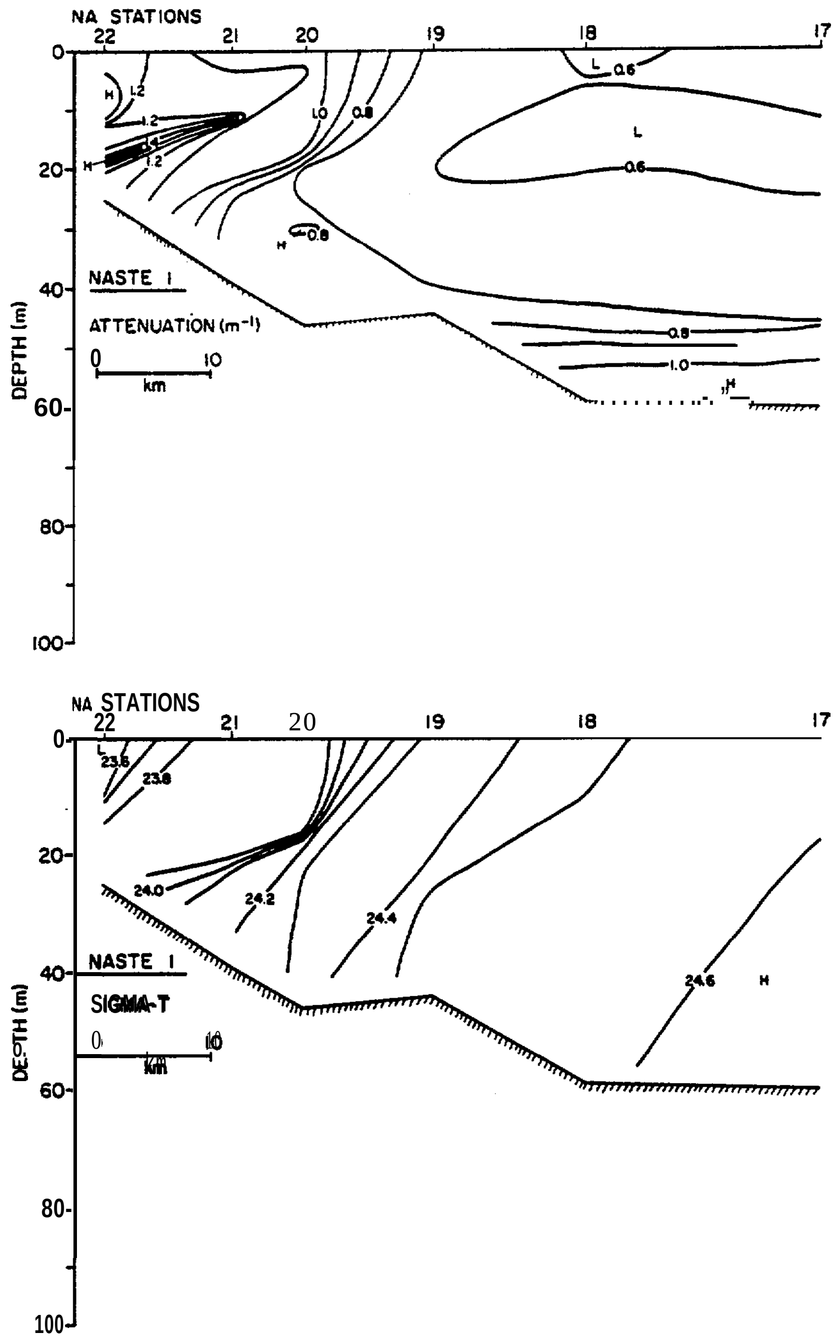

Figure 15. Attenuation (top) and density (bottom) cross-sections for line 1 (stations **NA17-22)**, August 1980.

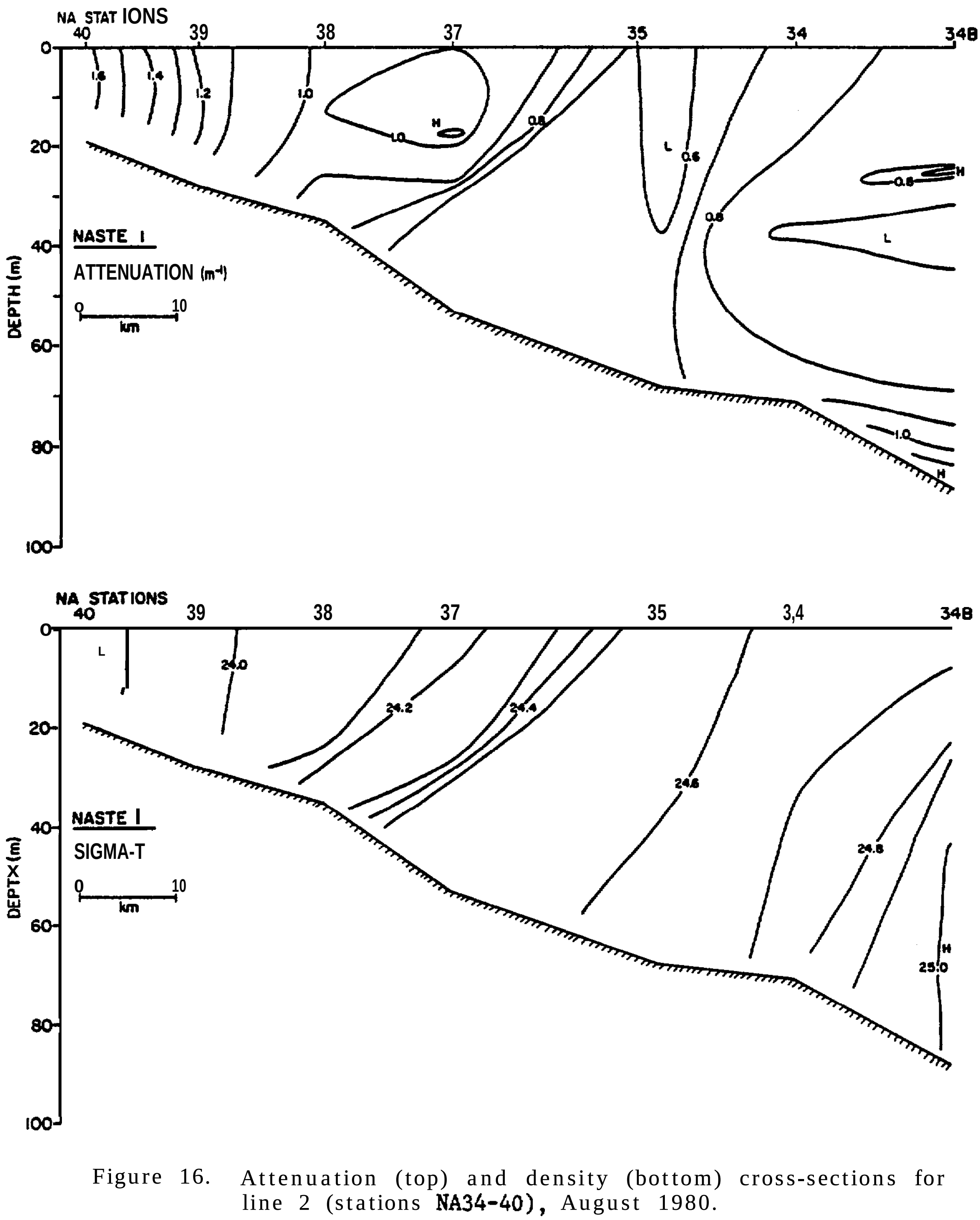

Figure 16. Attenuation (top) and density (bottom) cross-sections for line 2 (stations NA34-40), August 1980.

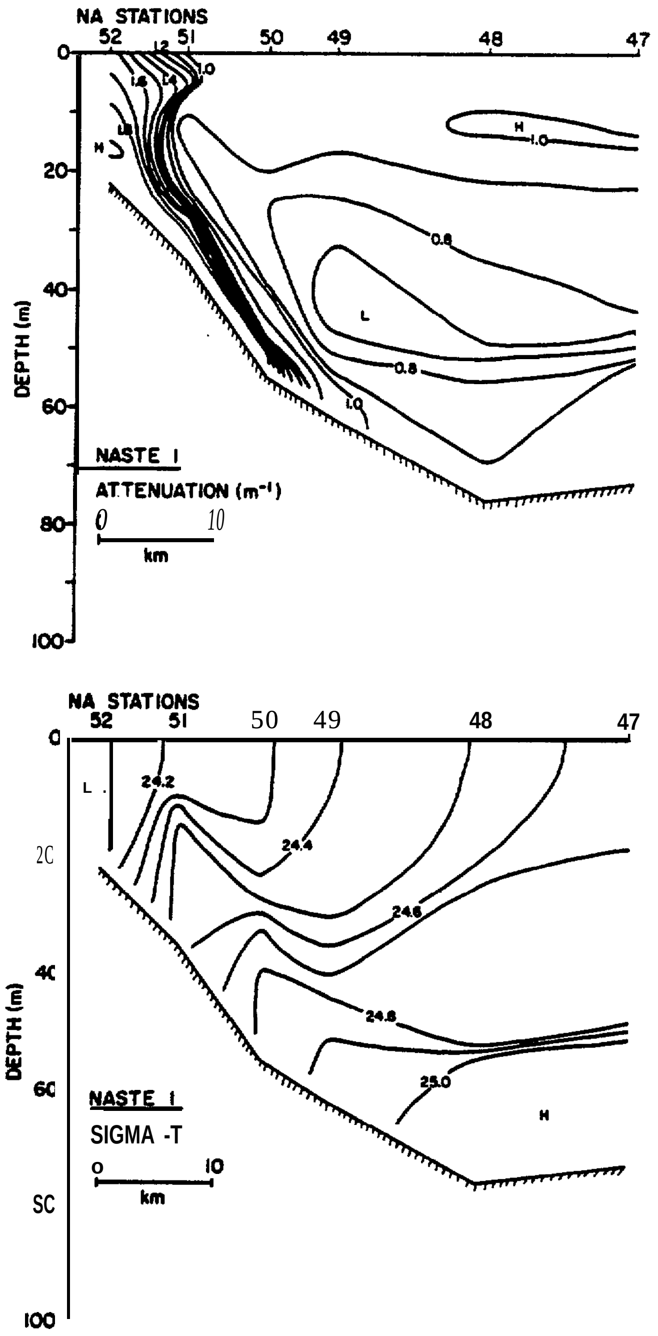

Figure 17. Attenuation (top) and density (bottom) cross-sections for line 3 (stations NA47-52), August 1980.

followed the trend of the σ_t contours, becoming vertically mixed on lines 2 and 3 and vertically stratified on line 1. Seaward of Stations NA20, NA37, and NA51 (i.e., ~the 40-m isobath), the vertical SPM distributions became typical of nearly all offshore stations in the study area. A strong three-layer distribution was well developed; a horizontally uniform mid-depth minimum zone separated horizontally variable layers of higher turbidity in the surface and bottom waters. This distribution is characteristic of the middle domain (Kinder and Schumacher, 1981a) in the southeastern Bering Sea. Line 3 was particularly interesting because it showed an excellent example of relatively clear deep water intruding along the seafloor until blocked by the coastal front produced by strong tidal mixing of water and particulates in the near-shore zone. High attenuation values in the near-bottom waters at Stations NA49, NA50, and NA51 were presumably due to resuspended sediment trapped in a thin bottom nepheloid layer below the intruding deep water.

Conditions during the winter cruise, NASTE 2, were significantly different both for density and SPM distributions (Figs. 18, 19, and 20). Density stratification was weak or absent throughout the region; only line 2, off Port Moller, showed signs of freshwater input in the density structure. SPM distributions were also generally unstratified. Absence of the middle domain stratification characteristics to at least a depth of 80 m resulted in a vertically uniform SPM distribution on all lines.

Late spring (NASTE 3) was a return to a period of strong vertical stratification throughout the study area (Figs. 21, 22, and 23). A surface mixed layer ~10 m thick was present along each line, separated from the underlying waters by 0.2 - 0.4 σ_t units at the offshore stations. Tidal mixing produced vertically homogeneous water landward of about 30 m.

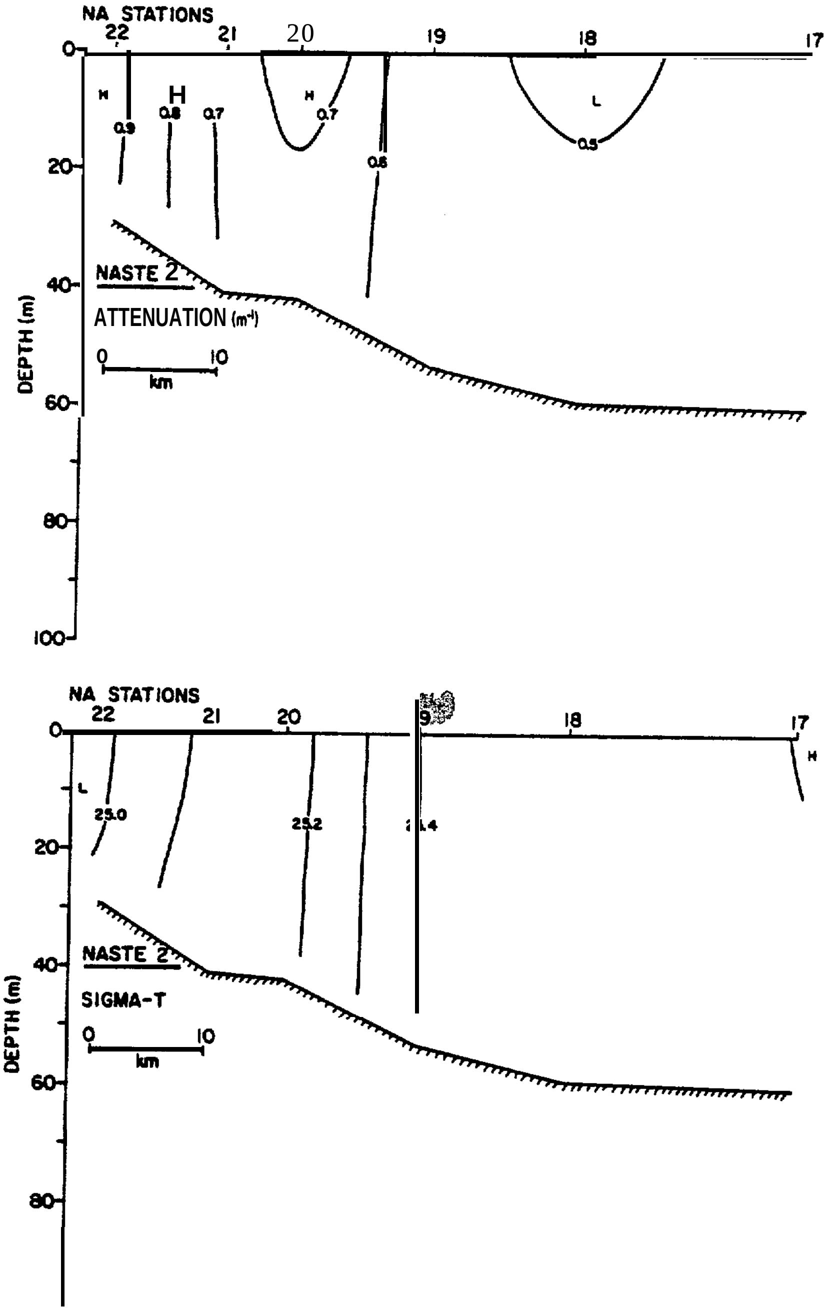

Figure 18. Attenuation (top) and density (bottom) cross-sections for line 1 (stations NA17-22), January 1981.

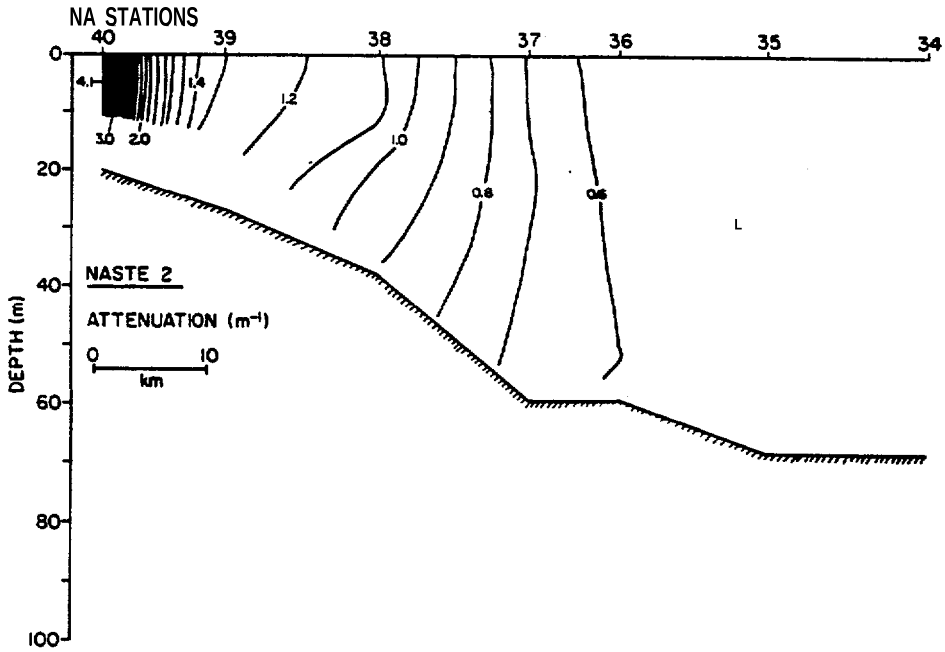

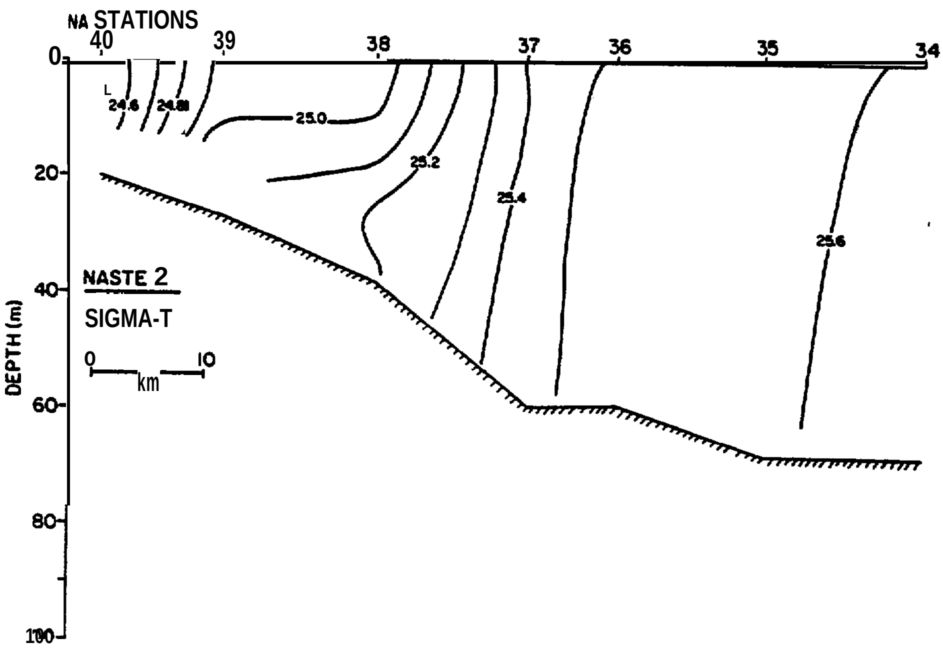

Figure 19. Attenuation (top) and density (bottom) cross-sections for line 2 (stations NA34-40), January 1981.

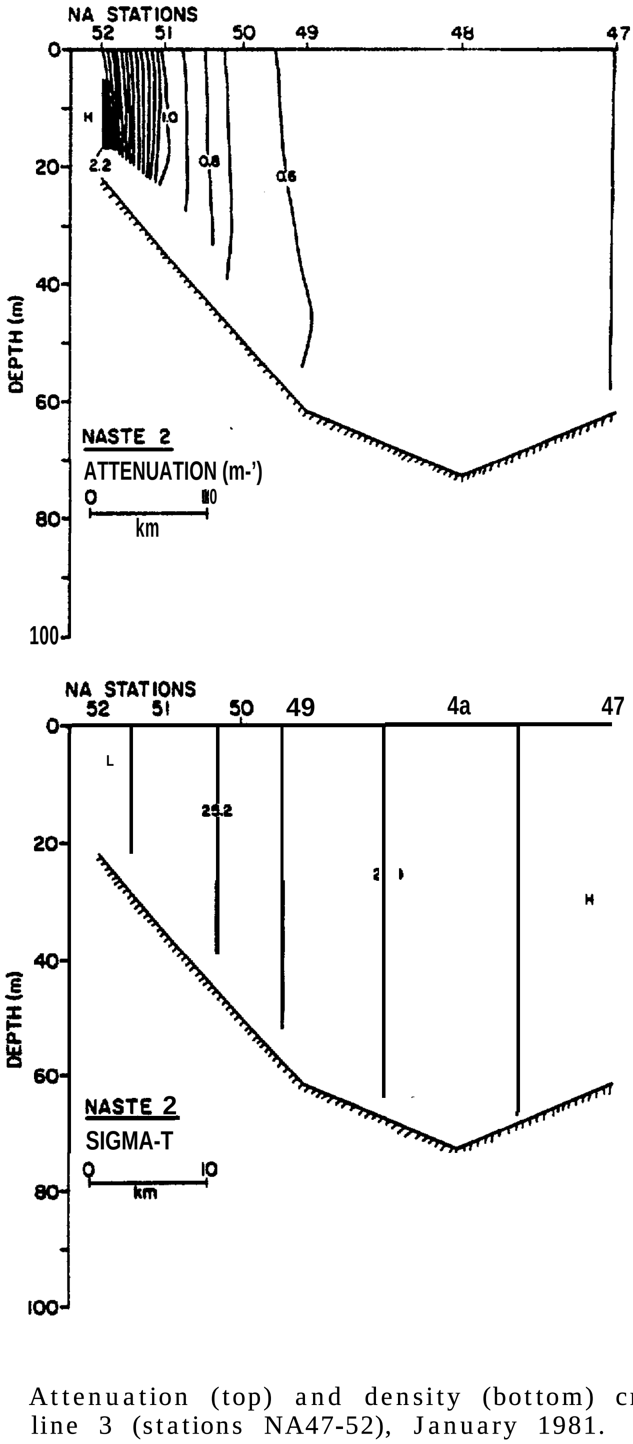

Figure 20. Attenuation (top) and density (bottom) cross-sections for line 3 (stations NA47-52), January 1981.

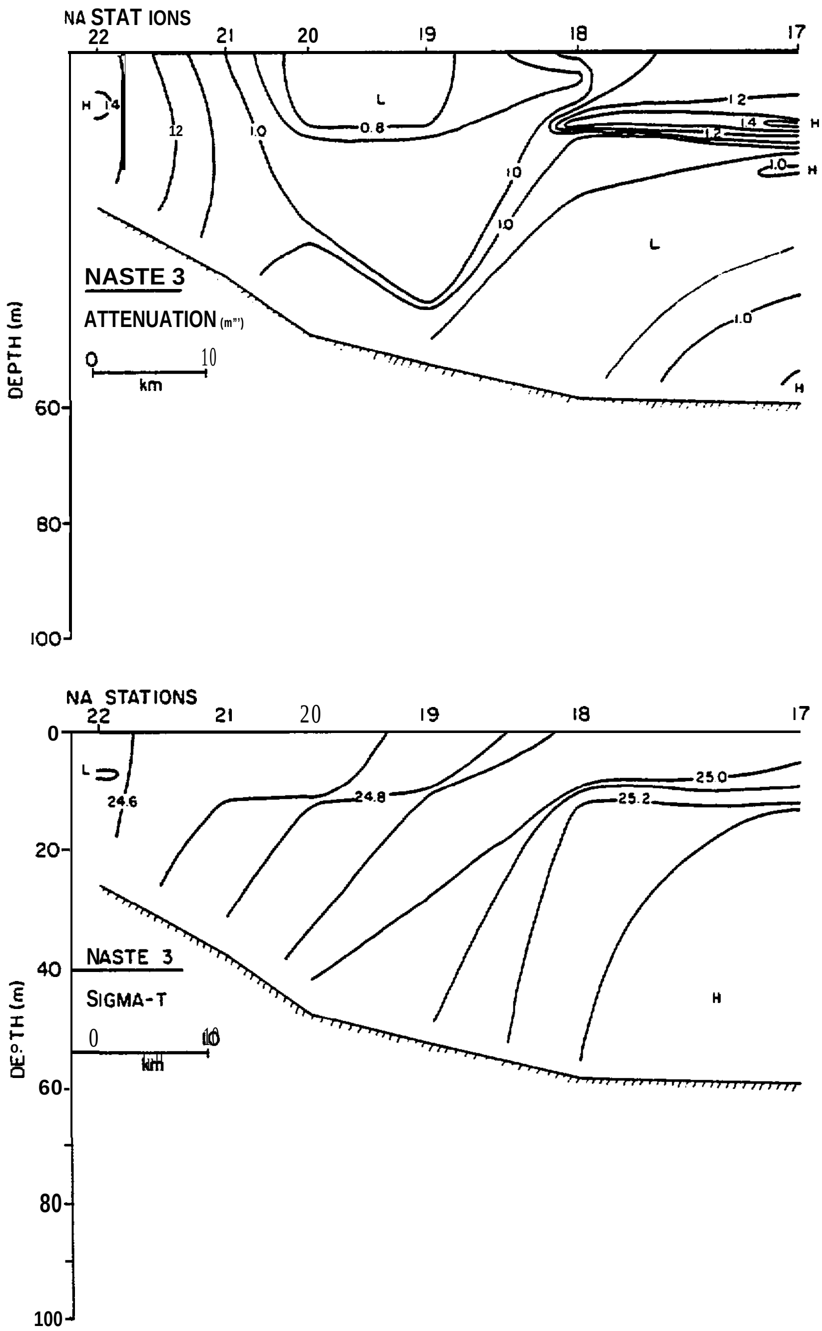

Figure 21. Attenuation (top) and density (bottom) cross-sections for line 1 (stations NA17-22), May 1981.

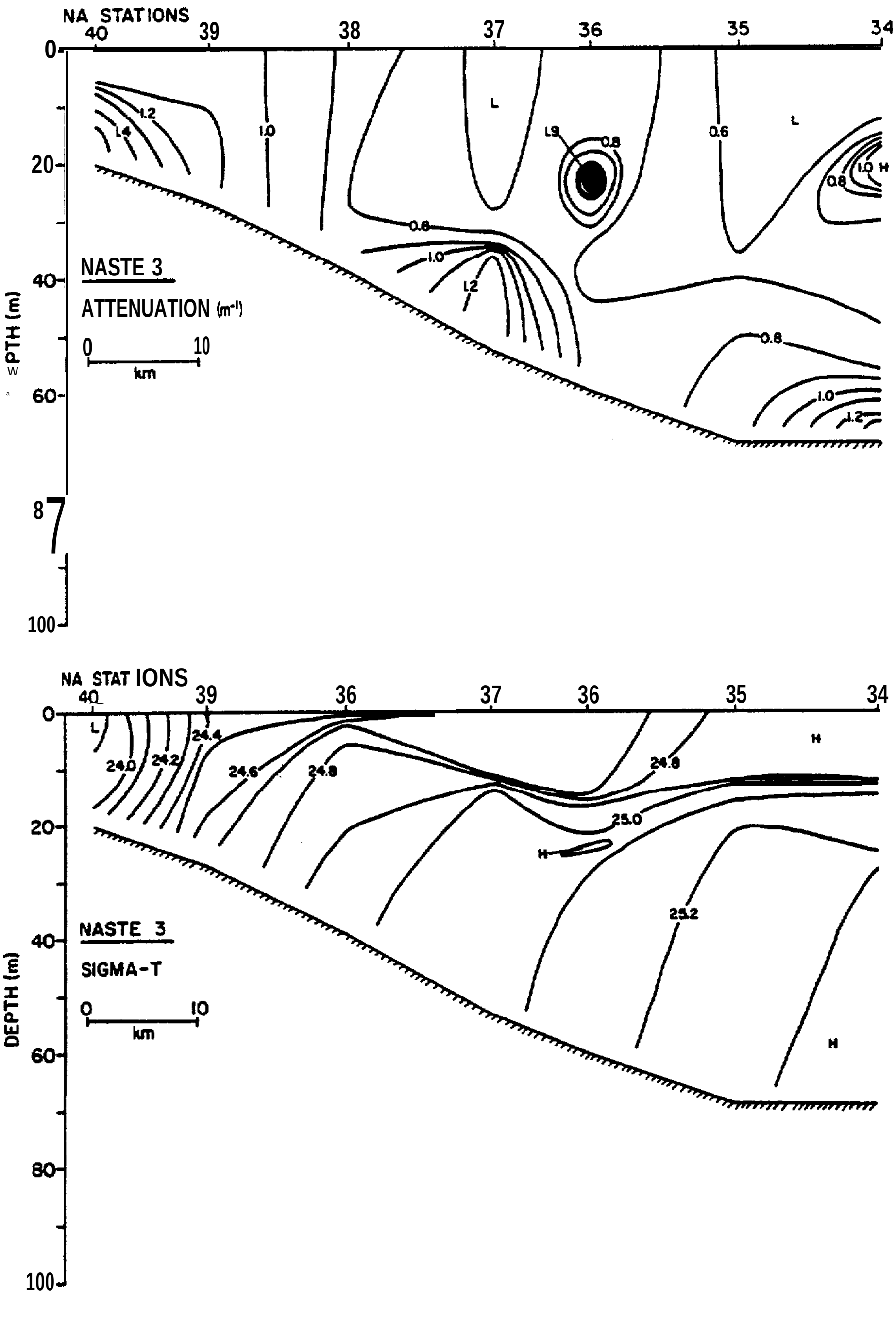

Figure 22. Attenuation (top) and density (bottom) cross-sections for line 2 (stations NA34-40), May 1981.

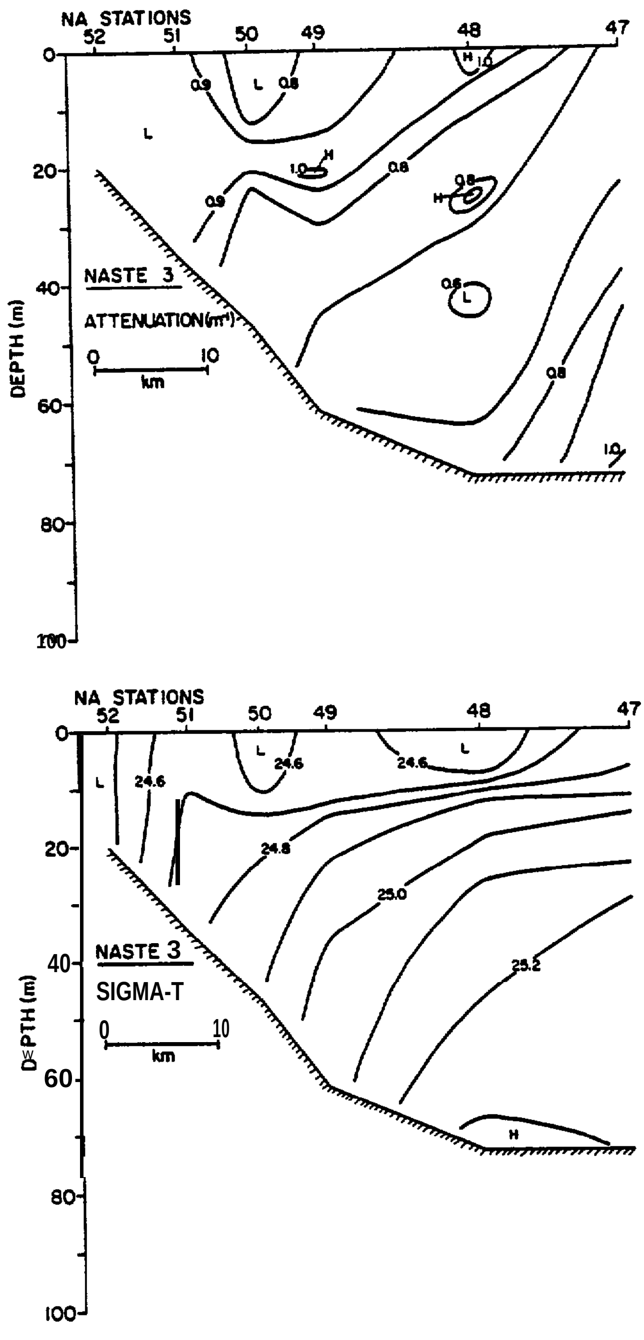

Figure 23. Attenuation (top) and density (bottom] cross-sections for line 3 (stations NA47-52), May 1981.

Beneath the surface mixed layer, σ_t contours dipped steeply landward.

SPM distributions were controlled by the strong pycnocline, weak stratification below the pycnocline, and inshore tidal mixing. Stations where the pycnocline was strongest (NA18, NA17, NA36, and NA34) had intense SPM maxima at the bottom or just below the surface mixed layer. Based on information from particle size distributions and phytoplankton pigment concentrations, these subsurface highs were produced by in-situ phytoplankton growth.

Weak stratification below the pycnocline allowed bottom resuspension to produce a thick nepheloid layer. The mid-depth ❑inimum typical of NASTE 1 was only found along line 3 where vertical stratification below the pycnocline was slightly greater than along lines 1 and 2.

Inshore vertical density stratification was almost nonexistent on lines 1 and 3, and attenuation values were likewise vertically uniform. Freshwater input from Port Moller produced weak stratification at stations NA40 and NA39 (line 2) and induced a similar stratification in attenuation, by preventing the upward mixing of resuspended sediments.

In a highly energetic region such as the North Aleutian Shelf, instantaneous occupations of a station line may be unrepresentative of the "average" conditions typical of an entire season. Transient weather conditions may completely interrupt the seasonal pattern of hydrographic structure and SPM distribution. For these reasons, certain transects were occupied several times during the NASTE 1, 2, and 3 cruises in order to gauge the magnitude of short-term variability in the particle distributions. During NASTE 1, line NA34-NA40 was traversed during the following (GMT) times (Fig. 24): 20 Aug. 1308-2139, 24Aug. 0706-1436, and 31 Aug. 1702 - 1 Sept. OO1O. An adjacent transect, line NA41-NA46, was occupied four separate times (Figs. 25

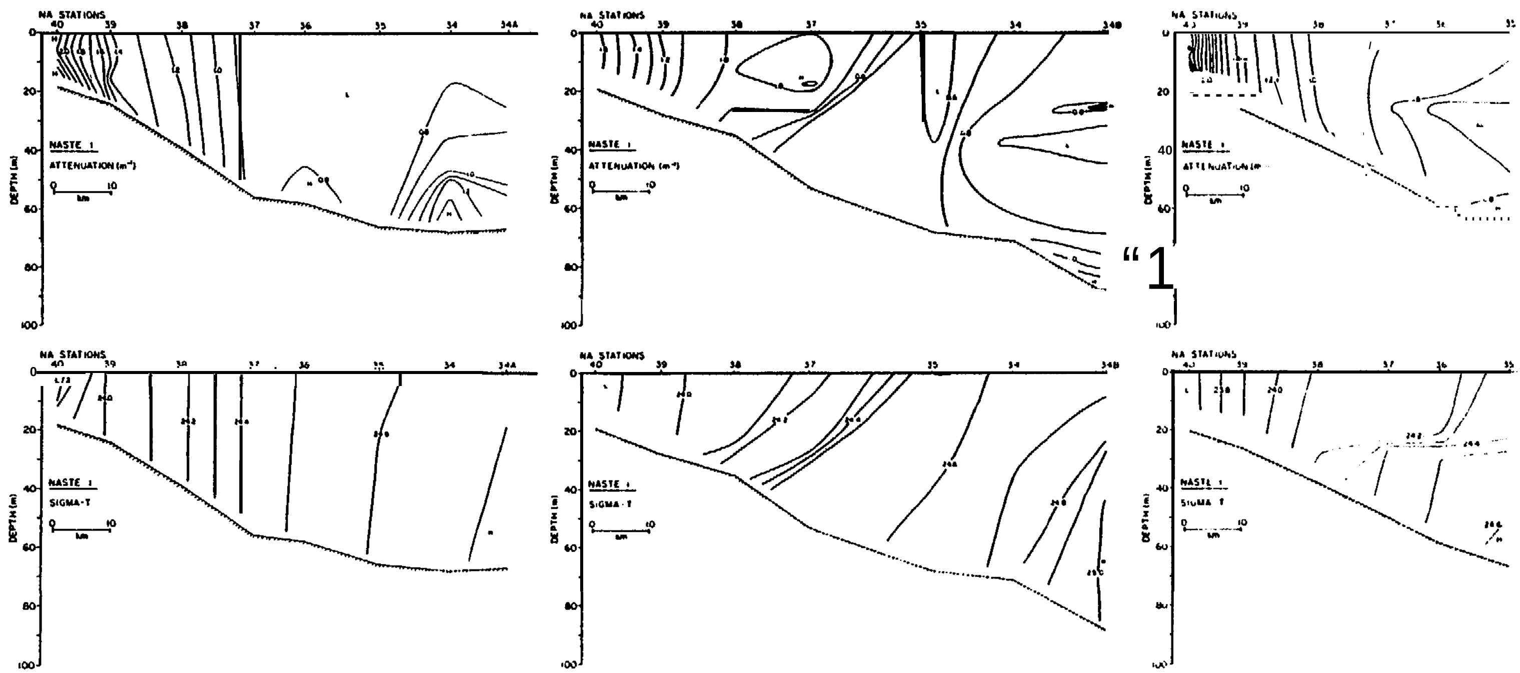

Figure 24. Attenuation (top) and density (bottom) cross-sections for stations NA34-40 on August 20 (left), August 24 (middle), and August 31, 1980 (right).

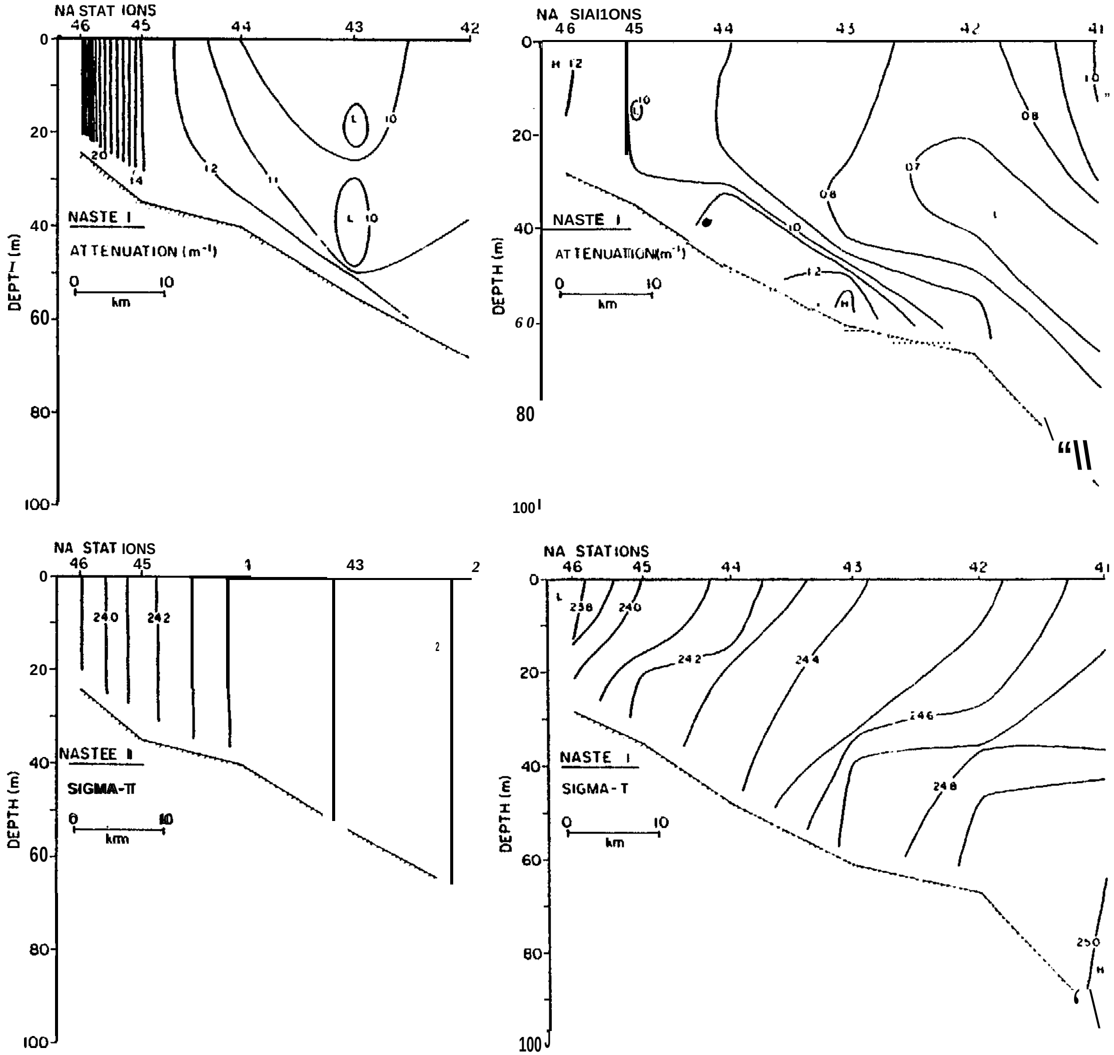

Figure 25. Attenuation (top) and density (bottom) cross-sections for stations **NA41-46** on August 19 (left), and August 24, 1980 (right).

and 26): 19 Aug. 0655-1344, 24 Aug. 1740-2354, 31 Aug. 0709-1225, and 2 Sept. 2009 - 3 Sept. 0035. During NASTE 2 line NA34-NA40 was occupied twice (Fig. 27): 31 Jan. 0330-1200 and 8 Feb. 1323-1945. During NASTE 3 line NA41-NA46 was occupied three times (Fig. 28): 15 May 0147-1135, 25 May 0420-1042, and 30 May 1237-1815.

The only significant short-term perturbations were noted during NASTE 1 as the result of a brief storm which destroyed the front separating the coastal and middle shelf hydrographic domains (Pearson et al., 1980). On 17-18 Aug. 1980 the remnant of typhoon MARGE passed through the study area with winds in excess of 30 m sec^{-1}. Transects run the following day (Figs. 24 and 25) showed that the density field was vertically homogeneous at least out to the 60-m isobath, with very weak stratification in deeper water. 5PM contours were also vertical out to -40 m; beyond that depth values increased from surface to bottom as a result of gravitational settling and resuspension. Transects occupied subsequently document the reestablishment of the frontal and domain characteristics typical of late summer. Prior to the 24 Aug. transects, a period of ❑ oderate (5-10 m sec^{-1}) northeasterly winds appeared to drive an offshore Ekman flux, resulting in vertical density and SPM stratification as far inshore as the 20-m isobath. At this time, however, stratification was best developed in waters deeper than ~60 m where a prominent SPM minimum had developed in association with the maximum density gradient. By the 31st of August, increasingly strong tides had firmly reestablished the well-mixed coastal domain and the inner front separating it from the two-layer middle domain (Figs. 24 and 26). 5PM distribution in the middle domain showed the typical mid-depth ❑ inimum zone separating the well-mixed surface layer from the resuspension-induced BNL. The thickness of the BNL was controlled by the thickness of the bottom-mixed

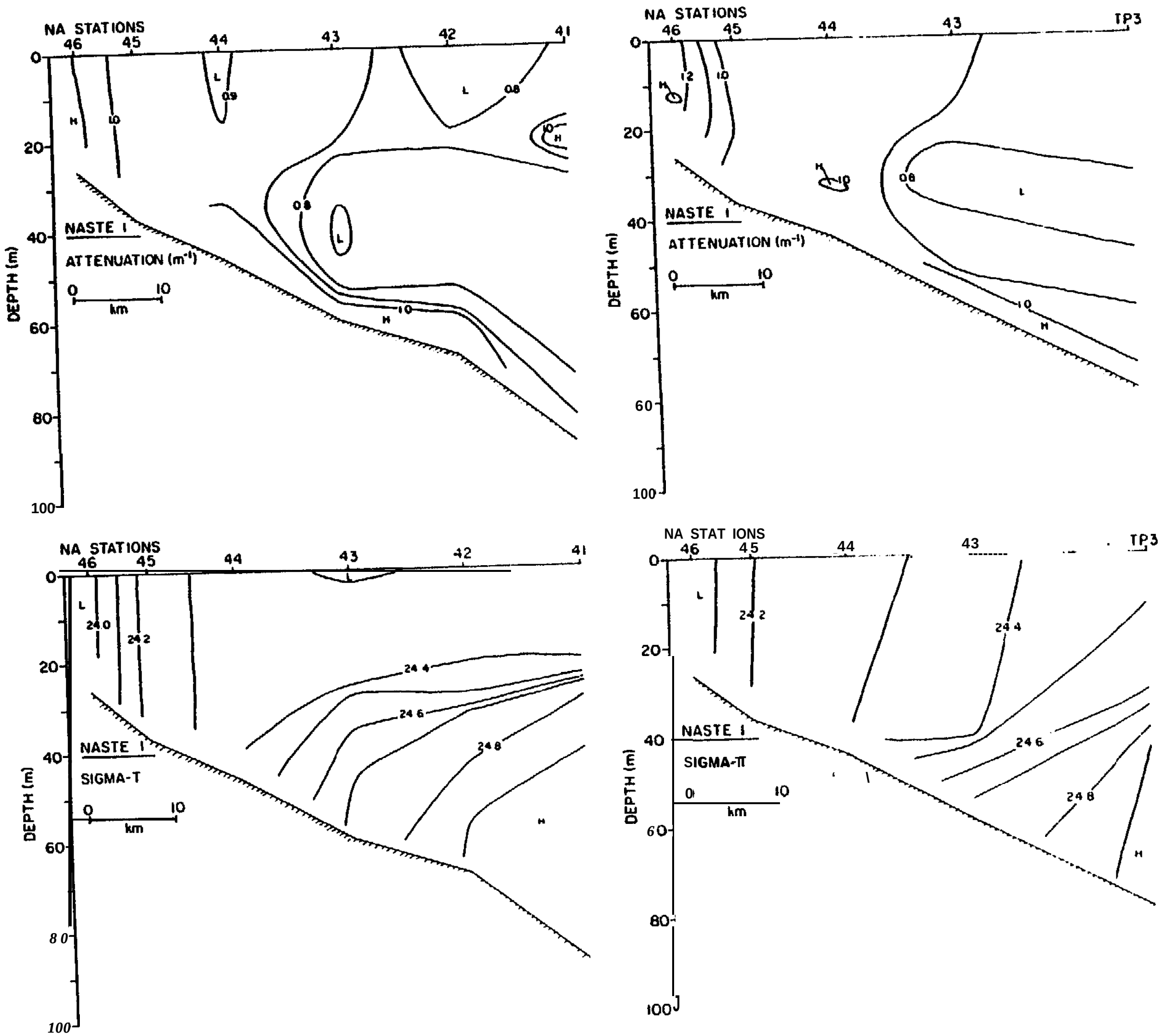

Figure 26. Attenuation (top) and density (bottom) cross-sections for stations **NA41-46** on August 31 (left), and September 2, 1980 (right).

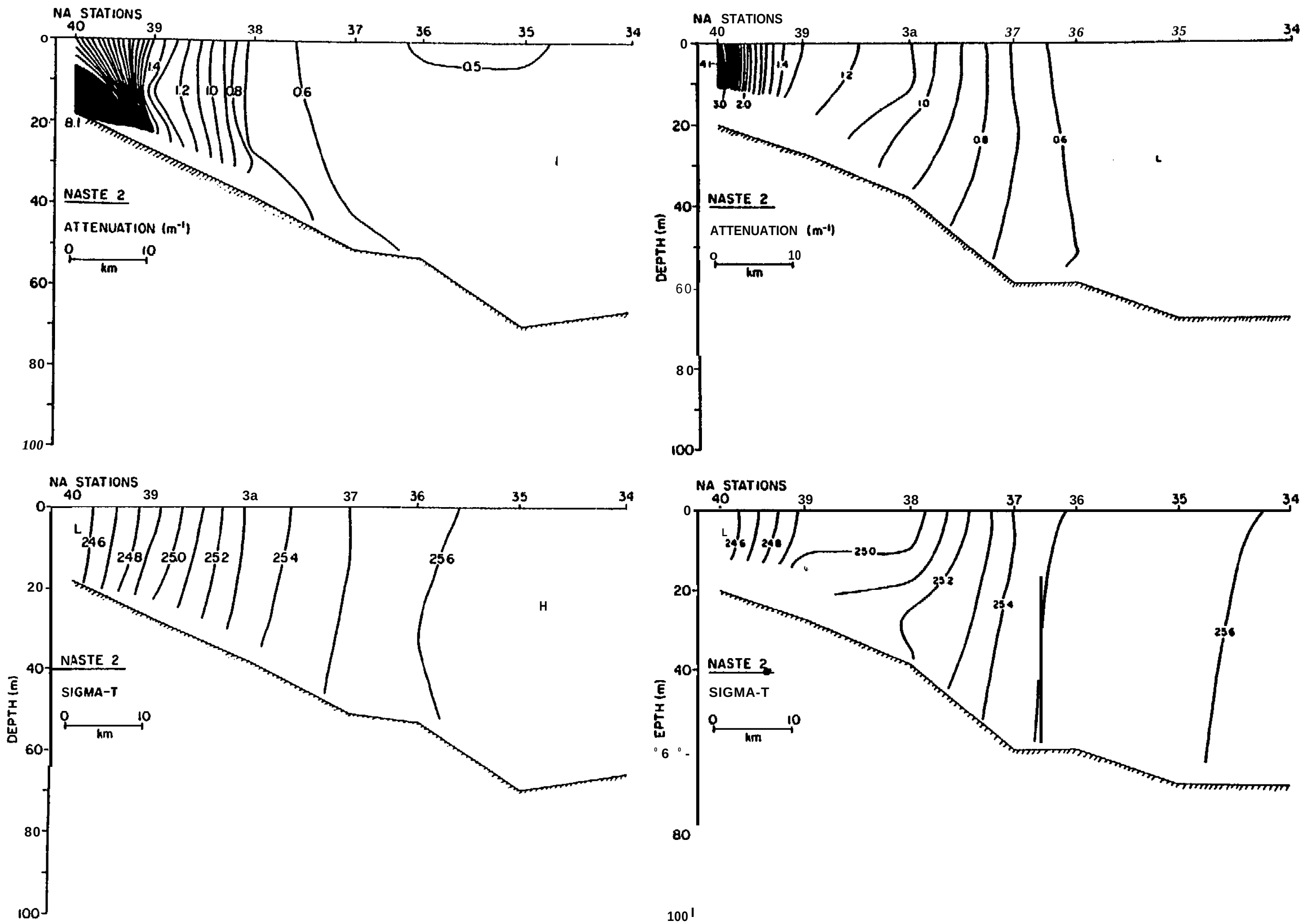

Figure 27. Attenuation (top) and density (bottom) cross-sections for stations **NA34-40** on January 31 (left), and February 8, 1981 (right).

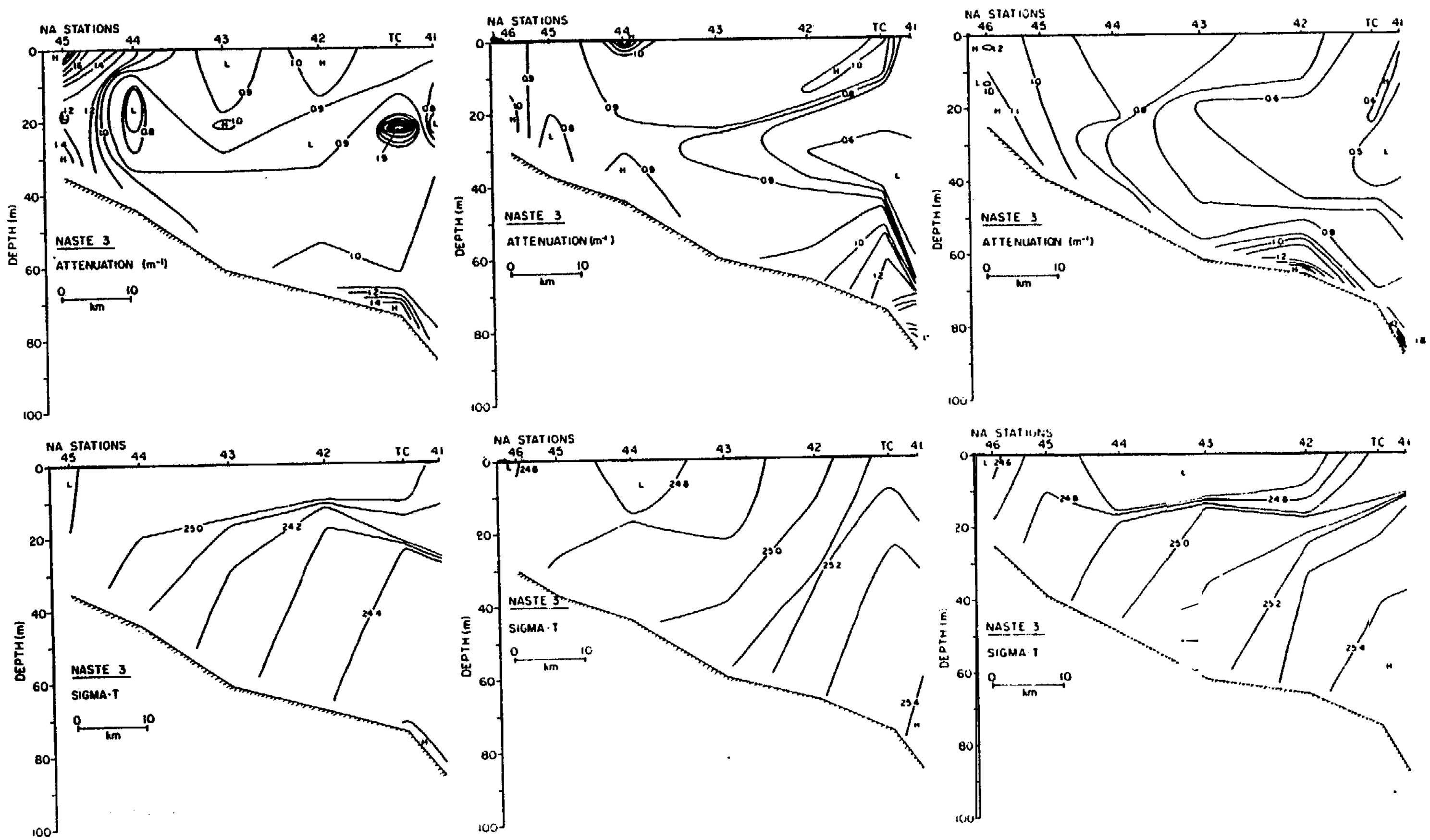

Figure 28. Attenuation (top) and density (bottom) cross-sections for stations NA41-45 on May 15 (left), May 25 (middle), and May 30, 1981 (right).

layer, which was generally greater along the NA40-NA34 line than along the NA41-NA46 line. Line NA41-NA46 was occupied a final time on 2 Sept. and found basically unchanged (Fig. 26).

Winter conditions along the NA34-NA40 line were found to be quite uniform on the scale of a week (Fig. 27). Density stratification was minimal except for just offshore of Port Moller where freshwater outflow caused a low density surface plume and higher attenuation values during the second occupation. Although the general structure of the density and SPM distributions remained constant throughout NASTE 3, the attenuation levels of individual stations showed high variability. During all three occupations of the NA41-NA46 line, a well-developed SPM mid-depth minimum zone was present seaward of Station NA45. Near-bottom attenuation values *were* always highest at the inner and outer ends of the transect, in good agreement with the regional pattern evident in the areal plot (Fig. 13). The surface layer showed numerous isolated high and low attenuation zones which were largely attributable to phytoplankton patchiness.

3. Particle size distributions

The particle size distribution (PSI.)) data from the North Aleutian Shelf area are summarized by reference *to* the NA34-NA40 station line. Variations along other transects during each cruise closely followed the changes observed along the NA34-NA40 line.

Data from NASTE 1 (Fig. 29A and B) indicated good agreement between PSD curves from surface and bottom waters. Slopes averaged 3.24±0.55 in the surface water and 3.35±0.50 5 m above bottom. Intercept values averaged 4.8 x 10^5 and 3.9 x 10^5 for surface and bottom samples. The inshore station, NA40, clearly showed the effects of fine-grained particle sources supplied

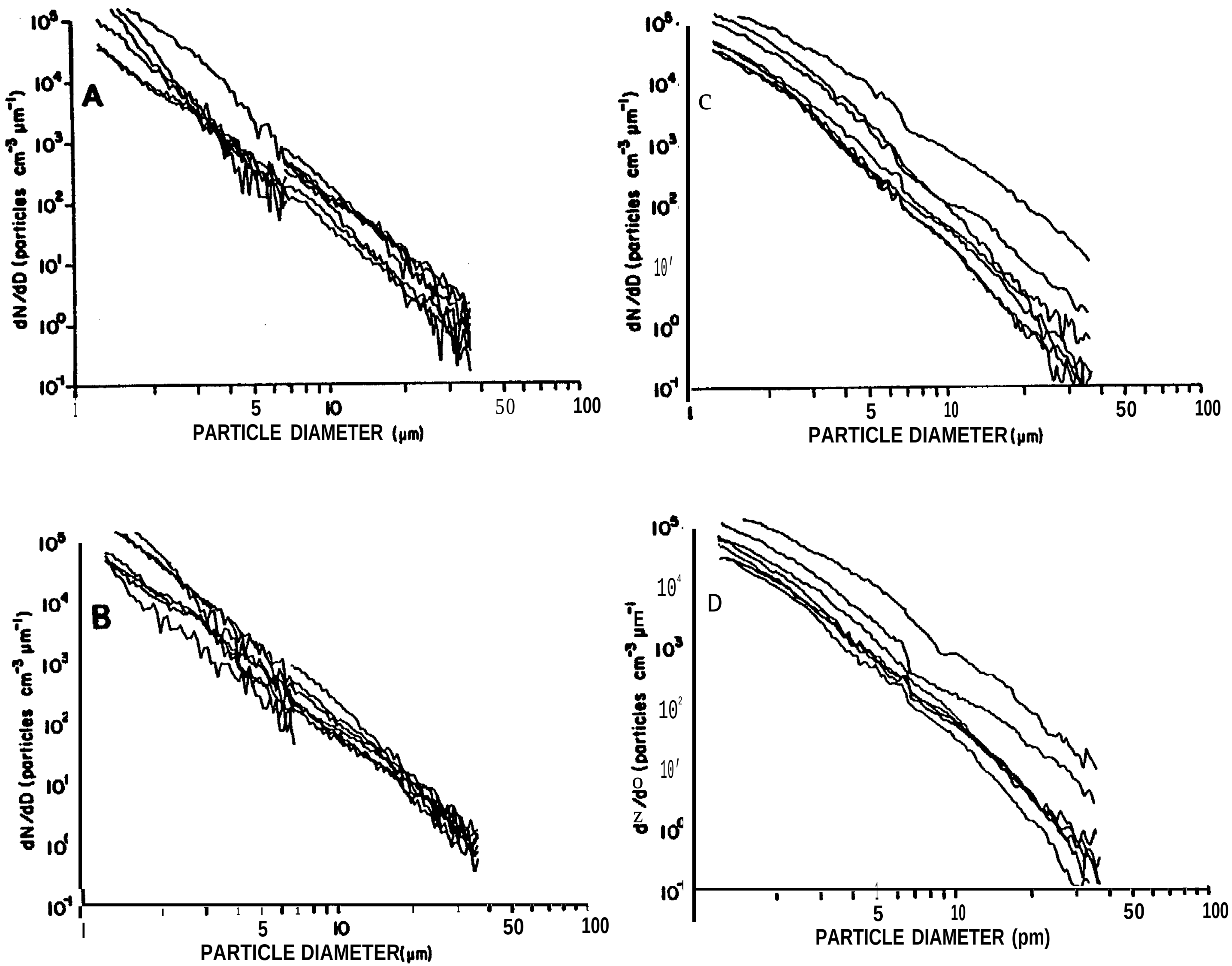

Figure 29. Incremental cumulative curves for particle populations along the **NA34-40** station line from surface (A) and bottom (B) samples from NASTE 1, and surface (C) and bottom (D) samples from **NASTE** 2.

from the adjacent lagoon environment: the slope and intercept for the surface water sample were 4.16 and 27.0 x 10^5, indicative of a turbid, fine-grained particle population.

PSD curves from NASTE 2 (Fig. 29C and D) show the influence of strong horizontal and weak vertical gradients in both density and SPM concentration typical of winter conditions. The family of curves for each depth horizon are virtually identical, while variation within each horizon is much greater than at any particular station. Particle populations in both surface and bottom waters became more turbid and relatively coarser grained progressing inward from Station NA34. Slope and intercept for surface and 5 mab at NA34 were 4.08, 3.1 x 10^5 and 3.74, 3.1 x 10^5, respectively. These values are relatively steady seaward of -50 m (NA37); landward of this position horizontal density and attenuation gradients increased markedly. By NA40, slope and intercept values for surface and 5 ❑ab were 3.10, 14.2 x 10^5 and 3.24, 17.7 x 10^5, significantly different than the surface and bottom averages for the entire line: 3.87 ± 0.41, 7.6 x 10^5 and 3.69 ± 0.32, 5.1 x 10^5.

The different conditions prevailing between NASTE 1 and 2 can be illustrated by comparing the individual inshore and offshore stations from each cruise (Fig. 30). Landwardmost and seawardmost stations during NASTE 1 were virtually indistinguishable from each other at the coarse end of the particle size spectrum and gradually diverged towards the fine-grained end. That is, the slope of the PSD curves was highest for the inshore station. The same stations during NASTE 2 showed far greater between-station than within-station variability.

Surface-bottom differences in the particle populations were also observed during NASTE 3 (Fig. 31). Horizontal variability in slope and

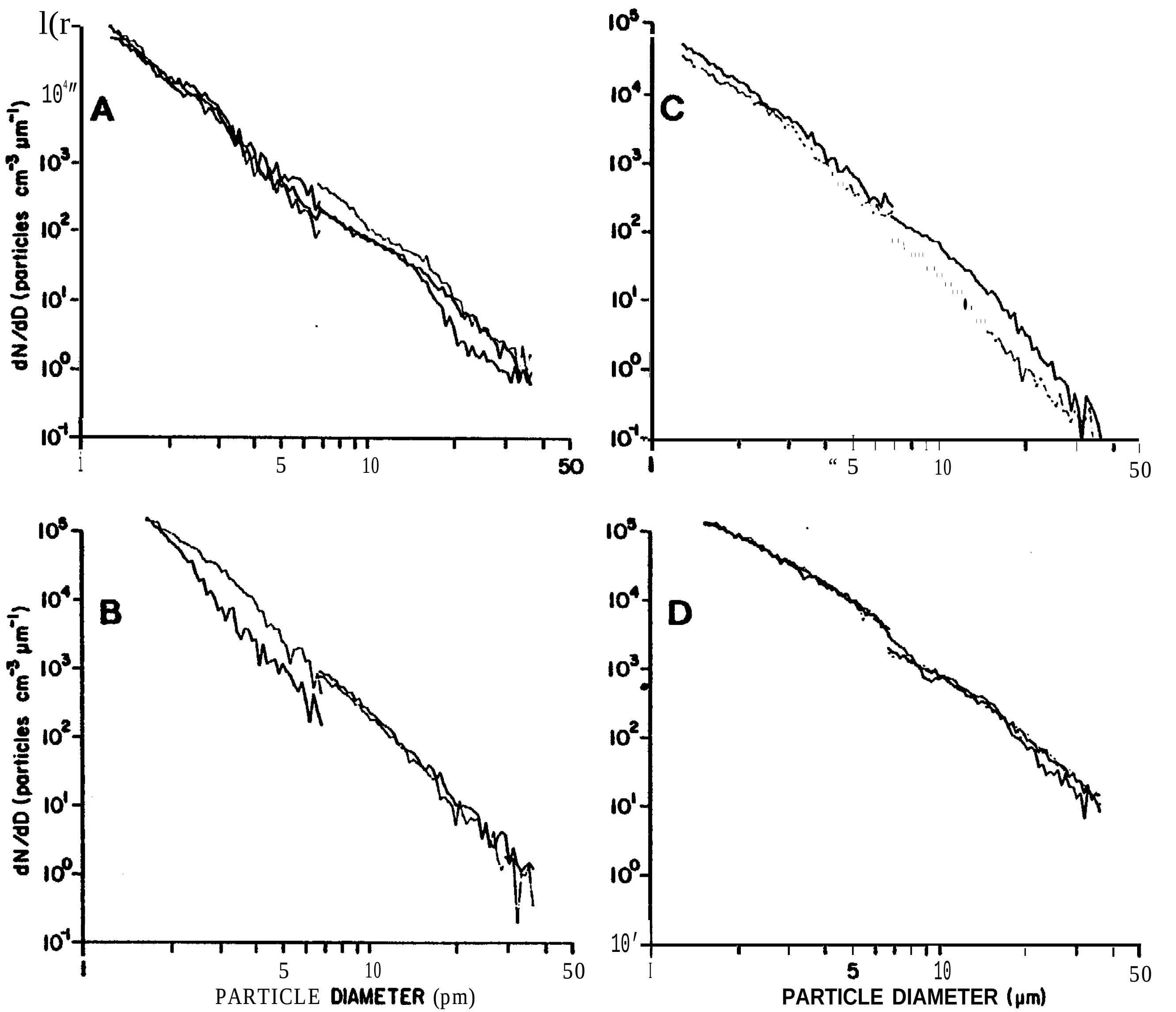

Figure 30. Incremental cumulative curves for particle populations at (A) an offshore station (NA34) and (B) an inshore station (NA40) during NASTE 1, and offshore (C) and inshore (D) stations during NASTE 2.

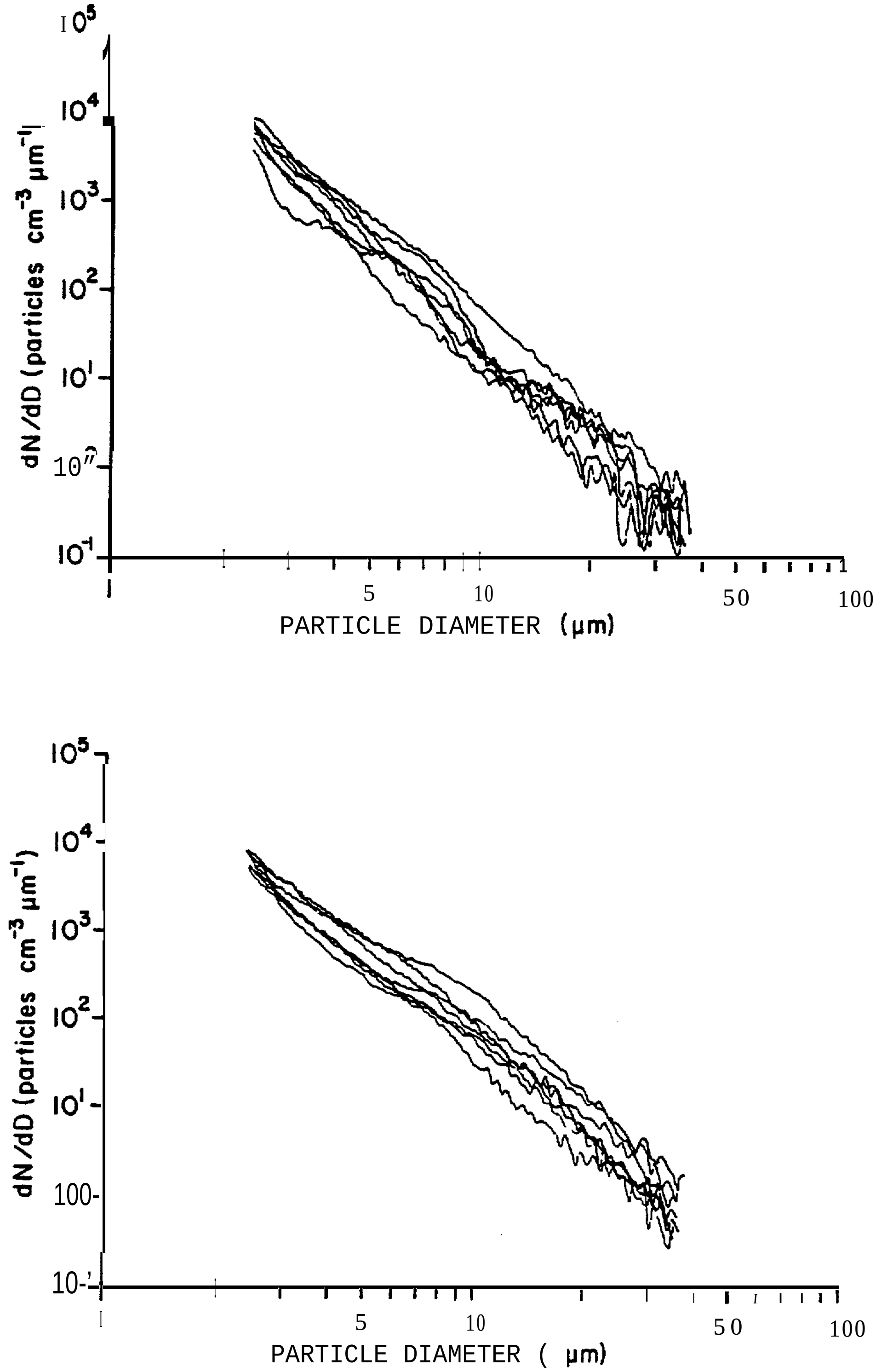

Figure 31. Incremental cumulative curves for particle populations along the NA34-40 station line from surface (top) and bottom (bottom) samples from NASTE 3.

intercept values was lower than in either of the two previous cruises, a fact which can be attributed to the well-developed surface and bottom mixed layers present during the spring (Fig.32). Average surface values of the slope and intercept were 3.76 ± 0.39 and 1.0 x 10^5 with no distinct spatial trend. Average bottom values were quite different: 2.91 ± 0.37 and 0.8 x 10^5, again with no definite spatial trend. As a group, these bottom samples were the coarsest measured on any cruise.

Although no clear spatial trends are evident within individual horizons, the influence of changing hydrographic regimes between the inshore and offshore stations can nevertheless be detected in the relationship between the surface and near-bottom samples. Figure 32 traces the surface and - near-bottom PSD curves from NA34 to NA40 during NASTE 3. Curves from the offshore stations vary independently; particularly obvious are broad peaks in the surface samples which do not occur in the bottom samples and the greater concentration of coarse-grained particles. Moving inshore, the curves become progressively more similar, until at NA40, well inside the well mixed coastal domain, the surface and bottom curves are virtually identical. As during NASTE 2, agreement in the particle population characteristics substantially improves landward of --40-50 m depth.

4. Organic matter concentrations

Available SPM samples from the seawardmost and landwardmost stations of all NA transects from each cruise were analyzed for organic matter content in order to characterize possible differences between the middle and coastal 5PM domains. Table 4 summarizes these results.

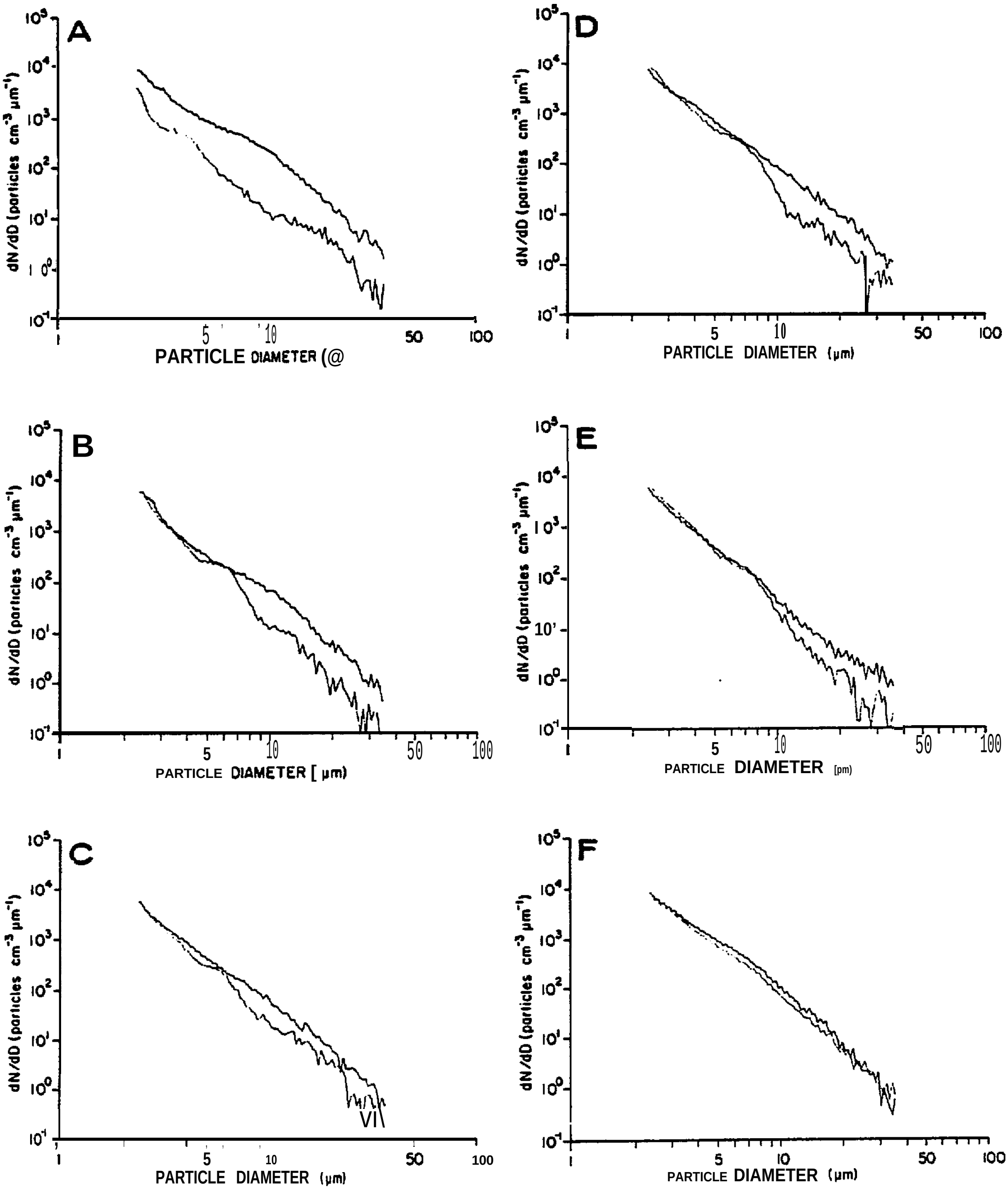

Figure 32. Incremental cumulative curves for particle populations at the surface and bottom at each station (NA34-40 station line) from NASTE 3. A is the outermost station and F is the imermost station.

TABLE 4

Percent organic matter in SPM samples from the North Aleutian Shelf region

Cruise	Surface						5 m above bottom					
	Onshore			Offshore			Onshore			Offshore		
	n	$\bar{x}$	s	n	$\bar{x}$	s	n	$\bar{x}$	s	n	$\bar{x}$	s
NASTE 1	15	42.8	9.6	12	47.9	7.4	14	38.5	11.4	13	32.8	8.2
NASTE 2	15	25.7	6.4	15	46.3	9.0	15	24.7	5.3	16	40.4	9.2
NASTE 3	7	45.6	15.6	10	57.5	15.3	7	39.7	11.9	10	29.3	5.7

The highest overall percentage of organic matter (43.0%) was recorded during NASTE 3, the cruise conducted during the normally highly productive spring bloom period. The percent organic matter was only slightly less during the late summer (40.5%, NASTE 1) and substantially lower in winter (34.3%). The lowest values recorded (~25%) were the surface and near-bottom values from the inshore winter stations; the offshore winter surface value was only slightly lower than its summer and spring counterparts. Offshore winter near-bottom values were higher than either spring or summer, an anomaly apparently caused by the relatively unimpeded vertical exchange between surface and bottom waters when density stratification is minimal.

Averaged over all three cruises, the surface offshore percent organic matter (50.6%) was significantly greater than the inshore value (38.0%), perhaps due to dilution of phytoplankton-produced organic matter in the coastal zone by inorganic detritus from shore and bottom erosion and re-suspension. Differences in phytoplankton standing stock or primary production between the coastal and middle domains, however, were not investigated during this study.

Near-bottom percent organic matter values were always less than the surface values, although the inshore-offshore pattern differed seasonally. Offshore near-bottom values in the spring and summer were lower than the corresponding inshore values because the offshore samples were insulated from the productive surface waters by the regional pycnocline. Resuspension of bottom sediment relatively poor in organic matter was a major source of particles to the offshore near-bottom water at these times. During winter, however, offshore near-bottom organic matter values were greater than the inshore values.

5. X-ray clay mineralogy

Results from the clay mineralogy analyses were inconclusive. The only peaks observed on any diffractogram were from silt-sized particles such as quartz and feldspars. Clay mineral concentrations in the water column were not great enough to yield measurable results by standard sampling techniques. Future efforts to quantify the clay mineral suite in suspension must encompass special techniques to recover, filter, and concentrate large volumes (10-20 ℓ) of seawater.

6. Particle flux measurements

a) Vertical particle flux

Vertical particle flux was measured at Stations TP2B, TP7, TP8, and TP9 between NASTE 1 and NASTE 2 (Fig. 3). Sequentially sampling sediment traps (S^3T) were deployed 11 to 15 m above bottom at each station in conjunction with transmissometers to measure light attenuation and current meters to measure current flow and water properties. Each sediment trap collected 9 separate flux samples of 11.25 days each, begiming on February 3 0600 **(TP2B)**, February 3 0540 **(TP7)**, February 6 0020 **(TP8)**, and February 4 0400 **(TP9)** and ending on or around May **16** (all times local).

Average total sedimentation rates **(TSR)** varied from **<2 g** m^{-2} **day**$^{-1}$ at TP8 to **>9** g m^{-2}**day**$^{-1}$ at TP7 and TP9, the shallowest and deepest stations, respectively (Table 5). Stations TP7, TP2B, and TP9 were along a transect normal to the coast, while **TP8** was located -56 Ion to the southwest at about the same depth at **TP2B.** Thus the TSR appears to be depth controlled, with large values found both close inshore and seaward of the coastal front, whereas smaller values were found near the zone where the SPM distribution changed from vertically stratified to horizontally stratified during **NASTE** 3 (see Figs. 21, 22, and 23). This zone may be considered the location of the coastal front along the North Aleutian Shelf region. Other indications also point to a higher energy environment at the TP7 and TP9 locations relative to TP8 and **TP2B.** The average flux of particles **>38μm** at TP7 and TP9 was 4 to 16 times greater and comprised **51.2%** of the total flux compared to only **31.0%** at TP8 and **TP2B.**

Much of the mixing energy in the nearshore waters of the Alaskan Peninsula is provided by wind events whose energy output varies greatly in time (Kinder and Schumacher, 1981a). Similarly, the flux of organic matter is dependent on seasonal plankton cycles. Thus "average" characterizations of the vertical SPM flux, while useful for defining regional variability, can not adequately describe the processes which control the flux. This point is illustrated by the temporal flux variability as recorded by the 11.25 day samples from each of the S^3T (Fig. 33). The TSR at TP7 and TP9 varied by as much as a factor of 15 between successive collection periods;

TABLE 5

Vertical particle flux measurements

Mooring Location	Water Depth (m)	Trap Depth (m)	Average Sedimentation Rate ($g\ m^{-2} day^{-1}$) Total	Phyto-plankton pigments	Organic matter	Particles <38μm	Particles >38μm	Average Composition (%) Organic matter	Particles <38μm	Particles >38μm
TP7	24	13	11.23±5.54	2.24±1.18	1.04±0.56	3.96±1.64	6.87±4.24	10.5±1.8	37.5±12.7	58.8±13.1
TP8	31	16.5	1.76±0.81	0.69±1.07	0.25±0.12	1.0710.52	0.4220.22	14.6±2.5	61.0± 5.3	23.4± 7.2
TP2B	35	20.5	3.25±1.72	0.94±0.87	0.48±0.20	1.73±1.20	1.30±0.75	16.515.5	53.4±14.0	38.7*14.5
TP9	89	77	9.60±8.26	2.22±3.56	1.1710.86	3.94±2.89	4.96±6.40	13.812.8	48.3±14.6	43.6115.2

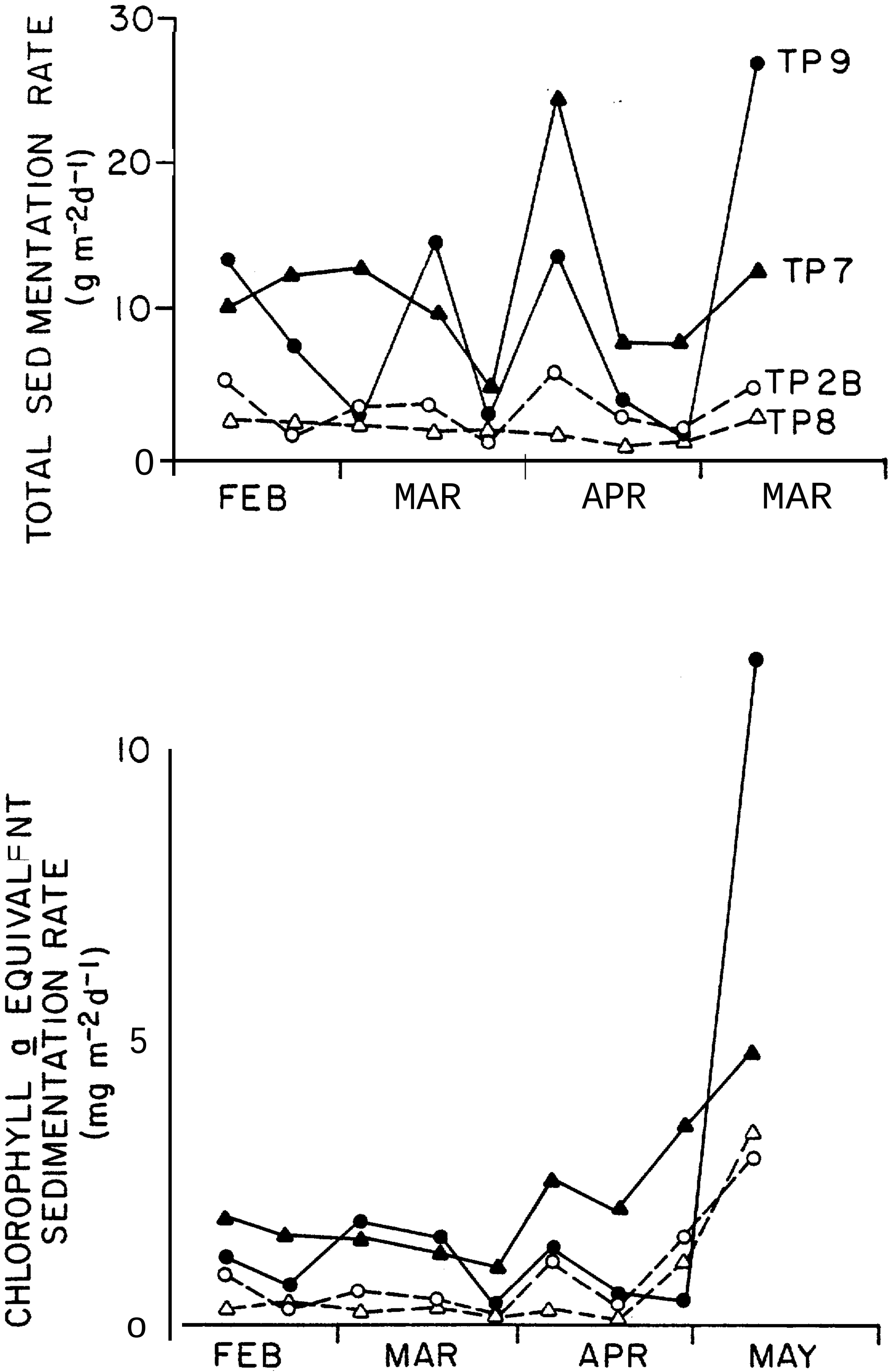

Figure 33. Flux values from NAS sediment traps. Each point represents an 11.25 day average value.

changes on the order of 5x were common. At TP8 and TP2B, however, temporal variability was far lower; the maximum observed was a 7-fold change and changes >2x were rare. Changes in the flux of fine and coarse-grained particles followed the same trends (Fig. 34). It is clear from Figs. 33 and 34 that this variability was not random. Sedimentation rates showed clear maxima in collection periods 4 (March 8-19), 6 (March 31-April 1), and 9 (May 3-14) at TP9. The same sequence was recorded at TP7 (except for a shift from period 4 to period 3) and, in reduced fashion, at TP2B. TP8, located 56 km down the coast from the others, showed no clear pattern in its much lower flux rate. Although the grain-size composition was highly variable at each site (Fig. 35), there was no clear pattern to the changes.

The temporal pattern of the biogenic portion of the flux was dominated by onset of increased phytoplankton production in the spring (Fig. 33). The flux of phytoplankton pigments, expressed as chlorophyll a equivalents [= chlorophyll a + (1.52) pheophorbide, the chlorophyll a degradation product; see Shuman and Lorenzen (1975)], varied only slightly at all stations through the first seven collection periods. Towards the end of the deployment, however, the pigment flux rose sharply, especially at TP9 where density stratification could produce a stable surface mixed layer to encourage primary production.

b) Horizontal particle flux

Variations in attenuation at the mooring sites were primarily the result of tidal forcing. Both inshore and offshore records (Fig. 36) showed significant (at the 0.05 level) spectral peaks in the attenuation record at periods of approximately 1, 0.5, 0.33, and 0.25 days. Significant variations were also caused by longer period events such as the fortnightly waxing and

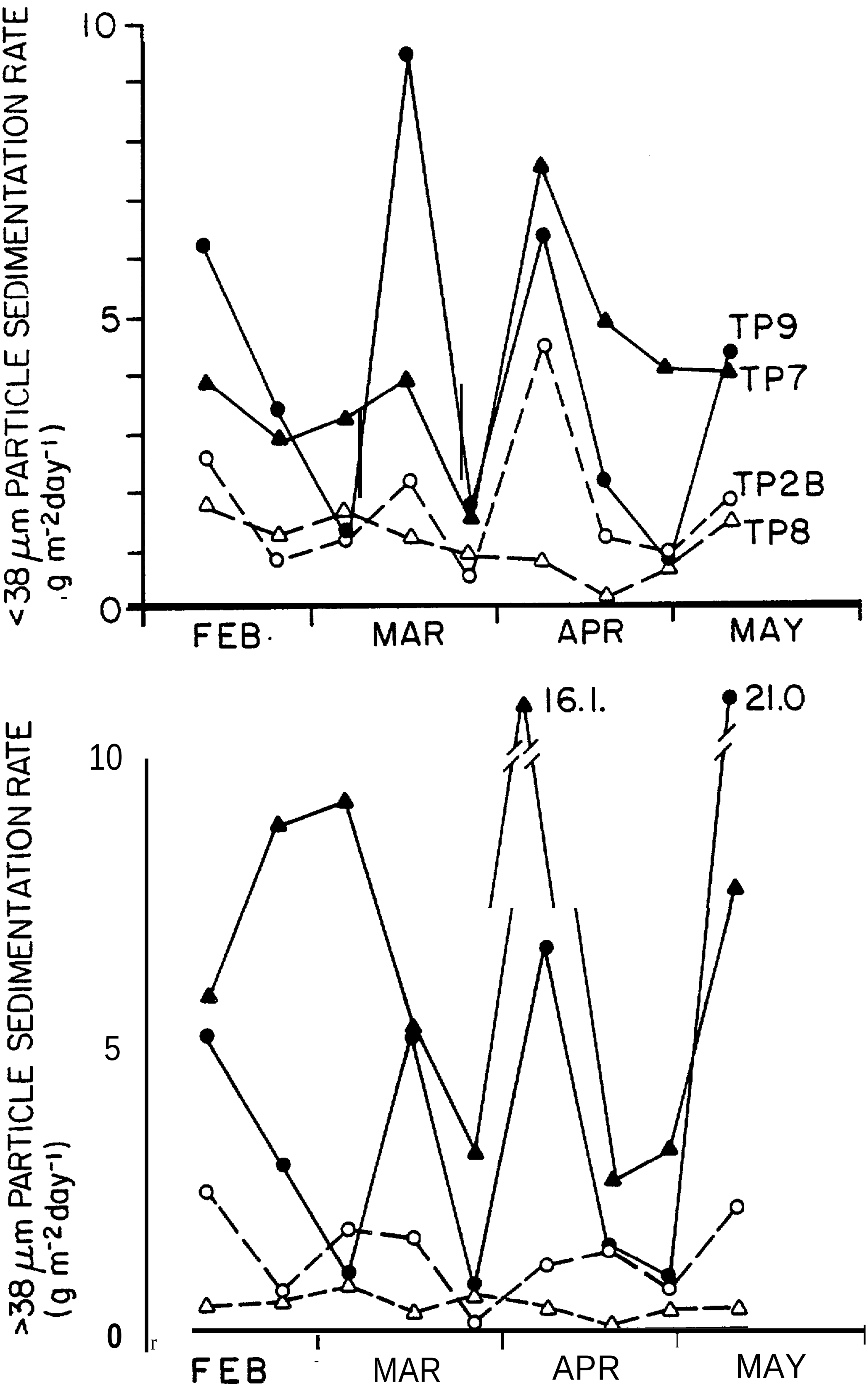

Figure 34. Flux values for fine- and coarse-grained particles in the NAS sediment traps.

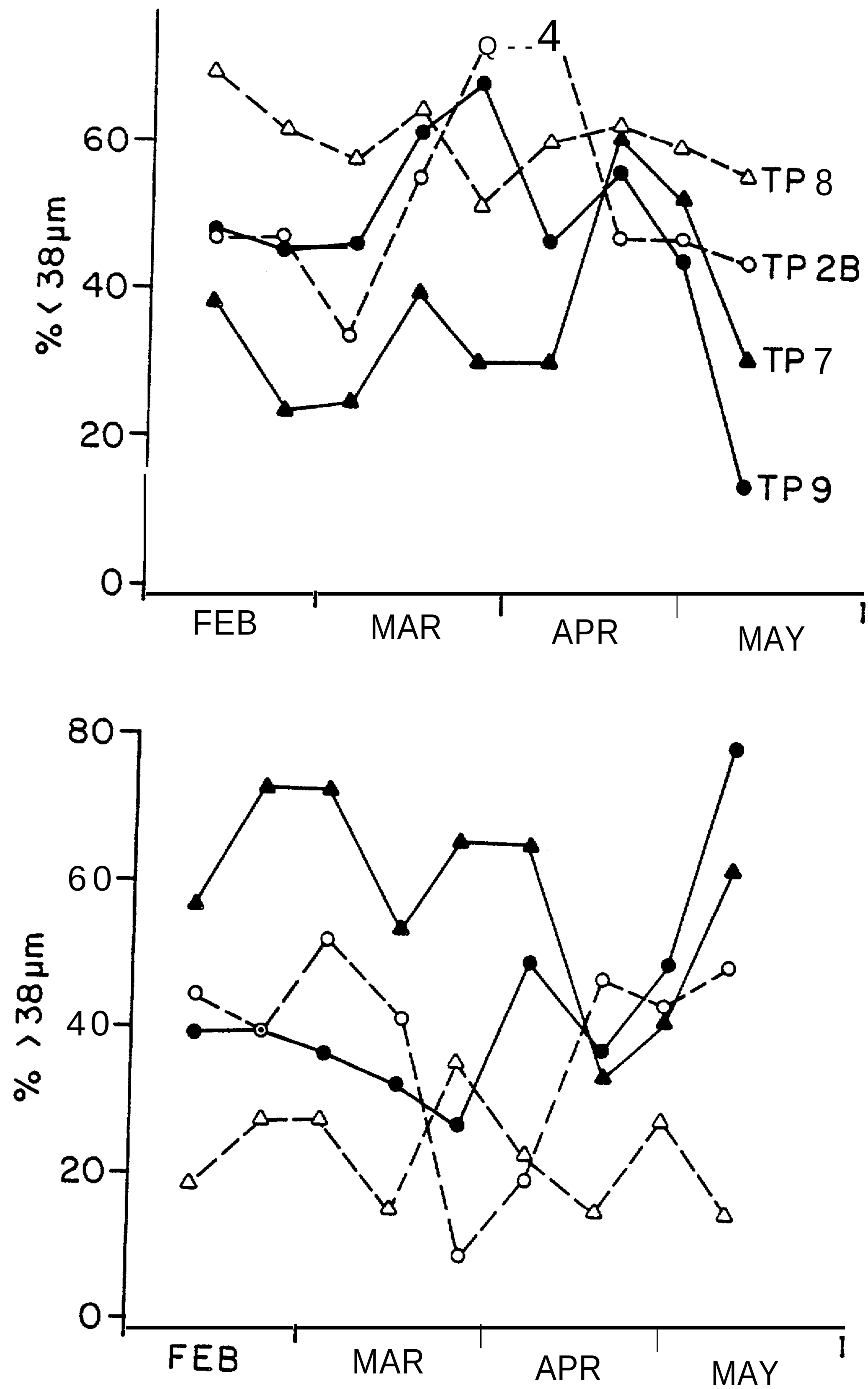

Figure 35. Variability of particle-size partitioning of sediment trap material.

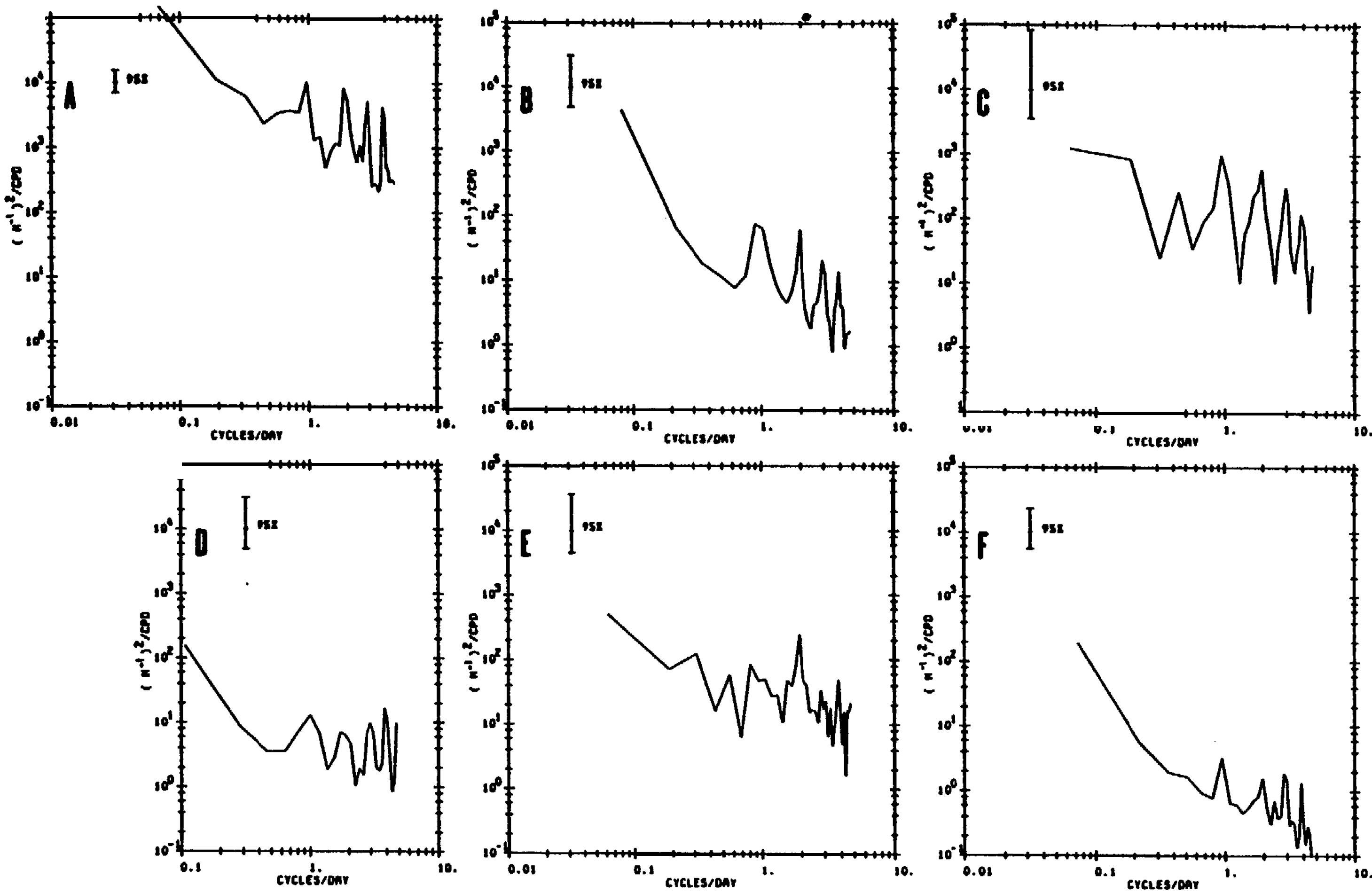

Figure 36. Variance spectra for attenuation records. A, TP7; B, TP2; C, TP8; D, TP6; E, TP4; F, TP9. Peaks occur at tidal frequencies.

waning of tidal energy, as expressed by the large proportion of spectral variance at periods of ~10 days. Attenuation variance levels were greatest at TP7, the shallowest station, and least at TP9, the deepest station. Variance at other stations was roughly proportional to the depth, but did not vary in a strictly linear fashion.

Figs. 37 and 38 illustrate the character of the mooring records from the landwardmost and seawardmost stations. Station TP7 shows very large daily variations throughout the record, as well as several 5- to 10-day intervals where the turbidity values were routinely 4x the "normal" value of ~2 m^{-1}. These aperiodic events are probably related to the local weather (at present, the local wind record from the temporary shore station has not finished the data processing routine). Station TP9 (Fig. 39) shows a very different attenuation record. (The record has been terminated at Mar. 27 since past that time fouling of the transmissometer lenses rapidly deteriorated the attenuation signal. Fouling was not found to be a problem in the much more energetic environment at TP7.) Daily changes are very small.

Sediment flux calculations (Table 6) show clear differences between inshore and offshore stations. SPM fluxes were >7 μg cm^{-2} see-l at TP7, TP2, and TP8, but <~2 μg cm^{-2} see-l in deeper waters. No consistent transport direction was found, but it should be remembered that net flow in this environment is difficult to interpret due to its very small ❑ agnitude relative to the tidal variations (Kinder and Schumacher, 1981b). The direction of net sediment flux usually agreed closely with that of the net water flow. Sediment flux at the offshore moorings was directed alongshore at the deepest two sites (TP4 and TP9) and inshore at TP6, a slightly shallower site. Sediment flux at the three inshore stations had a strong alongshore component to the southwest, away from Port Moller.

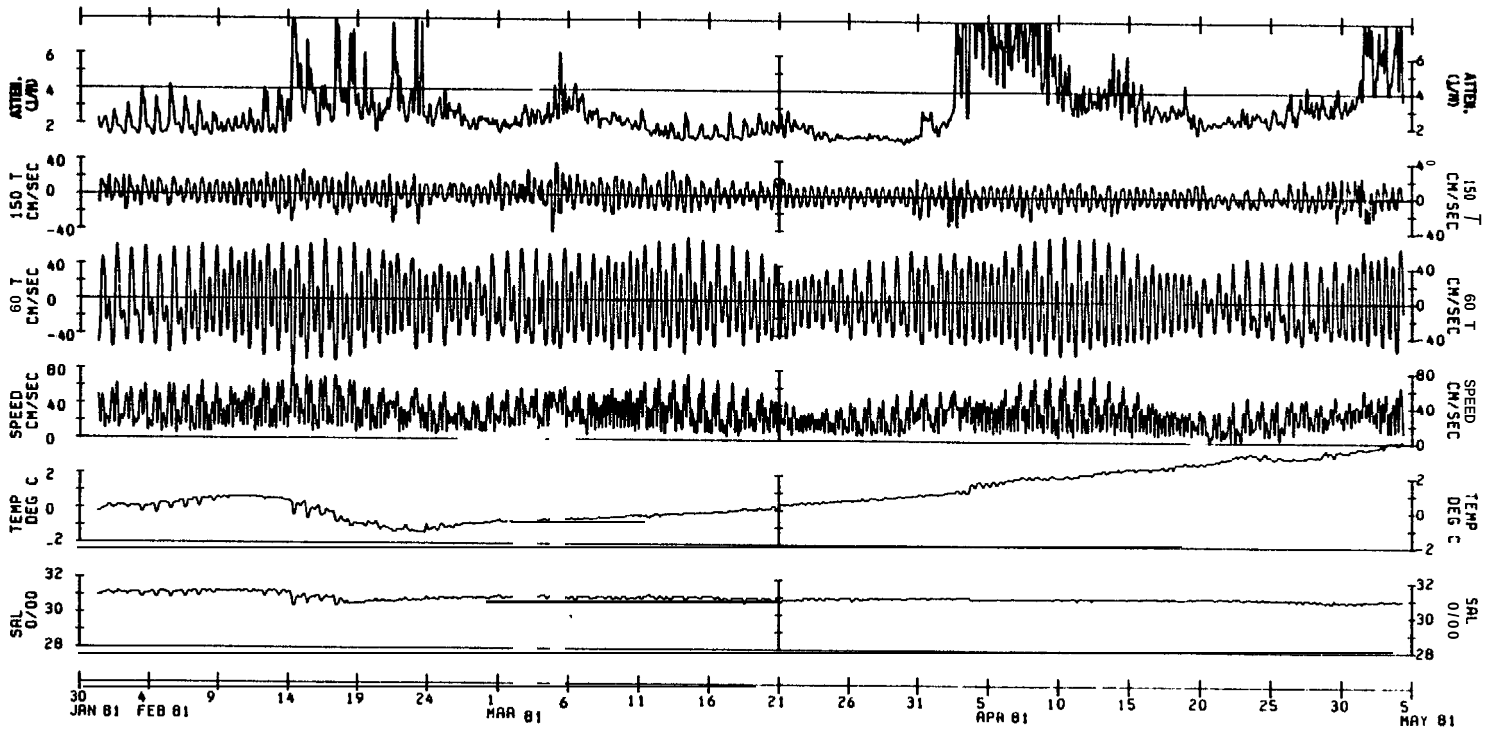

Figure 37. Current meter/transmissometer record at TP7.

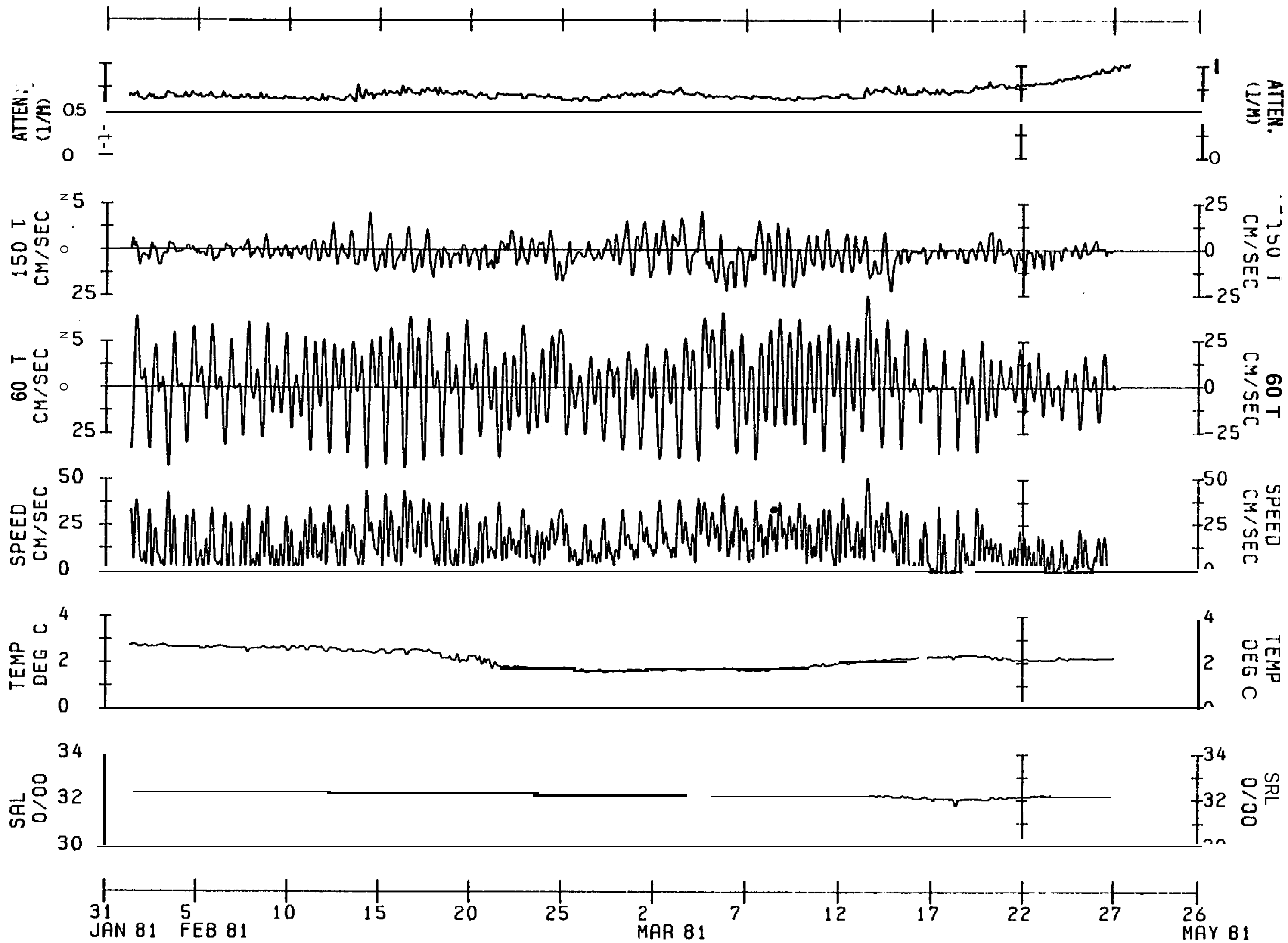

Figure 38. Current meter/transmissometer record at TP9. Note change in scales from Figure 37.

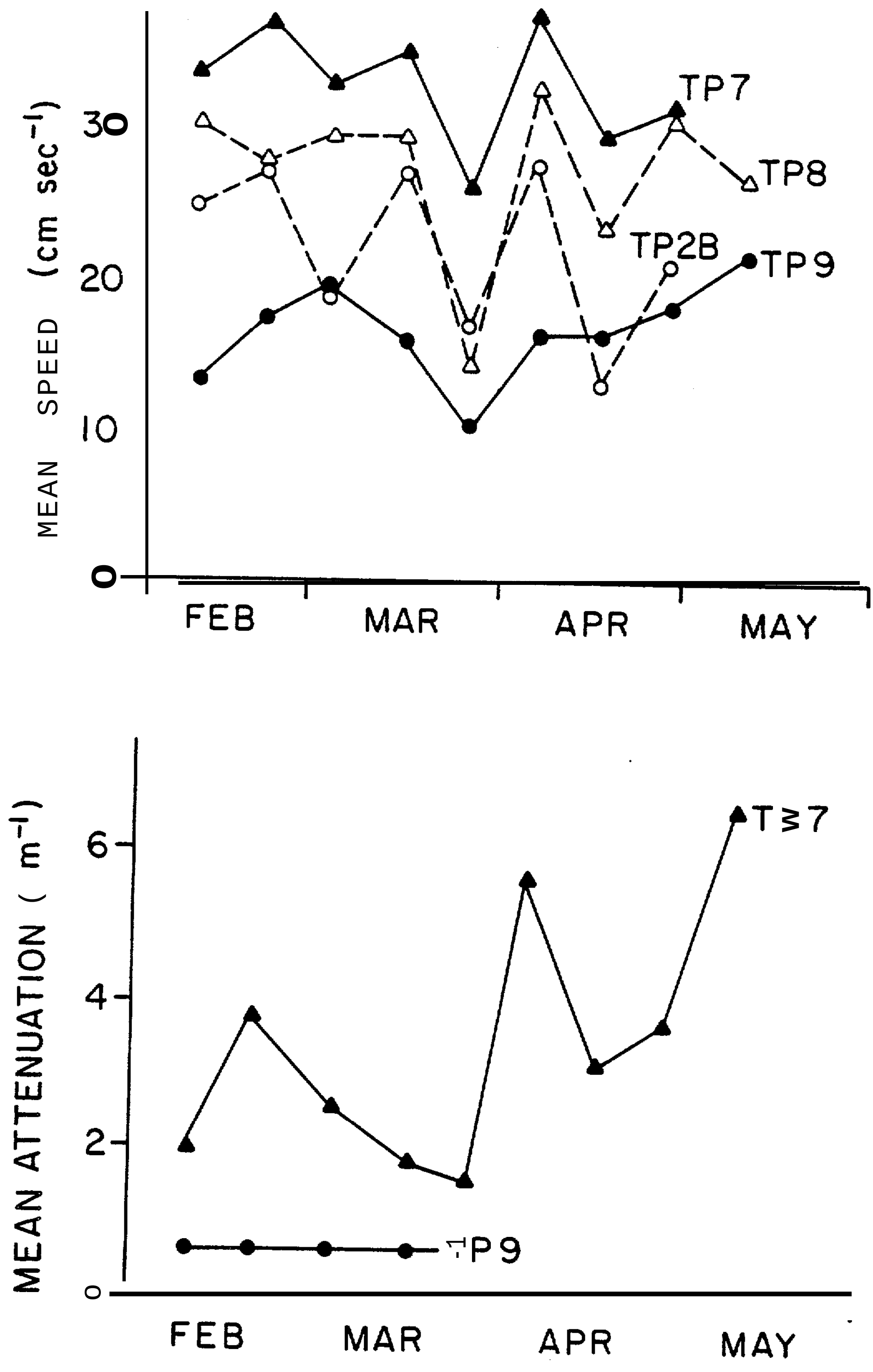

Figure 39. Mean speed and mean attenuation values averaged over sediment trap collection periods.

TABLE 6

Sediment flux calculations

Mooring	Meter Depth (m)	Sampling Interval	Particle Flux (µg cm^{-2} see-1)	Dir. (°)	Mean Speed (cm see-1)	Dir. (°)
Inshore						
TP7	15	30 Jan-5 May	17.5	238	33.0	206
TP2	20	19 Aug-25 May	7.6	219	27.8	212
TP8	21	2 Feb-19 Feb	7.0	205	30.4	210
Offshore						
TP6	55	20 Aug-17 Sep	1.1	153	22.4	150
TP4	63	19 Aug-20 Sep	2.1	45	14.9	47
TP9	89	31 Jan-27 Mar	1.2	15	15.5	13

It is also interesting to note that the correlation between mean current speed and sediment transport magnitude is poor. Mean current speed about doubles from TP9 to TP7, whereas sediment flux increases approximately fifteenfold. This difference can be explained on the basis of particle availability; the high SPM concentrations typical of the near-shore region result in much greater mass transport with only a moderate increase in current flow.

Comparison of the incremental sedimentation rate, mean current speed, and mean attenuation (Fig. 39) shows clear differences between nearshore and offshore environments. All three parameters follow similar trends at TP7, implying that the particles are thoroughly mixed throughout the water column and that these mixing processes are more important in controlling the distribution and transport of particles in the water than are sedimentation processes. At TP9, the TSR and mean speed trends are nearly independent, except for a mutual minimum during period 5 (a quiescent time over the entire region). Similarly, the truncated attenuation record shows essentially no change even with a near doubling of mean speed between periods 1 and 3. These results arise from the fact that the TSR at TP9 is strongly influenced by settling particles originating in the surface layers as well particles resuspended and advected within the BNL. TP8 and TP2B appear to be intermediate between these extremes in the relationship between sedimentation and current speed.

B. St. George Basin Region

Field work in this region was done to ascertain SPM distributions characteristic of the hydrographic domains as described by Kinder and Schumacher (1981a). Extensive descriptions of the physical oceanography of the southeastern Bering Sea are available, but data on the particle distributions are sketchy and related almost exclusively to purely biological processes (e.g., chlorophyll a distributions; Iverson et al., 1979).

Because the field emphasis in this project was the North Aleutian Shelf region, station coverage in St. George Basin was not uniform for all three cruises. Furthermore, equipment problems during NASTE 2 resulted in only a few CTD casts having acceptable transmissometer data. Data coverage was most complete during NASTE 3.

1. Density and SPM cross-sections

The longest continuous line of stations across the southeastern Bering Sea hydrographic domains was occupied during NASTE 1 and encompassed

Stations PL1 to PL24 (Fig. 40). (This line duplicated a standard station line used by the NSF PROBES Program.) The density cross-section clearly reveals the various **hydrographic** domains. The coastal domain, identified by vertically homogeneous water, was found inshore of about Station PL19 (approximately the 45-m **isobath).** The imer front, characterized by a high horizontal density gradient in the bottom water, occurred between Stations PL18 and **PL16.** Seaward of this zone, a strong two-layer stratification marks the middle domain. The broad ❑ iddle front appeared to be centered around Station PL8. Further seaward the stratification separating the wind ❑ ixed surface layer and the tidally mixed bottom layer became ❑ ore moderate and typical of the outer shelf domain. Surface expression of the shelf break front was seen between Stations PL2 and PL3.

Several features of the **SPM** distribution reflect these **hydrographic** domains. In the coastal domain, particles were well mixed throughout the water column with only slight increases in near-bottom attenuation levels due to gravitational sinking of large particles. Both the middle and outer shelf domains were characterized by a three layer **SPM** distribution. Particles in the bottom water were trapped below the regional **pycnocline** and created a bottom **nepheloid** layer with a sharp vertical gradient. Both bottom **nepheloid** layer concentrations and vertical gradients appeared substantially lessened at stations where horizontal near-bottom density gradients increased (i.e., Stations PL9 and **PL18).** Above the **nepheloid** layer was a broad zone where SPM concentration gradients were low in both horizontal and vertical directions. This zone was terminated in the **landward** direction by the inner front. Above the mid-depth minimum zone, SPM concentrations are highly variable and probably controlled by **phyto-** plankton patchiness,

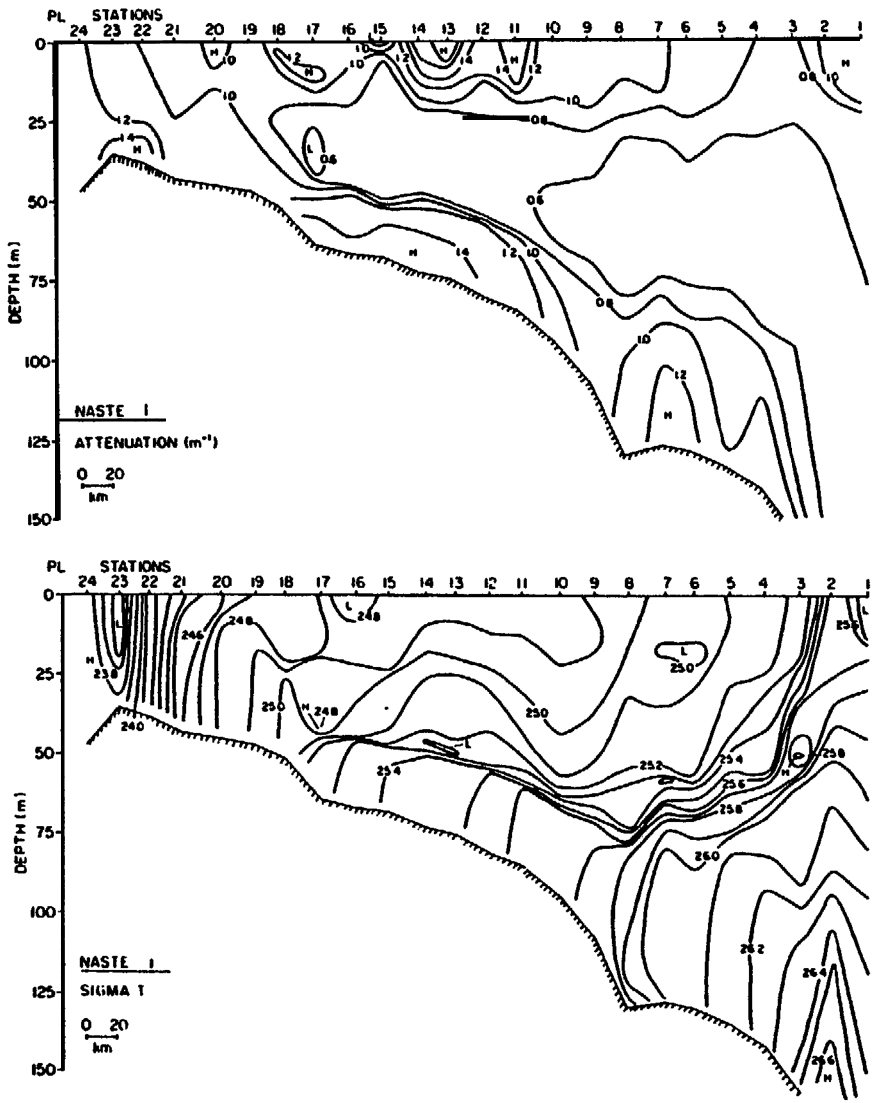

Figure 40. Attenuation (top) and density (bottom) cross-sections for the PL line during NASTE 1.

The data set from **NASTE** 3 is both geographically and temporally more extensive. An abbreviated portion of the PL line was occupied twice, once on May 17 and May 18 (Fig. 41) and again May 23 and 24 (Fig. 42).

The middle and outer shelf domains were again identified during the spring cruise. Sampling did **not** extend **landward far** enough **to** reach the coastal domain. The most significant change appeared to be in the strength and position of the **pycnocline** in the middle domain. During **NASTE** 1, **Brunt-Väisälä** frequencies averaged 10.9 ± 1.4 cph in the middle shelf **pycnocline;** during **NASTE** 3 the stability averaged 10.1 ± 1.2 **cph** during the first **PL** occupation and only 8.7 ± 0.6 cph during the second. Maximum **Brunt-Väisälä** values were found an average of 16 ± 4 ❑ above bottom during **NASTE** 1; during NASTE 3 the average was 47 ± 8 ❑ above bottom during the first occupation, lowering to **25** ± 9 ❑ above bottom during the second.

Although the general character of the SPM distribution was similar to NASTE 1, these alterations in the density distribution had demonstrable effects on the details of the SPM cross-sections. During the first **PL** occupation (Fig. 41), the extreme thickness of the bottom mixed **layer** effectively destroyed the mid-depth minimum zone landward of the middle shelf by allowing resuspended particles to be mixed high into the water column. Six days later, **during** the second FL occupation, the horizon of maximum stability had lowered to within ~ 25 m of the seafloor and thus allowed the reestablishment of a mid-depth minimum zone throughout the PL line (Fig. 42).

Data collected along three other lines parallel to the PL line (Fig. 2) also exhibited similar relationships between the density stratification and the vertical **SPM** distribution.

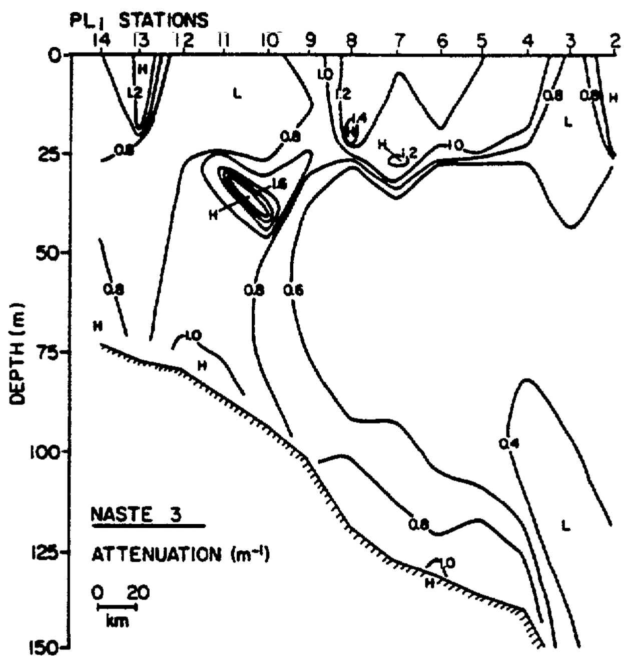

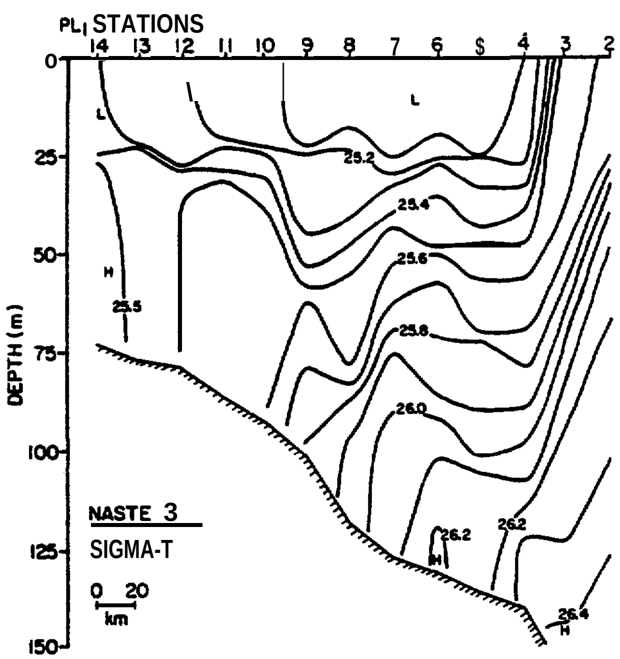

Figure 41. Attenuation (top) and density (bottom) cross-sections for the PL line, May 17-18, 1981.

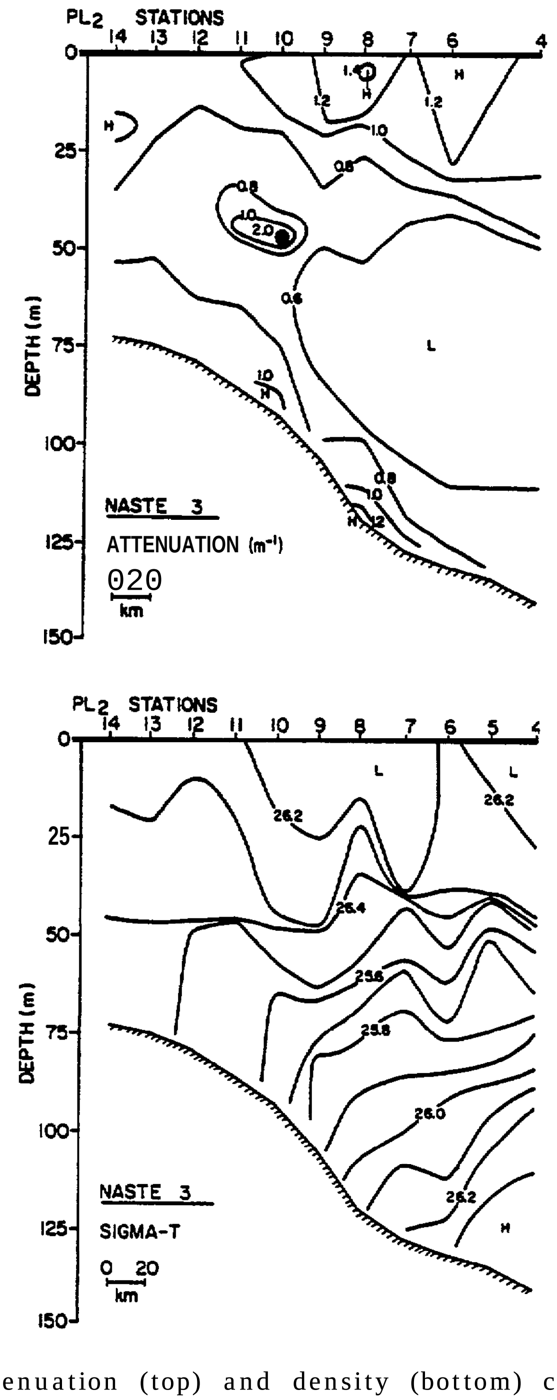

Figure 42. Attenuation (top) and density (bottom) cross-sections for the PL line, May 23-24, 1981,

2. Particle size distributions

Although particle size distribution data was collected at all St. George Basin stations, only samples from stations along the PL **line** will be discussed in detail. This transect was the only one occupied on each cruise and is representative of the entire region.

All distributions show excellent correlation with a power law distribution (see Section IV. B.I.). Correlation coefficients (r^2) for all samples were >0.95. The power law distribution **fails** only at diameters **>~20 µm** in the surface water where **large** concentrations of particles over a narrow size range (i.e., **phytoplankton)** result in deviations from the linear trend. During NASTE 1 and 2, a slight change of slope was observed **at ~4 µm** diameter (see Fig. 43; data from **NASTE** 3 was inconclusive on this point). This intersection has been noted in other oceanic samples processed by **Coulter** Counter techniques (Bader, 1970; **Brun-Cottan,** 1976; and **McCave,** 1975). Its origins and implications are unknown at present. To compare distribution slopes between cruises and depths, then, only the range between 4 and 20 **µm** was considered in calculating the power law regression coefficients.

Surface water along the PL line during NASTE 1 contained particle size distributions **(PSD)** with both the steepest slope and highest particle concentrations of any portion of the water column during any cruise **(Table** 7, Fig. 43). Variability in the family of PSD curves is high, with peaks in both the -20 **µm** and 3 - 5 **µm** range perhaps indicative of specific kinds of **phytoplankton. PSD** curves in the mid-depth minimum zone are much ❑ ore coherent. The average slope (4.19) shows a ❑ arked decrease from the surface samples (4.54) and the intercept value is lower by an order of magnitude (Table 7). The slope of the near-bottom samples decreases still further,

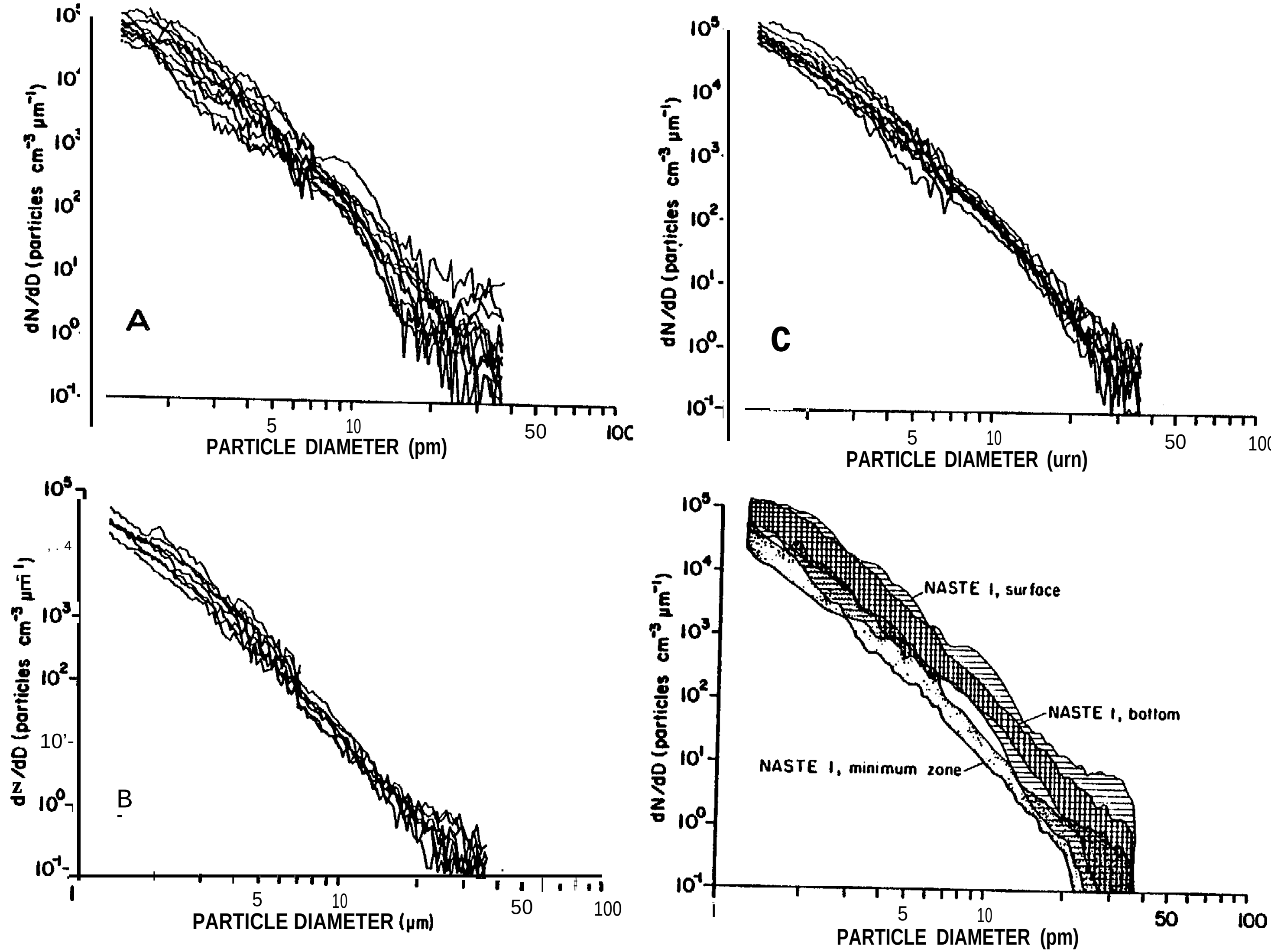

Figure 43. Incremental cumulative curves from the PL line during **NASTE** 1 for surface water (A), minimum turbidity *zone* (B), bottom water (C). Curve envelopes for each group are also shown.

TABLE 7
Particle size distribution parameters from PL line in St. George Basin

Cruise	Depth Zone	a[1] ($\times 10^5$)	b[1]	n[2]
NASTE 1	surface	40.3 ± 90.0	4.54 ± 0.62	10
	mid-depth	4.0 ± 3.0	4.19 ± 0.32	9
	bottom	12.8 ± 7.4	4.06 ± 0.22	9
NASTE 2	surface	3.0 ± 1.6	4.04 ± 0.17	6
	bottom	12.6 ± 14.4	4.13 ± 0.43	7
NASTE 3-PL_1	surface	1.1 ± 6.6	3.34 ± 0.27	13
	mid-depth			
	stas. 2-8	0.4 ± 0.2	3.79 ± 0.34	6
	stas. 9-14	1.2 ± 0.9	3.44? 0.45	6
	bottom			
	stas. 9-9, 13-14	3.1 ± 1.2	4.00 ± 0.18	7
	stas. 10-12	0.8 ± 0.4	3.04 ± 0.78	3
NASTE 3-PL_2	surface	0.8 ± 0.2	3.40 ± 0.14	10
	mid-depth			
	stas. 4-9	0.6 ± 0.4	3.88 ± 0.30	6
	stas. 10-14	0.8 ± 0.3	3.42 ± 0.16	5
	bottom			
	stas. 4-8, 14	4.8 ± 2.0	4.14 ± 0.27	6
	stas. 10-13	0.6 ± 0.2	2.98 ± 0.05	4

[1] Mean and standard deviation of constants determined from fitting the observed distributions to the form $dN/dD = aN^{-b}$.

[2] Sample size for each depth zone.

although the intercept value is greater than for the minimum zone samples.

The relative characteristics of the family of PSD curves from each depth horizon are compared in Fig. 43. Samples from the surface and bottom are seen to occupy very similar plot coordinates, while those from the minimum zone are distinct. Furthermore, PSD curves in all three horizons are uniform throughout the PL line (through PL20). This uniformity may be traced to the strong vertical stratification which prevailed during NASTE 1 (Fig. 40), thereby allowing the particle populations in the surface and bottom mixed layers to be internally consistent and distinct from the intermediate minimum zone.

PSD curves from the surface and bottom waters along the PL line during NASTE 2 are shown in Fig. 44 (no minimum zone data was collected). The average slopes of these lines are similar to each other and to the minimum zone and near-bottom samples from NASTE 1 (Table 7). Concentrations are slightly higher in the near-bottom samples. Comparison of the family of PSD curves from the minimum zone of NASTE 1 and the surface waters of NASTE 2 (Fig. 44) shows them to be nearly identical. This agreement indicates that in the absence of active phytoplankton growth and strong vertical stratification (as is the case in January-February in the southeastern Bering Sea), the particle populations of the surface layer and the mid-depth zone are indistinguishable and form what may be considered the "background" population of this region. Changes to this background thus occur when additional sources, such as bottom resuspension, phytoplankton growth, or river runoff, are influential.

Particle populations in the surface water during NASTE 3 again showed the strong influence of phytoplankton peaks (Fig. 45) at diameters >~20 µm. Below 20 pm, the PSD curves are quite coherent with slopes less than those

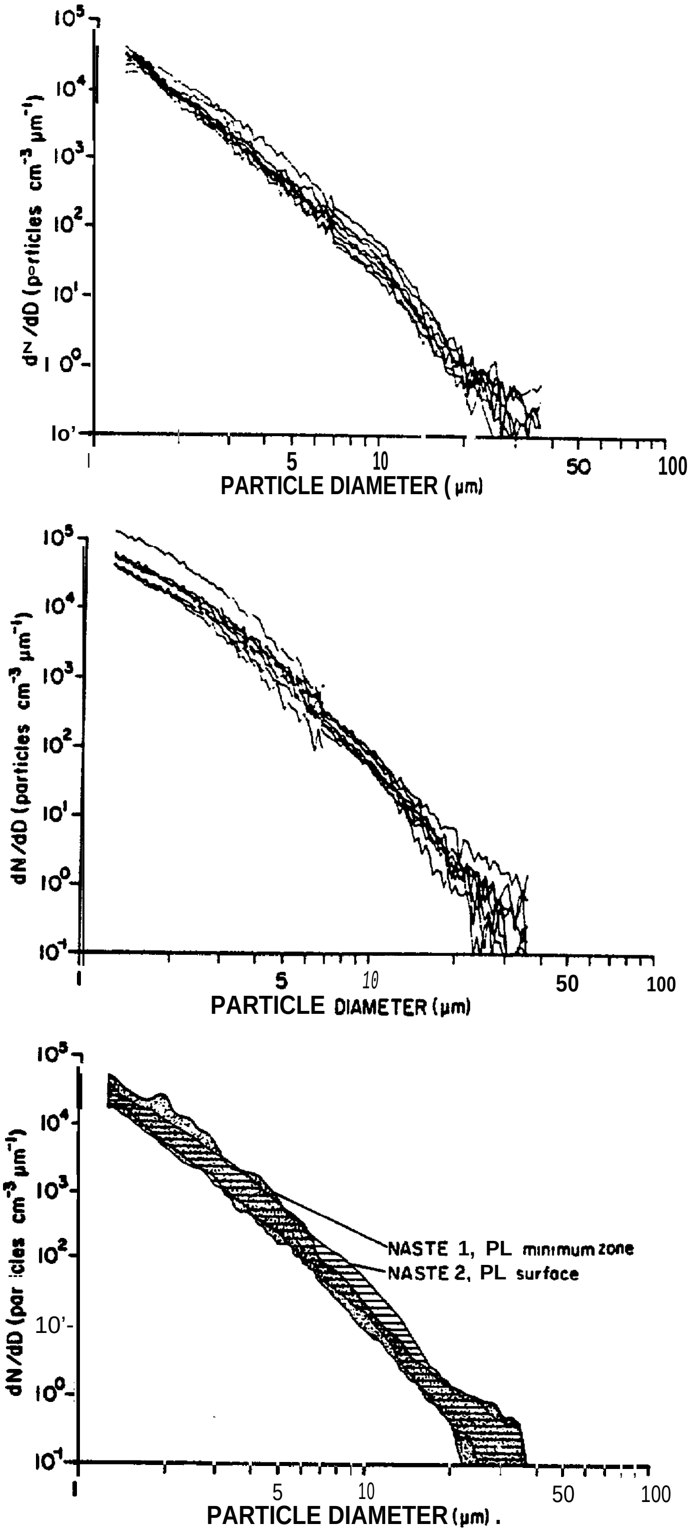

Figure 44. Incremental cumulative curves from NASTE 2 surface (top) and bottom (middle) waters. Curve envelopes (bottom) demonstrate the similarity of the two populations.

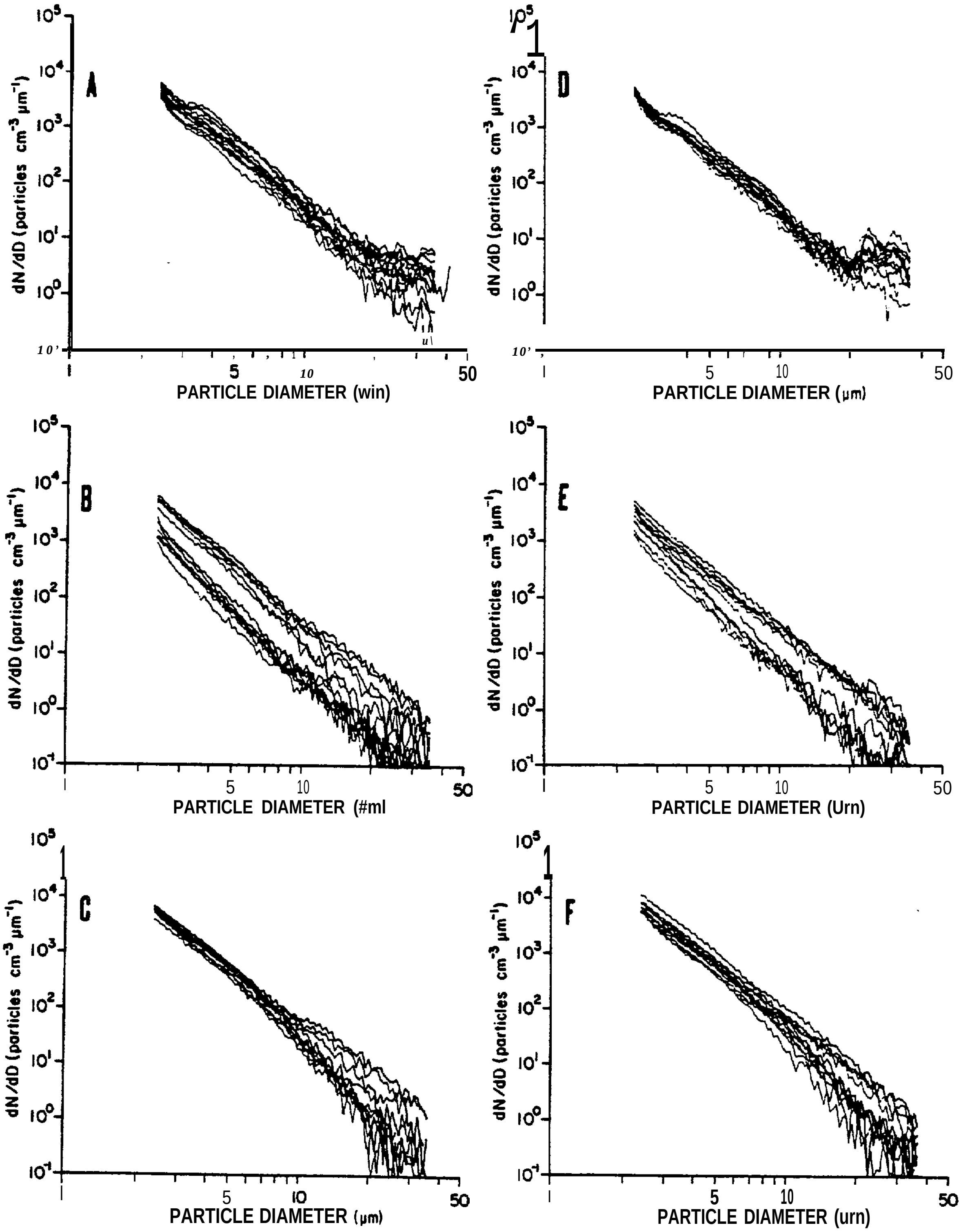

Figure 45. Incremental cumulative curves from NASTE 3 PL_1 surface (A), minimum turbidity (B), and bottom (C) zones. Panels D, E, and F show analogous curves for the PL_2 transect.

typical of the late summer and winter periods (Table 7). During both occupations of the PL line, there was a definite indication of a non-linearity in the PSD curves centered at ~3.5 μm, the same size range where prominent peaks were observed in the NASTE 1 surface data. Below the surface water, the mid-depth minimum zone can be separated into two distinct sub-populations (Fig. 45B and E): one sub-population, seaward of stations PL8 or 9, is characterized by slopes of -3.8; another sub-population, inshore of these stations, is characterized by slopes of -3.4, similar to the surface waters (Table 7). A similar, but less exaggerated situation also exists in the near-bottom water (Fig. 45C and F; Table 7). In the bottom water, however, the region of PSD curves with low slopes is more restricted and does not include the landwardmost stations.

VI. DISCUSSION

A. Relationship Between Vertical Distributions of Particles and Density

The vertical distribution of fine-grained particles in the ocean is principally governed by the density structure, since the density structure controls the vertical distribution of turbulence. 'Fine-grained' in this context is taken to mean those particles whose settling velocity is much less than the mean horizontal current speeds of a given environment. For inorganic particles, the upper limit is ~ 10pm; for organic particles and floccules, the upper limit may be several times larger. Since the hydrographic domains of the southeastern Bering Sea are also determined by the density structure (Kinder and Schumacher, 1981a), it is reasonable to expect that the various hydrographic domains are characterized by specific kinds of particle distributions.

Figure 46 summarizes the types of particle distributions found during this study and illustrates their dependence on the density distribution. In the outer domain (PL6), the particle distribution consists of well-mixed layers at the boundaries of the water column and a mid-depth low turbidity zone. These layers are separated by zones of relatively uniform change in the particle concentration. In this figure, values of total light attenuation have been uniformly reduced by the clear water attenuation value of 0.4 m^{-1} (see Section IV, A.2.) in order to plot only the curvature resulting from the particle attenuation. Plotting the resultant values on semi-log paper identifies zones where the eddy diffusion is uniform. These zones are characterized by a uniform slope in the particle attenuation curve. Several such increments are apparent at PL6. The bottom nepheloid layer consists of two such layers, a layer of relatively high diffusion (steep slope) in the bottom 30m and an overlying layer of much lower diffusion between 70 and 95 m. According to Bassin (1974), the maintenance of a nepheloid layer requires both a particle source and an overlying layer of increased stability (minimum turbulence) to inhibit diffusion of the particles upward and out of the nepheloid layer. At PL6 there was excellent agreement between the attenuation profile and the shape of the stability distribution (Brunt-Väisälä frequency). Tidal mixing along the bottom created a zone of low and uniform stability in which the particles were well mixed. Above this zone, mixing diminished and the stability increased towards a maximum at ~70 m. Particle concentrations decreased rapidly through this zone. Close correspondence between particle and density gradients at the top of the bottom nepheloid layer has been previously observed in other environments as

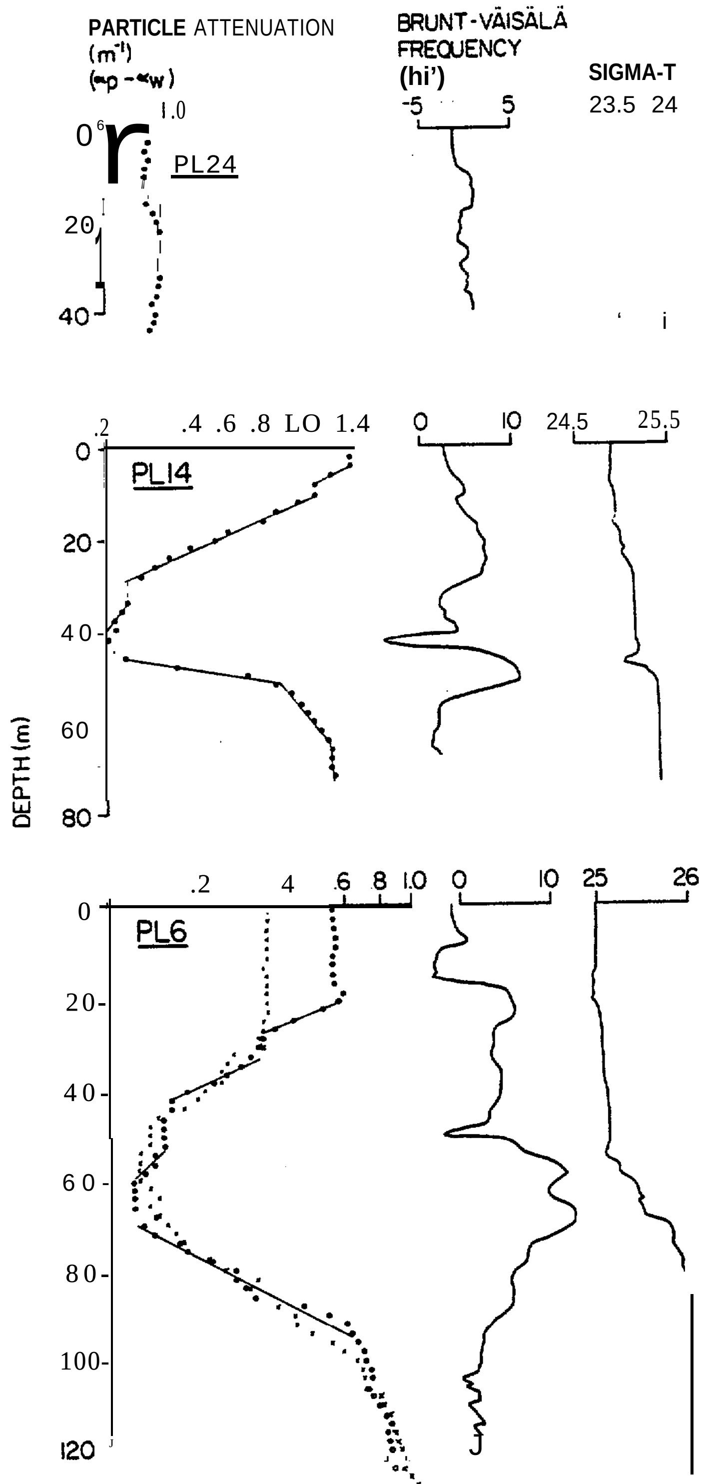

Figure 46. Net particle attenuation profiles, stability profiles, and density profiles from the coastal (top), middle (middle), and oceanic (bottom) domains. Note the stability maximum at the top of each bottom nepheloid layer.

diverse as the northwest Atlantic Ocean (Biscaye and Eittreim, 1974), Vema Channel in the southwest Atlantic (Johnson et al., 1976), and over the continental shelf off Oregon (Newberger and Caldwell,1981).

A similar situation prevailed in the surface waters. Wind mixing created a layer of uniform density and particle concentrations underlain by a series of. stability maxima and minima. Zones of low and uniform diffusion on Aug. 29 (e.g., 20-28 m, 34-44 m, and 54-62 m) were associated with stability peaks, while the relatively well-mixed layers separating them were associated with stability minima. This step-like decrease in particle concentrations, also seen during the Sept. 3 station occupation at PL6, may be attributable to discrete mixing events affecting the upper water column.

Distributions in the middle domain (Fig. 46, PL 14) were similar although the vertical particle gradients were generally steeper because of the sharper density gradients. The sigma-t curve, for instance, exhibited more of a discrete two-layer character without the intermediate middle layer seen in the outer domain. This change was reflected in a very low diffusion cap on the bottom nepheloid layer. Also, this layer at PL14 was partitioned into three mixing zones instead of the two observed at PL6.

As expected, distributions in the coastal zone were vertically uniform (Fig. 46, PL24). Water column stability was near zero everywhere and turbulence had thoroughly mixed the particles.

Coefficients of vertical eddy diffusion for particles can be estimated from the attenuation profiles in Fig. 45 using a sediment mass continuity equation:

$$\frac{\delta C}{\delta t} + \bar{u}\,\frac{\delta C}{\delta x} + \bar{v}\,\frac{\delta C}{\delta y} + (\bar{w} - w_s)\,\frac{\delta C}{\delta z} =$$

$$\frac{\delta}{\delta y}\left(K_y\,\frac{\delta C}{\delta y}\right) + \frac{\delta}{\delta z}\left(K_z\,\frac{\delta C}{\delta z}\right)$$

where C is the SPM concentration in mass per unit volume; $\bar{u}$, $\bar{v}$, and w are the mean advective flows in the horizontal and vertical directions; ws is the SPM settling velocity; and K_y and K_z are the horizontal and vertical eddy diffusion coefficients. This equation can be simplified by assuming a steady state situation ($\delta C/\delta t$ = O), and $\delta C/\delta y$ and $\delta C/\delta x$ negligible compared to $\delta C/\delta z$; thus:

$$0 = \frac{\delta}{\delta z} \left[K_z \frac{\delta}{\delta z} + (\bar{w} - w_s)C\right]$$

and

$$\frac{C_z}{C_a} = \exp \left[-\int_a^z \frac{(\bar{w} - w_s)}{K_z} dz\right]$$

where C_z is the concentration level of SPM at some level z above a reference level C_s" Levels of approximately constant K_z are assumed wherever a semi-log plot of C vs. depth yields a straight line, and K_z in these intervals may be evaluated by the expression:

$$K_z = \frac{(\bar{w} - w_s)\,(z-a)}{\text{in}\ (C_z/C_a)}$$

Station PL6 was visited twice (August 29 and September 3) and showed little change in the vertical gradients, justifying the steady state assumption.

K_z can be accurately estimated for each interval only if the term $\bar{w}$ - ws (the sum of vertical advection and particle settling velocity) is known. The settling velocity can be estimated from the Stokes equation

$$w_s = \frac{2g\,(\rho_s - \rho)r^2}{9\,\eta}$$

if the particles are assumed to be spherical and their radius (r) and net density (ρ_s - p) is known, and if the viscosity of the water (η) is known. The PSD's yield limits on the size range at various depths, but the in-situ density of the particles is unknown at present. Furthermore, since w_s for most particles is likely to be in the range of 10^{-2} to 10^{-4} cm see-l, the vertical advection term is likely to be an important factor. J. Schumacher (personal communication) has suggested that the vertical advection term in the southeastern Bering Sea, particularly in frontal areas, may be on the order of 10^{-3} cm see-l.

For comparative purposes, then, Table 8 gives values of $K_z/(w - w_s)$ for each interval. Values of K_z are also calculated for some reasonable values of $(\bar{w} - w_s)$. Certain trends are clear from these data. Turbulent mixing is always highest in the tidally mixed bottom layer. Above this layer, values of K_z decrease either abruptly or by means of a transition layer into a layer of low K_z which ends in the uniform concentrations of the mid-depth low turbidity zone. At PL14, this decrease in K_z was a factor of 100 in the space of -20 m.

The presence of diffusive barriers to particle mixing from the surface and bottom layers implies that transport of fine-grained particles from the surface to the bottom layers must occur primarily by large particles (e.g., biological aggregates such as fecal pellets) whose transit is not seriously impeded by the density structure. Similarly, fine-grained particles in the bottom layer are not easily mixed up into the overlying waters except when stratification breaks down, as in the coastal domain and in the middle domain during winter or during major storm events.

Table 8

Calculation of vertical eddy diffusion coefficients (K_z) from SPM profiles

STA.	z (m above bottom)	a	$\ln(C_z/C_a)$	$K_z/(\bar{w} - w_s)$	K_z ($cm^2 sec^{-1}$): $\bar{w} = 0$, $r = 5\ \mu m$, $(\rho_s - \rho) = 1.5$	$\bar{w} = 0$, $r = 5\ \mu m$, $(\rho_s - \rho) = 0.15$	$\bar{w} = 10^{-3}$, $r = 5\ \mu m$, $(\rho_s - \rho) = 1.5$	$\bar{w} = 10^{-3}$, $r = 5\ \mu m$, $(\rho_s - \rho) = 0.15$
PL-6	35	5	-0.38	-7905	14.8	1.5	6.9	0.7
	60	35	-1.47	-1700	3.2	0.3	1.5	0.2
PL-14	12	5	-0.01	-74549	139.4	13.5	64.9	6.5
	24	12	-0.31	- 3912	7.3	0.7	3.4	0.3
	31	24	-1.18	- 594	1.1	0.1	0.5	0.1

B. Characteristics of the particle domains and domain boundaries

1. Offshore transport of suspended particles

One of the goals of this project was to evaluate the effectiveness of the coastal front off the NAS region in prohibiting offshore transport of particles. To examine this question, offshore trends of average attenuation and average salinity were plotted against water depth for each survey period (Fig. 47). Figure 47 was constructed by averaging all NA stations (except NA 1-16, where properties were largely controlled by rivers in Kvichak Bay) within each of eight successive depth increments: 10-19, 20-29, 30-39, 40-49, 50-59, 60-69, 70-79, and ≥80 m. Average water column attenuation and salinity from each of these intervals then gave a meaningful picture of the offshore gradations of these properties.

The offshore trends of salinity and attenuation followed each other closely during each survey period. The steepest gradients were always found inshore of the 50-m isobath, with attenuation increasing sharply in the 10-19 m interval. Average attenuation seaward of 50 m was essentially uniform, with a value of ~0.8 m^{-1} during NASTE 1, 0.5 ❑ -l during NASTE 2, and 0.7 m^{-1} during NASTE 3. Salinity showed a continual decline in the deeper waters, however, except during the winter when values were stable.

As reported in the RESULTS section, the coastal front was best developed during NASTE 1 and 3; during NASTE 2 vertical stratification was absent throughout the region and so the coastal front, defined as the zone separating two differing structural domains, did not exist. Nevertheless, offshore attenuation gradients were virtually identical to the fall and spring cruises. This situation implies that the coastal front should not be thought of as a "barrier" to the passage of suspended particles in the

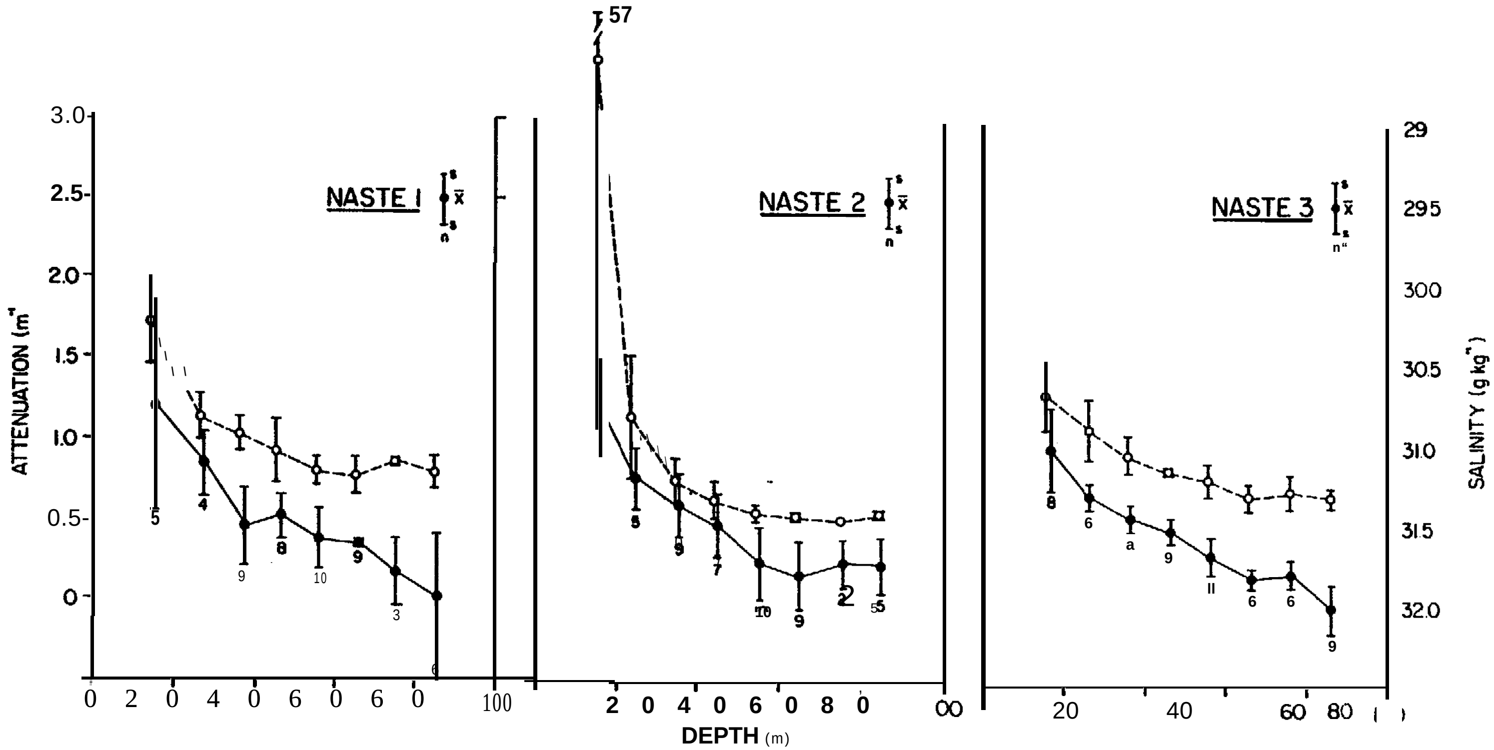

Figure 47. Attenuation (open circles) and salinity (closed circles) gradients normal to the Alaska Peninsula for each cruise. Mean attenuation and salinity values from each NA station were grouped and averaged over 10-m station depth increments.

water column. Particle concentrations are high inshore of 50 m because mixing energy, both tidal and wind, is highest there. Mean near-bottom current speeds at stations TP4, TP6, and TP9 (z >59m) ranged from 15 to 22 cm sec^{-1}. At stations TP2, TP2B, TP8, and TP7 (z < 35 m), the range was 28 to 33 cm sec^{-1}. Bathymetry determines the positions of the fronts in the southeastern Bering Sea (Kinder and Schumacher, 1981a) and also exerts a powerful influence on the offshore transport of particles. This influence can most clearly be seen during winter, when in-situ particle sources (phytoplankton) are minor and local particle maxima and minima are reduced by vigorous vertical mixing. Examination of the areal distribution of attenuation during NASTE 2 (Figs. 10 and 11) shows that the 0.6 m^{-1} contour precisely follows the 50-m isobath. The 50-m isobath also marks the onset of a change in the bottom sediment texture (Fig. 5). Inshore, the mean size is almost exclusively 125 µm or greater. Seaward of 50m, the mean grain sizes become more variable and finer grained, attributes of a lower energy environment.

2. Vertical ❑ixing of particles

Vertical mixing of particles is complete in the coastal zone except for isolated instances where large freshwater sources form a low-density surface plume. Direct evidence for this mixing comes from the many transmissometer casts taken in the nearshore zone. Records from the moored transmissometers showed significant peaks in the attenuation spectra at tidal frequencies (Fig. 36), implying that variation in current speeds is a principal controlling element in the variation of particle concentrations. The correlation of sedimentation rate, turbidity record, and mean current speed was also highest at TP7 in the nearshore zone (Fig. 39).

These results describe a high energy environment where particles are routinely cycled throughout the water column. Median particle sizes in the water column are typically an order of magnitude lower than the bottom sediments. The suspended particles are thus largely in a state of transit through this zone, with little deposition occurring. The major particle sources are local rivers, shore erosion, and biogenic detritus; the influence of rivers such as the Kvichak and Nushagak is not important south of about 57°N along the coast. Port Moller is the only major source of particles in the study region, and even its influence is not felt beyond about 100 km from its mouth (Fig. 10). Particle losses to the middle domain occur by mixing and diffusion of low-salinity coastal water with the higher salinity offshore water, as well as by advective processes such as upwelling by which coastal water is replaced by offshore water.

Vertical mixing in the middle and outer domains is highly dependent on density stratification. Following Coachman and Charnell (1979), the fronts separating the middle and outer domains can be identified by a sharp increase in the horizontal gradient of the 0-100 m average salinity (Fig. 48). Increases in the vicinity of PL8-9 (~110 m) and PL3 (~150 m) were apparent during NASTE 3, agreeing with historical values of ~ 9.3×10^{-3} g kg^{-3} m^{-1} (Coachman and Charnell, 1979). Frontal characteristics were much less apparent during NASTE 1.

These hydrographic differences directly influenced the horizontal and vertical distributions of particles. During NASTE 3, the mid-depth low-turbidity zone was well developed and uniform seaward of PL9; the minimum attenuation value for these stations averaged 0.42 ± 0.026 m^{-1} (Fig. 49). Landward of PL9, the comparable value was 0.76 ± 0.093, a 76% increase.

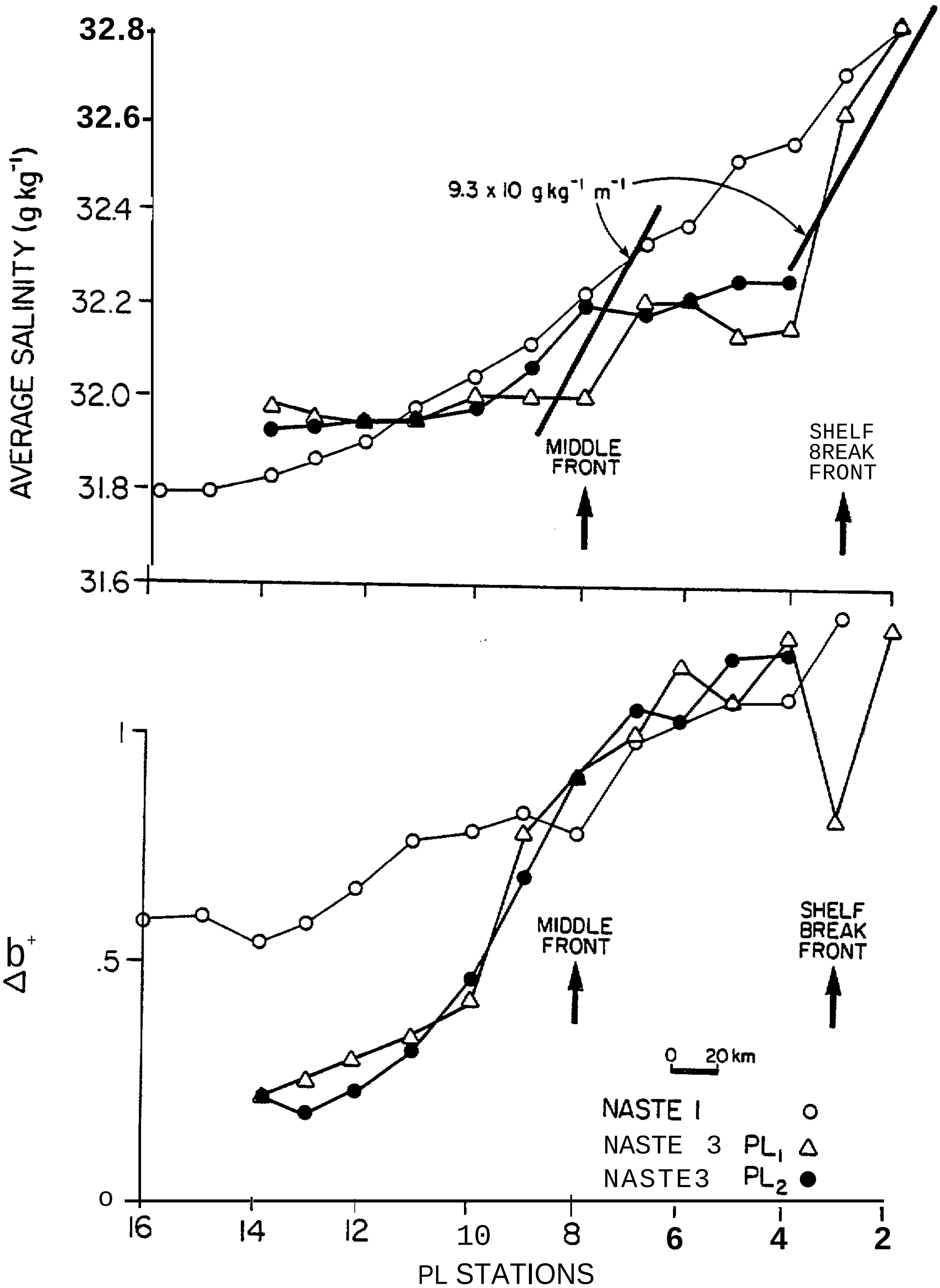

Figure 48. Salinity and $\Delta\sigma_t$ gradients along the PL line during **NASTE** 1 and **NASTE** 3.

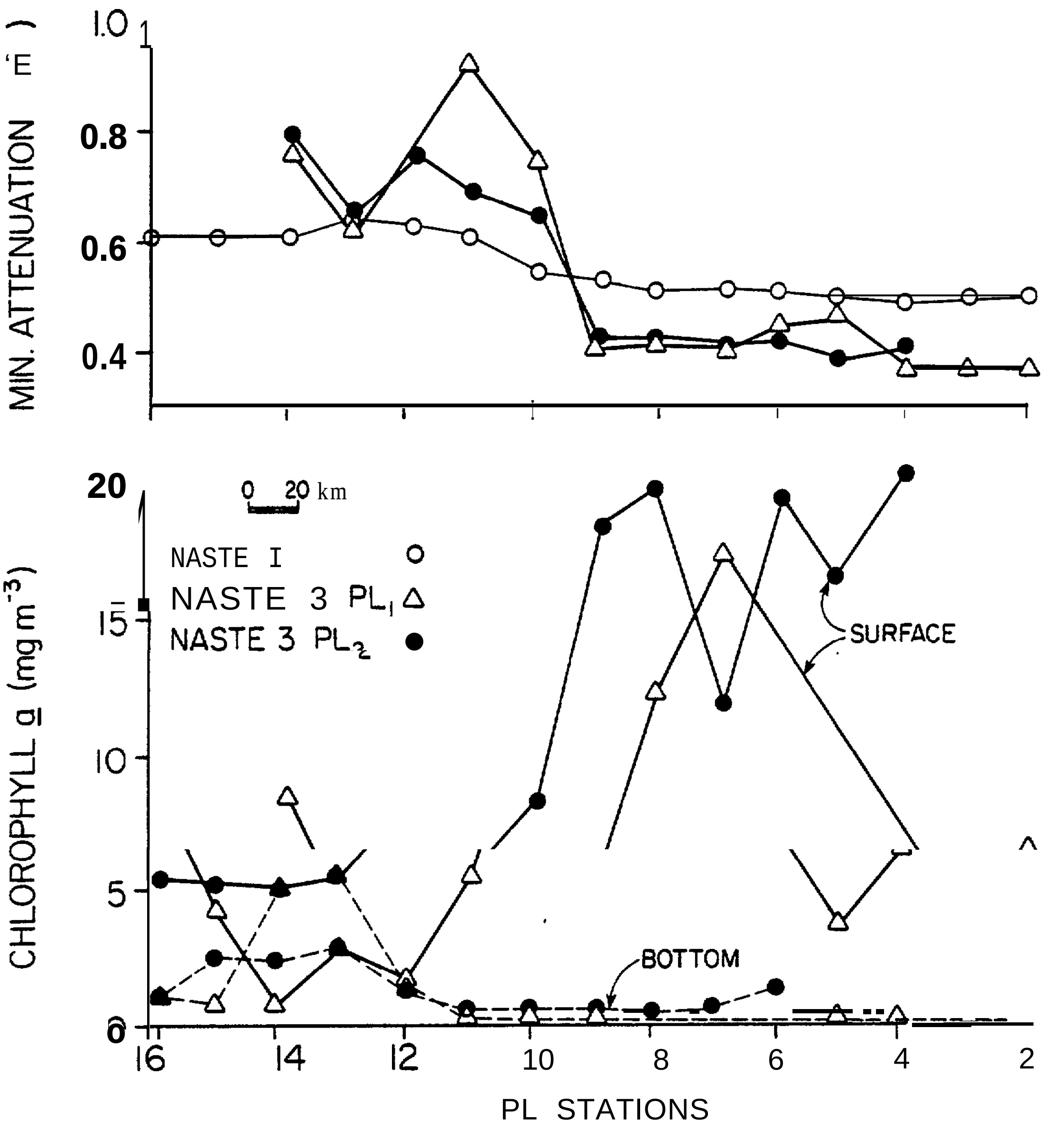

Figure 49. Changes in the attenuation value in the turbidity minimum and in the concentration Of surface and bottom chlorophyll a along the PL line. Compare the position of these changes with the hydrographic changes in Figure 48.

Average attenuation over the entire water column increased by **only** 22% (from $0.70 \pm 0.056\ m^{-1}$ to $0.86 \pm 0.051\ m^{-1}$) from the outer to middle domain. These figures imply that increases in the mid-depth region of the water column are attributable *to* enhanced vertical mixing of *the* surface and bottom layers which were previously isolated by high $\Delta\sigma_t$ values. This interpretation is supported by the PL cross-sections in Figs. 41 and 42. Particle concentrations in the surface and bottom layers decline crossing the middle front region from outer domain to middle domain. **This** vertical mixing is also graphically demonstrated by a plot of the surface and bottom chlorophyll a concentration along the **PL** line during **NASTE** 3 (Fig. 49). In **the** outer domain, surface values are -30 x greater than bottom values. **In** the middle domain, however, surface values decline and bottom values increase until both are about equal. Particle size distribution curves similarly show dramatic differences between middle and outer domain stations (Fig. 45).

During **NASTE** 1, however, stratification remained relatively high throughout the middle domain (Fig. 48), resulting in the maintenance of a well-defined, three-layer particle distribution seaward of **PL18** (Fig. 40). Average value of the minimum attenuation between PL2 and PL10 was $0.52 \pm 0.02\ m^{-1}$; between **PL11** and 16 this value increased only 19%, to $0.62 \pm 0.01\ m^{-1}$. The change in the average water column attenuation over the same interval was **28%**, from $0.78 \pm 0.06\ m^{-1}$ to $1.00 \pm 0.09\ m^{-1}$. Unlike the situation during NASTE 3, vertical mixing of fine-grained particles was inhibited throughout the middle domain. The particle size distribution data also showed homogeneity in the minimum zone throughout the middle and outer domains (Fig. 43).

The mixing processes described above should not be interpreted to mean that no particle exchange occurs between the surface and bottom layers.

Fine-grained particles of both biogenic and non-biogenic origin are continually packaged into large biological particles such as fecal pellets which rapidly fall to the seafloor. On the seafloor, or in the water column, these large particles may be broken up and their constituent particles dispersed into the water column. This transport method is only applicable to particles dense enough to overcome the buoyancy effects of stratification and turbulence in the surface layer. Thus large organic-rich, low-density floes may not be important in the vertical transport of material in stratified waters.

C. Particle Influences on the Transport of Spilled Oil in the Southeastern Bering Sea

The vertical sediment flux ❑ easurements reported here, combined with data on oil loading on various sediment types from SAI studies (Payne et al., 1981), can be used to produce crude estimates of the vertical transport of spilled oil to the seafloor. It must be emphasized that such calculations are extremely speculative. Sediment trap data give the mass of particles passing through a particular depth horizon over a given time with no implications about the origin of such material. Material may be added by surface fallout, mid-depth horizontal advection, or bottom sediment resuspension, and so the interpretation of sediment trap data as it affects the removal of oil from the water column is difficult.

Similarly, the SAI data relating oil loading on various sediment types may not be directly applicable to suspended particles. The SAI studies were all performed on samples of deposited sediments, which may have oil absorption characteristics quite different from the suspended particles described in this report.

Bearing these difficulties **in** mind, we ❑ ay use the available data to generate some oil transport figures to set the scale of the problem. Five sediment types were tested in-the SAI study: (1) Kasitsna Bay 1: fine-grained terrestrial sediment plus diatoms, many flakes $\leqq$ 5 **µm,** total **aliphatic** plus aromatic loading of 527 mg per kg of sediment; (2) **Kasitsna** Bay **2A:** surface **(<** 1 cm deep) sediment mostly > 5 pm, terrestrial material plus-some plant debris, 1216 *mg oil* per **kg** sediment; (3) **Kasitsna** Bay 2B: below surface (l-8 cm) sediment mostly> 5 pm, 744mg oil per kg sediment; (4) **Kasitsna** Bay 3: consolidated sediment >90% diatoms , some **terrigenous** material **$\leqq$5** pm, 122 **mg** oil per kg sediment ; and **(5) Kasitsna** Bay 4: salt marsh material, organic matter plus fecal pellets, 694 ❑ g oil per kg sediment.

The oil loading data can be combined with the sediment data in two ways. First, the range **of** oil loadings observed can be combined with typical sediment concentrations from different depth zones of the North Aleutian Shelf (Fig. 47) to derive a range of accommodated **oil** loadings for the NAS waters. Average attenuation values from Fig. 47 were transformed into particle mass concentrations using the regression equations in Table 1. The calculations in Table 9 indicate that sediment accommodated oil loadings ❑ ight vary from -10 to 100 **mg** m^{-2} in the near-shore zone, and from -5 to 60 ❑ g m^{-2} in the offshore zone if **all** the suspended particles were loaded with oil in the manner of the sediments tested by SAI. These loadings translate into -0.7 to 7 ppb total concentration of oil in the near-shore zone water column and **~0.06** to 1.1 ppb in the offshore zone. Oil not associated with particles, of course, is not considered here.

A second method of treating the data is to consider the possible delivery rates of accommodated oil to the benthos by combining the sediment trap data with the oil-loading studies. The figures in Table 10 represent the oil sedimentation expected under the minimum, mean, and maximum fluxes observed at each trap site if the sedimenting material had the characteristics of the various sediments tested in the SAI study. The maximum value is ~30 mg m^{-2} day^{-1} for KB2A at either TP7 or TP9. Mid-shelf values (TP8 and TP2B) never exceed 7 mg m^{-2} day^{-1}. Mean values are generally in the range 1-10 mg m^{-2} day^{-1}.

Table 9

Estimated oil loading on NAS suspended sediments

Depth Zone (m)	Average Sediment Loading ($g m^{-2}$)	Sediment Accommodated Oil Loading (mg m^{-2})				
		KBI (527 mg kg^{-1})[1]	KB2A (1216 mg kg^{-1})	KB2B (747 mg kg^{-1})	KB3 (122 mg kg^{-1})	KB4 (694 mg kg^{-1})
10-19	79.0	41.6	96.1	58.8	9.6	54.8
40-49	41.1	21.7	50.0	30.6	5.0	28.5
80-89	48.4	25.5	58.8	36.0	5.9	33.6

[1]Measured SAI oil loading per kg of sediment (Payne et al., 1981).

Table 10

Estimated oil sedimentation rates in NAS waters

Trap Site	Water Depth (m)	Oil Sedimentation Rate ($mg\ m^{-2}\ day^{-1}$) KBI min	KBI mean	KBI max	KB2H min	KB2H mean	KB2H max	K2B min	K2B mean	K2B max	KB3 min	KB3 mean	KB3 max	KB4 min	KB4 mean	KB4 max
TP 7	24	2.4	5.9	12.8	5.6	13.6	29.4	3.4	8.3	18.0	0.6	1.4	3.o	3.2	7.8	16.8
TP8	31	0.1	0.9	1.3	0.3	2.2	2.9	0.2	1.3	1.8	0.03	0.2	0.3	0.2	1.2	1.7
TP2B	35	0.4	1.7	3.0	1.0	3.9	6.9	0.6	2.4	4.2	0.1	0.4	0.7	0.5	2.2	4.0
TP9	89	0.9	5.1	13.9	2.2	11.7	32.1	1.3	7.1	19.6	0.2	1.2	3.2	1.2	6.7	18.3

VII. ACKNOWLEDGEMENTS

This study could not have been conducted without the support of many other people in both the field and the laboratory. D.A. Tennant and S.L. Walker were of continuing help throughout this project. The captains and crews of the NOAA ships *Surveyor* and *Discoverer* made the field studies possible. The work was supported by the Office of Marine Pollution Assessment, Alaska Office.

VIII. REFERENCES

Bader, H. (1970). The hyperbolic distribution of particle size. J. Geophys. Res. 75, 2822-2830.

Baker, E.T. (1973). Nephelometry and mineralogy of suspended particulate matter in the waters over the Washington Continental slope and Nitinat Deep-Sea Fan. Ph.D. dissertation, Univ. of Washington, Seattle, 142 PP.

Baker, E.T. (1982), Suspended particulate matter in Elliott Bay. NOAA Tech. Rept. ERL 417-PMEL 35, 44pp.

Baker E.T., J.D.Cline, R.A.Feely, and J. Quan (1978). Seasonal distribution, trajectory studies, and sorption characteristics of suspended particulate matter in the northern Puget Sound region. EPA-600 17-78-126, 140 pp.

Baker, E.T., R.A. Feely, and K. Takahashi (1979). Chemical composition, size distribution, and particle morphology of suspended particulate matter at DOMES sties A, B, and C: Relationships with local sediment composition. In Marine Geology and Oceanography of the Pacific Manganese Nodule Province (J. Bischoff and D.Z. Piper, eds.), Plenum, New York, pp. 163-201.

Baker, E.T., and H.B. Milburn (in press). An instrument system for the investigation of particle fluxes. Cont. Shelf Res.

Bartz, R., J.R.V. Zaneveld, and M. Pak (1978). A transmissometer for profiling and moored observations in water. SPIE Ocean Optics V, 106, 102-108.

Bassin, N.J. (1974). Suspended matter and the stability of the water column: Central Caribbean Sea. In Suspended Solids in Water (R.J. Gibbs, cd.), Plenum, New York, pp. 271-279.

Biscaye, P.E. and S.L. Eithreim (1974). Variations in benthic boundary layer phenomena: Nepheloid layer in the North American Basin. In Suspended Solids in Water (R.J. Gibbs, cd.), Plenum, New York, pp. 271-279.

Brun-Cottan, J.C. (1976). Stokes settling and dissolution rate model for marine particles as a functioning size distribution. J. Geophys. Res., 81, 1601-1606.

Carder, K.L., and F.C. Schlemmer, II (1973). Distribution of particles in the surface waters of the eastern Gulf of Mexico: An indicator of circulation. J. Geophys. Res., 78, 6286-6299.

Coachmen, L.K., and R.L. Charnell (1979). On lateral water mass interaction--A case study, Bristol Bay, Alaska. J. Phys. Oceanogr., 9, 278-297.

Crecelius, E.A., M.M. Bothner, and R. Carpenter (1974). Geochemistries of arsenic, antimony, mercury, and related elements in sediments of Puget Sound. Env. Sci. Tech., 9: 325-333.

Feely, R.A., G.J. Massoth, A.J. Paulson, M.F. Lamb, and E.A. Martin (1981). Distribution and elemental composition of suspended ❑atter in Alaskan coastal waters. NOAA Tech. Memo. ERL PMEL-27, 119 pp.

Gardner, W.D. (1980a). Sediment trap dynamics and calibration: a laboratory evaluation. J. Mar. Res., 38, 17-39.

Gardner, W.D. (1980b). Field assessment of sediment traps. J. Mar. Res., 38, 41-52.

Hannan, C.A., and W.D. Grant (1982). Evaluating sediment trap biases in natural flows. EOS, 63, 46.

Helm-Hansen, O., C.J. Lorenzen, R.W. Holmes, and J.D.H. Strickland (1965). Fluorometric determination of chlorophyll. J. Cons. Int. Explor. Mer., 30, 3-15.

Iverson, R.L. L.K. Coachman, R.T. Cooney, T.S. English, J.J. Goering, G.L. Hunt, Jr., M.C. MaCauley, C.D. McRoy, W.S. Reeburgh, and T.E. Whitledge (1979). Ecological significance of fronts in the southeastern Bering Sea. In Ecological Processes in Coastal and Marine Systems (R.S. Livingston, cd.), Plenum, New York, pp. 437-466.

Johnson, D. A., S.E. McDowell, L.G. Sullivan, and P.E. Biscaye (1976). Abyssal hydrography, nephelometry, currents, and benthic boundary layer structure in the Vema Channel. J. Geophys. Res., 81, 5771-5786.

Kinder, T.H. and J.D. Schumacher (1981a). Hydrographic structure over the continental shelf of the southeastern Bering Sea. In The Eastern Bering Sea Shelf: Oceanography and Resources, vol. 1,(D.W. Hood and J.A. Calder, eds.), NOAA/Office of Marine Pollution Assessment, pp. 31-52.

Kinder, T.H. and J.D. Schumacher (1981b). Circulation over the continental shelf of the southeastern Bering Sea. In The Eastern Bering Sea Shelf: Oceanography and Resources, vol. 1, (D.W. Hood and J.A. Calder, eds.), NOAA/Office of Marine Pollution Assessment, pp. 53-75.

Kitchen, J.C., J.R.V. Zaneveld, and M. Pak (1978). The vertical structure and size distributions of suspended particles off Oregon during the upwelling season. Deep-Sea Res., 25, 453-468.

Lal, D. and A. Lerman (1973). Dissolution and behavior of particulate biogenic matter in the ocean: Some theoretical considerations. J. Geophys. Res., 78, 7100-7111.

Landing, W.M. (1978). The chemistry and vertical flux of particulate materials in the N.E. Gulf of Alaska. M.S. Thesis, Univ. of Washington, Seattle, 101 pp.

Lerman, A., K.L. Carder, P.R. Betzer (1977). Elimination of fine suspensoids in the oceanic water column. Earth Planet. Sci. Lett., 37: 61-70.

Liss, P.S. (1976). Conservative and non-conservative behavior of dissolved constituents during estuarine mixing. In Estuarine Chemistry (J.D. Burton and P.S. Liss, eds.), Academic Press, London, pp. 93-130.

McCave, I.N. (1975). Vertical flux of particles in the ocean. Deep-Sea Res., 22, 297-310.

Meyers, P.A. and J.G. Quinn (1973). Factors affecting the association of fatty acids with mineral particles in seawater. Geochim. Cosmochim. Acts, 37, 1745-1759.

Natrella, M.G. (1963). Experimental Statistics, Nat. Bureau of Standards, 504 pp.

Newberger, P.A. and D.R. Caldwell (1981). Mixing and the "bottom nepheloid layer. Mar. Geol., 41, 321-327.

Payne, J.R., B.E. Kirstein, R.E. Jordan, G.D. McNabb, Jr., J.L. Lambach, M. Frydrych, W.J. Paplawsky, G.S. Smith, P.L. Mankiewicz, R.T. Redding, D.M Baxter, R.E. Spenzer, R.F. Shokes, and D.J. Maiero (1981). Multivariate analysis of petroleum weathering in the marine environment--Sub Arctic. Annual Rept. to NOAA/Office of Marine Pollution Assessment (Alaska Office).

Pearson, C.A., E.T. Baker, and J.D. Schumacher (1980). CTD and SPM observations during reestablishment of a structural front: Bristol Bay, Alaska. EOS, 61, 1002.

Sharma, G.D. (1979). The Alaskan Shelf: Hydrographic, Sedimentary, and Geochemical Environment. Springer Verlag, New York.

Schuman, F.R. and C.J. Lorenzen (1975). Quantitative degradationof chlorophyll by a marine herbivore. Limnol. Oceanogr., 20, 580-586.

Tyler, J.E., R.W. Austin, and T.J. Petzald (1974). Beam transmissometers for oceanographic measurements. In Suspended Solids in Water (R.J. Gibbs, cd.), Plenum, New York, pp. 51-60.

IX. APPENDICES

Appendix A: Discrete sample data from Cruise RP4SU804. NASTE 1

Station	Cast #	Depth m	SPM mg/ℓ	% Organic Matter	Size Distribution Slope
NA46	6	2	2.304	42	
		17	5.908	32	
NA44	8	2	1.262		
		35	1.412		
NA42	10	2	0.350		
		66	1.356		
PMI	11	2	0.459		
NA40	12	2	1.958	36	
PM3	13	2	1.725		
NA38	15	2	1.782		
		35	0.263		
NA36	17	2	0.736		
NA34	19	2	0.600	37	
		40	1.158		
NA4-A	24	2	4.068	39	
		17	2.586	42	
NA3-A	26	2	1.996	32	
NA2-A	2?	2	1.490	34	
		25	2.448	27	
NA1-A	28	2	0.994	52	
		36	2.792	40	
NA5	29	2	0.636	61	
		37	6.134	32	

Station	Cast #	Depth m	SPM mg/ℓ	% Organic Matter	Size Distribution Slope
NA6	30	2	0.793	47	
		36	1.730	30	
NA7	31	2	1.484		
		38	1.872	31	
NA8	32	2	1.036	38	
		34	1.046	41	
NA9	33	2	1.165	32	
		28	2.984	35	
NA1O	34	2	1.320	65	
		24	4.371	45	
NA16	36	2	1.683		
NA15	37	2	1.020	43	
		37	1.614	21	
NA14	38	2	1.303	55	
		44	6.241	32	
NA12	40	2	0.840	48	
		40	3.721	32	
NA18	44	2	0.732	46	
NA20	46	2	0.194	4	
NN22	48	2	1.837	44	
		17	2.253	40	

Station	Cast #	Depth m	SPM mg/ℓ	% Organic Matter	Size Distribution Slope
NA27	49	2	2.315	34	
		18	3.004	35	
NA25	51	2	1.221	42	
		45	1.222	57	
NA23	53	3	0.575	57	
NA29	55	2	0.461	53	
		58	2.509	28	
NA31	57	2	0.196	44	
		45	1.304	15	
NA33	59	2	1.805	47	
		22	1.731	48	
NA40	61	2	1.308	35	4.16
		12	3.168	27	3.23
NA39	62	2			2.84
		17			3.62
NA38	63	2	0.873		2.75
		32	0.999		4.14
NA37	64	2			3.10
		47			3.40
NA35	65	2	0.426		3.73
		64	0.649		3.45
NA34	66	2			3.38
		65			2.50
NA34-B	67	2	0.589	36	2.70
		84	0.595	44	3.12

Station	Cast #	Depth m	SPM mg/ℓ	% Organic Matter	Size Distribution Slope
NA41	68	2	0.273	46	
		86	1.340	27	
NA43	70	2	0.421		
		56	3.116		
NA45	73	2	0.789		
NA52	75	4	4.363	26	
		19	5.685	22	
NA50	77	2	0.867	40	
		50	2.371	22	
NA48	79	2	0.383	45	
		72	0.413	32	
NA47	80	2	0.404	44	
		68	0.518	30	
NA58-A	81	2	0.713	50	
		32	0.643	44	
NA40	83	2	3.535	33	
NA59	86	2	0.464	44	
NA61	87	2	1.397	40	
NA64	89	3	0.894	48	
		35	1.682	31	

Station	Cast #	Depth m	SPM mg/ℓ	% Organic Matter	Size Distribution Slope
NA72	91	2	1.144	46	
		34	1.078	3s	
NA69	93	2	0.392	74	
		105	1.147	20	
SG5	96	2	1.021		
		124	1.822		
SG4	97	2	0.395		
SG2	98	3	0.195		
		50	0.132		
		150	0.204		
		296	0.222		
PL3	106	2			4.26
		50			4%12
PL4	107/108	2	0.205		3.52
		50			3.95
		100	0.265		
		137	1.024		4.15

Station	Cast #	Depth m	SPM mg/ℓ	% Organic Matter	Size Distribution Slope
PL6	110	2	0.409		4.75
		126	1.924		4.26
PL8	112	2			5.32
		60			4.09
		118	1.463		4.10
PL1O	114	2	0.048		4.97
		40	0.494		
		60			4.41
		85	1.144		4.26
PL12	116	2	0.303		5.30
		40	0.317		4.27
		75	1.915		4.26
PL14	118	2			4.75
		40	0,231		4.25
		60	1.554		
		72	1.526		4.16
PL16	120	2	0.362		4.75
		50	1.627		
		63	1.477		3.92
PL18	122	2	0.590		3.81
		30			3.86
		46	4.148		3.71
PL20	125	2			4.01
		40			3.73

Station	Cast #	Depth ❑	SPM mg/ℓ	% Organic Matter	Size Distribution Slope
NA45	139	2	0.564		
		31	1.370		
NA36	142	2	0.550		
		52	0.735		
NA38	144	2	0.439		
		30	1.364		
NA40	147	2	0.201	53	
NA33	149	2	1.566	44	
		10	1.464	46	
NA31	151	2	0.651	68	
		39	0.452	67	
NA29	153	58	0.308	45	
NA24	156	2	0.497	94	
		54	0.823	39	
NA26	158	2	0.942	58	
		24	0.193		

Appendix B: Discrete sample data from cruise RP4SU81A NASTE 2

Station	Cast #	Depth m	SPM mg/ℓ	% Organic Matter	Size Distribution Slope -
NA28	2	2	0.435	54	
		17	0.544		
		65	0.518	57	
NA31	5	2	0.940	38	
		36	1.418	33	
NA40	8	2	5.506	27	
		16	16.202	20	
NA38	10	2	0.871	51	
		31	1.125	37	
NA36	12	2	0.434	39	
		25	0.435		
		49	0.578	45	
NA34	15	2	0.438	40	
		24	0.422		
		54	0.520	56	
NA46	16	2	2.250	27	
		21	2.183	32	
NA44	18	2	0.991	47	
		30	0.954	51	
NA41	21	2	0.326	50	
		80	0.459	41	
SG11	22	2	0.146		
		44	0.208		
		50	0.216		
		78	0.811		

Station	Cast #	Depth m	SPM mg/ℓ	% Organic Matter	Size Distribution Slope
PL10	24	2	0.217		
		48	0.217		
		68	0.562		
		79	1.032		
NA52-B	29	2	9.851	18	
		10	7.662	23	
NA50	31	2	0.569	48	
		42	0.649	45	
NA47	34	2	0.416	43	
		55	0.511	40	
NA1-A	35	2	2.601	25	
		7	2.401		
		24	3.454	26	
NA4-A	39	2	3.893	17	
		11	2.890	23	
NA10	41	2	1.789	24	
		17	2.008	23	
NA8	43	2	0.905	48	
		23	1.228	68	
NA5	46	2	0.786	50	
		15	0.821		
		31	1.065	45	
NA11	47	2	0.495	38	
		45	0.638	43	
NA14	50	2	0.546	46	
		31	0.742	60	

Station	Cast #	Depth m	SPM mg/ℓ	% Organic Matter	Size Distribution Slope
NA16	52	2	1.417	34	
PM3(A)	57	2	6,821		
		14	5,596		
		12	3.404		
PM3(C)	60	2	4.898		
		5	5.031		
		10	4.481		
PM3(D)	62	2	17.058		
		12	19.022		
		15	18.302		
PM3(F)	65	2	12.300		
PM3(G)	67	2	4.464		
		15	4.489		
PM3(H)	69	2	3.996		
		13	4.016		
PM3(I)	71	2	7.015		
		13	5.736		
NA22	73	2	1.293	31	
		23	1.361	33	
NA20	75	2	1.933		
		35	0.874	47	

Station	Cast #	Depth m	SPM mg/ℓ	% Organic Matter	Size Distribution Slope
NA17	78	2	0.497	50	
NA23	79	2	0.552	35	
		60	0.629	40	
NA25	81	2	0.518		
NA27	83	2	3.687	31	
		21	3.134	28	
NA33	84	2	3.890	23	
NA31	86	2	0.729	30	
NA28	89	2	0.329	45	
NA34	90	2	0.371	47	4.08
NA35	91	2			4.29
NA36	92	2	0.440	43	3.84
NA37	93	2			3.94
NA38	94	2	1.606	33	4.24
		31	1.417	29	4.17

Station	Cast #	Depth m	SPM mg/ℓ	% Organic Matter	Size Distribution Slope
NA39	95	2			3.59
		14			3.36
NA40	96	2	11.506	17	3.10
		5	9.339		
		10	9.893	17	3.24
NA46	97	2	2.588	25	
		18	2.384	27	
NA44	99	2	0.702	42	
		40	0.832	25	
NA41	102	2	0.234	52	
		84	0.479	42	
NA47	103	2	0.212	53	
		67	0.417	42	
NA50	106	2	0.447	45	
		55	0.568	33	
NA52	108	2	3.556	16	
		16	4.697	16	
NA53	109	2	0.208	61	
		60	0.456		
		83	0.533	33	
NA56	112	2	0.444	45	
		39	0.489	37	
NA58	114	2	0.920	35	
		21	1.250	24	
NA65	115	2	0.538	29	
		15	0.423		
		31	1.601	21	

Station	Cast #	Depth m	SPM ❑ g/!2	% Organic Matter	Size Distribution Slope
NA63	117	2	0.328	44	
		44	0.496	35	
NA61	119	2	0.226	60	
NA59	121	2	0.264	57	
NA72	122	2	0.628	32	
		45	0.749	31	
NA70	124	2	0.368	39	
		66	0.596	31	
NA68	126	2	0.322		
		102	1.139	23	
PL4	127	2	0.175		3.84
		120	0.762		
		133	0.794		3.72
PL6	128	2			4.30
SG28	129	116			4.08
PL8	131	2			3.95
PL1O	132	2	0.181		4.11

Station	Cast #	Depth m	SPM mg/ℓ	% Organic Matter	Size Distribution Slope
PL12	133	2			3.91
		76			3.61
PL14	134	2			4.16
		69	0.603		
		38	0.182		
		78	1.204		
		110	1.165		
SG26	143	2	0.260		
SG43	146	2	0.183		
		60	0.216		
		128	0.599		
SG29	150	2	0.181		
		130	1.446		
SG46	152	2	0.250		
UP10	153	2	0.394		
		285	0.220		

Station	Cast #	Depth m	SPM mg/ℓ	% Organic Matter	Size Distribution Slope
UP12	155	2	0.465		
		56	0.439		
		74	0.385		
		82	0.378		
		105	0.377		

Appendix C: Discrete sample data from cruise RP4DI81A

Station	Cast #	Depth m	SPM mg/ℓ	% Organic Matter	Size Distribution Slope
NA41	9	2	0.664	64	
		40	1.069		
		81	1.189	30	
NA42	11	2	0.854	53	
		40	0.973		
		63	1.250	38	
NA43	12	2	0.649	37	
		30	1.265		
		56	1.185	36	
NA44	13	2	0,468	45	
		20	0.777		
		37	2.242	39	
NA45	14	2	0,893	52	
		27	2.714	35	
NA46	15	2	1.637	58	
NA40	16	2	2.139	20	
		11	2.749	31	
NA39	17	2	1.036	38	
NA38	19	2	0.535	49	
		20	0.396		
		28	0.769	47	

Station	Cast #	Depth m	SPM mg/ℓ	% Organic Matter	Size Distribution Slope
NA37	20	2	0.559	37	
		30	1.601		
		45	2.172	40	
NA36	21	2	0.757	55	
		30	1.234		
		55	1.535	43	
NA35	22	2	0.787	42	
		40	1.400		
		65	1.518	34	
NA34	23	2	1.413	72	
		40	1.415		
		63	1.263	33	
SG1O	25	2	0.331		
		30	0.332		
		88	1.253		
SG26	27	2	1.394		
SG27	29	2	0,806		
SG45	31	2	0.540		

Station	Cast #	Depth m	SPM mg/ℓ	% Organic Matter	Size Distribution Slope
PL2	33	2	1.142		3.02
		30	0.206		3.30
		365	0.377		3.65
PL3	34	2	0.591		3.64
		153	0.193		3.79
PL4	35	2	0.283		3.93
		100			3.44
		137	0.962		3.97
PL5	36	2	1.904		3.29
		50	0.175		4.16
		132	0.915		4.00
		127	1.487		4.14
PL7	38	2	2.034		3.64
		126	1.161		4.22
PL8	39	2	1.665		3.31
		117	0.203		
PL9	40	2	0.996		3.36
		80	0.629		2.97
		97	0.912		4.07

Station	Cast #	Depth m	SPM mg/ℓ	% Organic Matter	Size Distribution Slope
PL10	41	2	0.617		3.66
		70	0.836		3.53
		86	1.246		3.36
PL11	42	2	0.961		3.79
		40	1.213		3.18
		65	1.357		
		81	1.619		2.94
PL12	43	2	0.961		3.79
		40	1.213		3.18
		65	1.357		
		81	1.619		2.94
PL12	43	2	0.483		3.39
		74	1.750		2.82
PL13	44	2	1.032		3.04
		55	0.739		
		72	0.794		3.97
PL14	45	2	0.882		3.37
		66	1.098		3.65
SG69	46	2	0.769		
		65	0.615		
SG69	48	2	1.102		
		90	0.851		
SG5	51	2	1.122		
		113	0.933		
SG29	52	2	0.701		

Station	Cast #	Depth m	SPM mg/ℓ	% Organic Matter	Size Distribution Slope
UP3	54	2	0.915		
		70	0.324		
		138	0.324		
SG30	55	2	0.921		
		130	0.510		
SG21	56	2	0.391		
		72	0.721		
SG2	57	2	0.393		
		73	0.613		
SG15	58	2	0.576		
		70	0.458		
SG14	59	2	0.757		
		40	0.986		
		70	0.694		
SG74	60	2	1.060		
		87	0.949		
SG22	61	2	0.548		
		97	0.989		
SG3	62	2	0.912		
		120	0.963		
SG73	63	2	1.371		
		123	1.034		
SG5	66	2	2.194		
		60	0.199		
		121	1.644		

Station	Cast #	Depth m	SPM mg/ℓ	% Organic Matter	Size Distribution Slope
PL4	67	2	1.531		3.56
		70	0.143		
		100			4.16
		136	0.618		4.61
PL5	68	2	2.281		3.34
		130	0.984		4.17
PL6	69	2	2.165		3.50
		127	1.52		4.09
PL7	70	2	1.977		3.63
		70			3.73
		123	1.134		3.92
PL8	71	2	2.248		3.27
		50	0.228		3.46
		116	1.616		4,23
PL9	72	2	1.835		3.40
		60			4.29
PL10	73	2	1.456		3.50
		43	2.617		
		70			3.56
		87	1.633		3.06
PL11	74	2	0.837		3.24
		50			3.30
		81	2.101		2.94

Station	Cast #	Depth m	5PM mg/ℓ	% Organic Matter	Size Distribution Slope
PL12	75	2			3.34
		40			3.37
		74			2.99
		30			3.28
PL14	77	2			
		68			3.84
NA41	78	2	0.392	43	
		82	2.815	28	
NA43	81	55	1.198	40	
NA44	82	2	0.746	46	
		38	1.086	44	
NA46	84	2	0.307		
		22	1.640	40	
NA39B-2	89	17	0.965		
NA39A-3	91	2	2.615		
		20	1.256		
NA39B-3	92	2	1.465		
		21	1.935		
NA39C-3	93	2	1.420		
		14	2.185		
NA11	94	2	0.847	38	
		48	0.893	35	

Station	Cast #	Depth m	SPM mg/ℓ	% Organic Matter	Size Distribution Slope
NA16	99	21	1.017	53	
NA22	101	19	1.489	38	
NA19	104	2	0.487	31	
		48	0.768		
NA17	106	2	0.705	45	
		55	1.453	27	
NA23	107	2	0.291	52	
		61	2.345	28	
NA25	109	2	1.103	42	
		46	4.194	25	
NA27	111	2	0.977	54	
		19	1.085	25	
NA39A-4	112	2	0.971		
NA39B-4	113	2	0.788		
NA39C-4	114	2	1.082		
NA39B-8	125	2	0.960		
NA39C-8	126	2	1.150		
NA33	130	2	1.559	66	
NA30	133	2	0.289	39	
		56	1.024	40	
NA29	134	65	2.773	39	
NA28	135	2	0.211	51	
		67	0.378	31	
NA34	136	2	0.349	52	3.28
		65	2.646	32	2.50

Station	Cast #	Depth ❑	SPM mg/ℓ	% Organic Matter	Size Distribution Slope
		65			2.80
NA36	138	2	0.555	45	3.59
		56	1.049	38	3.11
NA37	139	2			. 3.80
		48			2.43
NA38	140	2	1.016	46	4.13
		33	2.605	45	2.96
NA39	141	2			4.26
		22			3.50
NA40	142	2	2.140	34	3.28
		16			3.07
NA52	146	2	1.047	46	
NA5 O	148	2	1.003	63	
		42	1.196	38	
NA48	150	2	1.675	73	
		69	1.438	34	
NA45	153	2	0.688	42	
		35	0.988	54	
NA43	155	2	1.755	77	
		57	0.808	17	
NA72	175	2	0.989	41	
		30	0.813	33	
NA69	178	2	0.993	60	
		98	0.785	22	

NA66	181	2	2.091	85	
		105	0.840	15	
PL8	183	114	1.470		